VOLUME XLIV

GEMS & GEMOLOGY

FALL 2008

Identifying Synthetic Yellow Melee Diamonds

Separation of Blue Beryl

Mexifire Synthetic Fire Opal

Color Durability of "Chocolate Pearls"

THE QUARTERLY JOURNAL OF THE GEMOLOGICAL INSTITUTE OF AMERICA

GEMS & GEMOLOGY®

Fall 2008

VOLUME 44, NO. 3

pg. 203

pg. 229

EDITORIAL

FEATURE ARTICLES

NOTES AND NEW TECHNIQUES

RAPID COMMUNICATIONS

REGULAR FEATURES

pg. 269

GEMS & GEMOLOGY

www.gia.edu/gemsandgemology

SUBSCRIPTIONS

Subscriptions to addresses in the U.S. are priced as follows: **$74.95** for one year (4 issues), **$194.95** for three years (12 issues). Subscriptions sent elsewhere are **$85.00** for one year, **$225.00** for three years. Canadian subscribers should add GST.

Special rates are available for GIA alumni and current GIA students. One year: **$64.95** to addresses in the U.S., **$75.00** elsewhere; three years: **$179.95** to addresses in the U.S., **$210.00** elsewhere. Please have your student or Alumni number ready when ordering. Go to www.gia.edu/gemsandgemology or contact the Circulation Coordinator (see above).

Single copies of this issue (print or PDF) may be purchased for **$19.00** in the U.S., **$22.00** elsewhere. Discounts are given for bulk orders of 10 or more of any one issue. A limited number of back issues are also available for purchase. Please address all inquiries regarding subscriptions and single copy or back issue purchases to the Circulation Coordinator or visit www.gia.edu/gemsandgemology.

To obtain a Japanese translation of *Gems & Gemology*, contact GIA Japan, Okachimachi Cy Bldg., 5-15-14 Ueno, Taitoku, Tokyo 110, Japan. Our Canadian goods and service registration number is 126142892RT.

DATABASE COVERAGE

Gems & Gemology's impact factor is 1.381 (ranking 11th out of the 26 journals in the Mineralogy category), according to Thomson Scientific's 2006 Journal Citation Reports (issued July 2007). *Gems & Gemology* is abstracted in Thompson Scientific products (*Current Contents: Physical, Chemical & Earth Sciences* and Science Citation Index—Expanded, including the Web of Knowledge) and other databases. For a complete list, see www.gia.edu/gemsandgemology.

MANUSCRIPT SUBMISSIONS

Gems & Gemology welcomes the submission of articles on all aspects of the field. Please see the Guidelines for Authors on our Website, or contact the Managing Editor. Letters on articles published in *Gems & Gemology* are also welcome.

Gems & Gemology is published quarterly by the Gemological Institute of America, a nonprofit educational organization for the gem and jewelry industry, The Robert Mouawad Campus, 5345 Armada Drive, Carlsbad, CA 92008.

Postmaster: Return undeliverable copies of *Gems & Gemology* to GIA, The Robert Mouawad Campus, 5345 Armada Drive, Carlsbad, CA 92008.

ABOUT THE COVER

Fine blue aquamarine has long been a highly sought-after gem. In this issue, Dr. Ilaria Adamo and coauthors examine several aquamarines and other natural and synthetic dark blue beryls, and discuss the criteria by which they can be separated. Shown here is a fine aquamarine crystal with several faceted aquamarines. The 12.8 cm crystal (from Pakistan) is courtesy of Roz and Gene Meieran, Phoenix, Arizona; the 9.68 ct oval stone is courtesy of Omi Gems, Los Angeles; the 13.18 ct round and 9.58 ct emerald-cut aquamarines are GIA Collection numbers 34397 and 34398.

Photo © GIA and Harold & Erica Van Pelt. Composite image designed by Karen Myers.

Color separations for Gems & Gemology *are by Pacific Plus, Carlsbad, California.*
Printing is by Allen Press, Lawrence, Kansas.

 ISSN 0016-626X

A New Gemological Challenge: Synthetic Diamond Melee

More than two decades ago, *G&G* published an editorial by then editor-in-chief Richard T. Liddicoat titled "The Ultimate Synthetic: A Jewelry-Quality Diamond," in the same issue (Winter 1986) that we published an article on the first commercially available gem-quality synthetic diamonds, manufactured by Sumitomo Electric Industries of Japan. Since then, thousands of carats of jewelry-quality synthetic diamonds have gradually entered the marketplace, though the quantities are still very small compared to the millions of carats of natural diamonds produced annually. Most gem-quality synthetic diamonds are grown through high-pressure, high-temperature (HPHT) processes, with the chemical vapor deposition (CVD) method just beginning to establish a presence.

While researchers have succeeded in developing identification methods for both HPHT and CVD synthetic diamonds, melee-size stones (those that weigh 0.20 ct or less) can be particularly troublesome. And the challenges are even greater when dealing with jewelry-set melee. Typically, sophisticated instrumentation is needed to identify even small synthetic goods, and at a certain size it is no longer cost-effective to test each specimen. As a result, most are never submitted to gemological laboratories for identification or grading and are thus sold without a report. Because these goods often have no obvious synthetic characteristics, they can be easily mixed in with a parcel of natural diamonds and sold as such, undisclosed, either to the jewelry manufacturer or—once set—to the consumer.

This *is* happening, and it's happening now. That's what makes the lead article in this issue—Hiroshi Kitawaki et al.'s "Identification of Melee-Size Synthetic Yellow Diamonds in Jewelry"—so important. The study, conducted by three researchers at the GAAJ-Zenhokyo Laboratory in Tokyo, found that 10% of loose yellow melee-size diamonds submitted to the lab over a four-month period were synthetic. Moreover, approximately half the jewelry items set with yellow melee that the lab received during the same period also contained synthetic diamonds. Although there have been many rumors of synthetic diamond melee in the trade over the last several years, this is one of the first research reports to confirm the potential extent of the problem.

To address this issue, the GAAJ-Zenhokyo Lab devised a procedure that combines standard gemological testing with micro-infrared spectroscopy and advanced imaging techniques to distinguish between natural and synthetic diamond melee as small as 0.001 ct. The identification is "fairly rapid," according to the authors, requiring only a few minutes for loose melee and slightly longer for mounted goods.

As the authors point out, synthetic diamonds have by no means saturated the gem market. We feel, though, that the issue comes down to a matter of perception and consumer confidence: Just *one* undisclosed synthetic diamond out of a hundred casts doubt on the entire parcel—or suite of jewelry. In the group tested by Kitawaki et al., as many as 10 out of a hundred loose yellow melee were synthetic, as was at least one stone in 15 out of 30 melee-set pendants and rings.

Similar problems surround treated melee-size natural diamonds, particularly those that have been HPHT color enhanced or fracture filled (or both). Nor are colored stones exempt, given the challenges posed, for example, by beryllium-diffused corundum in very small sizes. *Gems & Gemology* applauds the GAAJ-Zenhokyo Laboratory's groundbreaking work on the cost-effective identification of mounted synthetic diamond melee. At the same time, we also call on gemologists and research facilities everywhere to continue to develop realistic means to confront such identification challenges for small and lower-cost stones, for the sake of the consumer *and* the industry.

The words with which Richard Liddicoat concluded his 1986 editorial continue to resonate today: "... never has the role of the gemologist been more important."

Alice S. Keller • Editor-in-Chief • akeller@gia.edu

IDENTIFICATION OF MELEE-SIZE SYNTHETIC YELLOW DIAMONDS IN JEWELRY

Hiroshi Kitawaki, Ahmadjan Abduriyim, and Makoto Okano

Melee-size yellow synthetic diamonds have recently been seen in the gem market, mostly as loose stones but sometimes set in jewelry. The material identified to date is synthesized by the high-pressure, high-temperature (HPHT) process. Randomly occurring pinpoint or flux-metal inclusions are diagnostic identification clues. However, some synthetic diamonds require advanced laboratory methods. This report describes the effectiveness of a technique new to gemology, infrared microspectroscopy, in combination with cathodoluminescence imaging for the rapid and accurate separation of melee-size natural and synthetic diamonds based on their characteristic mid-infrared absorption spectra and growth structures, respectively. With these techniques, the GAAJ-Zenhokyo Laboratory in Tokyo determined that approximately 10% of loose—and dozens of mounted—yellow melee diamonds submitted over a four-month period were synthetic.

Two techniques are known today for the laboratory growth of gem-quality diamonds: high pressure and high temperature (HPHT) and chemical vapor deposition (CVD). Synthetic diamonds grown by the HPHT process began to appear on the gem market in the 1990s. Most of the laboratory-grown diamonds seen commercially to date in the GAAJ-Zenhokyo Laboratory are yellow type Ib's in faceted sizes under 2 ct, but some are type Ia synthetics that have been HPHT treated to display a green-yellow color. We have also seen small quantities of type IIa colorless synthetic diamonds, as well as pink to red or purple synthetics that are produced by a multi-step process (HPHT plus irradiation and/or heat treatment; see, e.g., Shigley et al., 2004). Apollo Diamond Inc. recently announced the production and commercial sale of diamonds lab-created by the CVD method (Wang et al., 2003, 2007); however, such material has not been seen in the market in any quantity.

The HPHT synthesis of gem-quality diamonds has for the most part been based on the Russian BARS technique. In recent years, however, the U.S.–based Gemesis Corp. has been mass producing yellow synthetic diamonds by a process that represents an improvement on the original Russian technology (Shigley et al., 2002). Chatham Created Gems has also been selling synthetic diamonds in pink, blue, or yellow hues produced by a different HPHT method (Shigley et al., 2004; e.g., figure 1).

Given the current availability of synthetic diamonds and the fact that melee-size (especially those smaller than 0.05 ct) stones are more difficult to test, it should not come as a surprise that such small synthetic yellow diamonds have started to become mixed with natural diamonds, both in parcels of loose stones and in manufactured jewelry (figure 2). Although synthetic diamonds still represent only a very small part of the gem market, they receive a

See end of article for About the Authors and Acknowledgments.
GEMS & GEMOLOGY, Vol. 44, No. 3, pp. 202–213.

Figure 1. The loose synthetic diamonds shown here, from Chatham Created Gems (San Francisco), illustrate some of the yellows produced by HPHT growth. Many are similar in hue and intensity to the natural yellow diamonds in this ring, which is courtesy of Alan Friedman, Beverly Hills, California. The loose synthetics weigh 0.05–0.30 ct; the Fancy Intense yellow center diamond in the ring is 1.09 ct, and the 93 yellow melee weigh a total of 1.12 ct. Photo by Robert Weldon.

great deal of attention within and outside the industry, so correct identification is of great importance. In the present article, we introduce a practical approach used routinely at the GAAJ-Zenhokyo Laboratory to identify melee-size HPHT-grown synthetic yellow diamonds (loose and in jewelry). Our laboratory also routinely checks for treatment in such stones, but that is beyond the scope of this study.

REVIEW OF IDENTIFICATION CRITERIA FOR HPHT-GROWN SYNTHETIC DIAMONDS

Today, most laboratories use a variety of indicators to identify HPHT-grown synthetic diamonds, as summarized below.

Inclusions. Most natural diamonds form in the earth's upper mantle at depths of 150–200 km. Associated minerals that may be present as inclusions in natural diamonds include pyrope, chrome diopside, enstatite, and olivine (see, e.g., Kirkley et al., 1991). Oriented needle-like inclusions may also provide proof of natural origin (Crowningshield, 1994). In contrast, the HPHT process generally uses Fe, Ni, and Co as flux solvents because carbon readily dissolves in them. These metals may become trapped in the lab-grown crystals as inclusions, in which case they provide proof of synthetic origin.

Although some minerals with a metallic luster (such as chromite) may be present in natural diamonds, their crystal forms are different from those shown by the metallic inclusions in synthetic diamonds. The latter may also contain breadcrumb-like or pinpoint inclusions that are characteristic of laboratory growth.

Anomalous Double Refraction due to Lattice Distortion. Diamond belongs to the cubic crystal system and is optically isotropic. However, most natural diamonds show anomalous double refraction (ADR) when they are viewed between crossed polarizing filters, due to lattice distortion. This ADR can be divided into two types—one that is created during the growth process deep in the mantle, and one caused by post-growth plastic deformation of the diamond. A good example of plastic deformation–caused ADR seen in type II diamonds is the so-called tatami pattern, which can distinguish natural type II diamonds from HPHT-grown synthetic type I diamonds (Lang, 1967). Although plastic deformation–caused ADR may be seen in type I natural diamonds, the fact that ADR due to distortion occurs only along internal growth sectors in HPHT-grown synthetic diamonds distinguishes them from natural diamonds (Shigley, 1986).

Ultraviolet Luminescence. Natural diamonds emit various fluorescence colors when exposed to UV radiation. Common colors are blue-white (originating from the N3 center), orange (the NV center), and yellow and green (the S1 or S3 centers and H3 center; Fritsch and Waychunas, 1994). These fluorescence

Figure 2. The GAAJ-Zenhokyo laboratory has identified yellow HPHT-grown synthetic diamond melee set with natural yellow melee in fine jewelry. In this ring, 12 melee (0.46 ct total weight) surround a 3.89 ct ruby. Only one of the 12 was natural (see arrow); all the others were synthetic. Photo by Masaaki Kobayashi.

colors and their intensities correspond to some extent to specific types or colors of diamonds (Eaton-Magaña et al., 2007).

HPHT-grown synthetic diamonds also often show characteristic reactions to UV radiation. Type IIa colorless synthetic diamonds exhibit strong yellow-white phosphorescence after exposure to short-wave UV, which is not seen in their natural counterparts. Likewise, the orange fluorescence seen in pink synthetic stones is an indication of growth in a laboratory (Shigley et al., 2004). Another characteristic feature of HPHT-grown synthetic diamonds is the uneven fluorescence in a cross-like pattern that is associated with cubic growth sector zoning. HPHT-treated synthetic stones in highly saturated yellow colors may show a strong green-yellow luminescence to long- and short-wave UV that originates from a defect related to nickel (Shigley et al., 1993).

Color Zoning. Color zoning may occur in natural diamonds due to differences in the incorporation of impurity elements (mainly nitrogen) during crystal growth. This uneven color distribution is generally observed parallel to the octahedral crystal faces. Plastic deformation after crystal growth or a vacancy disk lying on {111} planes also can produce brown or pink color zoning parallel to octahedral faces and often in intersecting patterns (Bangert et al., 2006); these features, too, may help identify natural diamonds.

HPHT-grown synthetic diamonds have a crystal morphology different from that of natural diamond. Each internal growth sector (such as those sectors underlying cubic or octahedral faces) incorporates impurity elements in different concentrations; as a result, distinct color zoning corresponding to the arrangement of growth-sector zoning is generally observed with magnification. Hence, synthetic diamonds often display color zoning with a combination cross and square pattern, which is also an important identifying feature.

Spectroscopy. Typically, synthetic diamonds cannot be identified by standard gemological testing alone, so more sophisticated spectroscopic and imaging techniques must also be employed. One key way to distinguish natural from synthetic diamonds is spectral analysis in the UV-visible region, with the presence of absorption due to the N3 center (415 nm). The N3 center is a defect caused by the aggregation of three nitrogen atoms surrounding a vacancy; it is present in most natural diamonds, but it is not produced by normal diamond synthesis processes (Welbourn et al., 1996). The DiamondSure instrument developed by the Diamond Trading Company (DTC) to distinguish natural and synthetic diamonds operates on the basis of detecting the N3 center. Another defect related to a Ni-N center may also be detected in the UV-visible spectrum of some synthetic diamonds (Lawson and Kanda, 1993).

Fourier-transform infrared (FTIR) spectroscopy can reveal diamond type, as well as the existence of defects related to hydrogen or to the B′ center that are characteristic of natural diamonds (Allen, 1981; Kiflawi and Lawson 1999).

X-ray Fluorescence Analysis. XRF analysis to detect the chemical composition of inclusions can be an effective way to recognize HPHT-grown synthetic diamonds. Since this method can analyze only the surface or near surface of an object, any inclusions need to be exposed on a polished facet of the diamond. In HPHT-grown synthetic diamonds, the flux-metal inclusions often reach the polished surfaces. In such cases, the presence of Fe, Ni, or Co can reveal the synthetic origin of the stone.

Cathodoluminescence (CL) Imaging. Sophisticated luminescence techniques can be very effective for the identification of natural or synthetic diamonds, because they clearly reveal the very different growth structures described above. One commonly used

instrument, the DTC DiamondView, employs strong deep-UV radiation to capture luminescence images of a diamond (Welbourn et al., 1996). Similarly, CL imaging employs an electron beam to create images of the gem's growth structure. While the DiamondView is easier to operate, luminescence images obtained by electron beam in the CL technique are sharper. Also, the lower limit for the DiamondView is about 0.05 ct (see, e.g., Welbourn et al., 1996), but—coupled with an optical microscope—the CL instrument can be used to test diamonds that are smaller than this.

Although CL images of natural diamonds ideally will show a rectangular growth structure that is caused by an octahedral {111} sector, variations in impurity concentrations and growth conditions typically lead to significant differences between stones in terms of observed growth pattern, interval of zoning, fluorescence, and intensity of CL. Some diamonds show very complicated images due to dissolution and plastic deformation processes. These images are unique for each diamond and possibly may be used to identify specific diamonds (Sunagawa et al., 1998; Miyata et al., 1999).

The CL images of synthetic diamonds are more predictable. They clearly show sector zoning, and an experienced operator will be able to visualize the morphology of the original crystal from this image.

Photoluminescence (PL) Analysis. This spectral technique can detect some point defects when excited by lasers in the UV or visible-light range. Since 2000, this has become an important method for detecting HPHT treatment at gemological laboratories (Chalain et al., 2000). In natural diamonds, PL analysis reveals spectral peaks that originate due to various point defects, nitrogen-containing defects, and defects for which the cause has not yet been identified. Conversely, in HPHT-grown synthetic diamonds, PL analysis can reveal peaks that are related to metal solvents such as nickel.

MATERIALS AND METHODS

The samples used in this study included 870 loose yellow melee (see, e.g., figure 3) and 500 yellow melee in 30 items of jewelry submitted to the GAAJ-Zenhokyo Laboratory by a number of clients for identification reports. These yellow melee were submitted over a four-month period from the end of 2006 into 2007. For the purposes of this study, we defined *melee* as diamonds smaller than 0.20 ct.

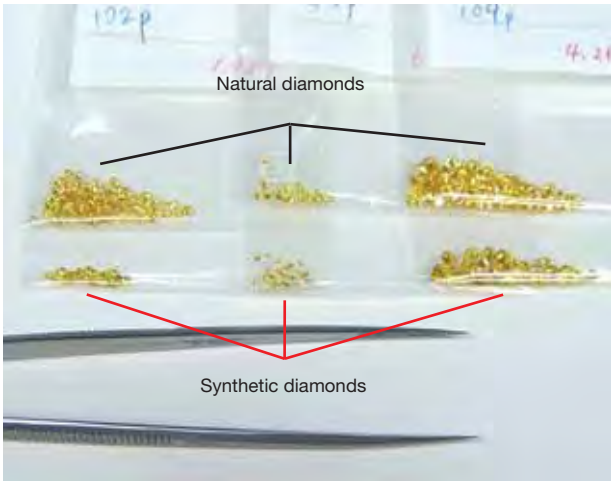

Figure 3. The study examined 870 loose yellow melee. All the samples shown here were originally submitted as a single parcel; testing revealed that a significant portion of them (the three bags in the lower row) were HPHT-grown synthetic diamonds. These samples ranged from 0.001 to 0.10 ct. Photo by H. Kitawaki.

Twenty of the 30 jewelry items were set with 3–12 yellow melee, and the remaining 10 items were set with 35 to as many as 66 stones. For the most part, the samples ranged between 0.01 and 0.15 ct, but the smallest weighed 0.001 ct (again, see figure 3). The jewelry items consisted of rings and pendants (figure 4).

We studied all the loose and jewelry-set samples with standard gemological instrumentation. We used an Olympus gemological microscope to examine inclusions, with magnification up to 60× and a narrow fiber-optic light source (diameter of 1–3 mm) for illumination. UV fluorescence was observed in a dark room using long- and short-wave UV lamps manufactured by Manaslu Co.

Infrared Spectroscopy. All the samples were tested by IR spectroscopy. The 870 loose stones were analyzed by a Shimadzu IR Prestige-21 instrument equipped with a KBr beam splitter and DLATGS detector. This instrument can analyze extremely small loose diamonds and requires less time than the micro-FTIR technique used for analyzing mounted stones. The analytical range was 4000–400 cm^{-1}, resolution 4 cm^{-1}, and total scans per spectrum 20. When the signal-to-noise ratio was not adequate, the measurement was made with 1.0 cm^{-1} resolution and 200–500 scans per spectrum. The monitor mode in 4 cm^{-1} resolution allows faster measurements. Although the data cannot be saved

Figure 4. The yellow melee in several items of jewelry were tested as part of this study. Although most of the stones were natural diamonds, HPHT-grown synthetic diamonds (indicated here by arrows) were identified in approximately half the jewelry items tested. Photos by H. Kitawaki.

to a computer in this mode, a measurement can be done in about 10 seconds (including positioning the sample on the microscope stage and data scanning).

The samples set in jewelry were measured by FTIR microspectroscopy (micro-FTIR). This kind of IR measurement under a microscope has emerged relatively recently compared to the better-known Raman microspectroscopy (e.g., Macmillan and Hofmeister, 1988). It has been used in various fields; in geology, micro-FTIR has been applied to minerals in thin section to analyze hydrous microphases in areas as small as 10 × 10 μm, to understand the

Figure 5. A Shimadzu IR Prestige-21 FTIR spectrometer in conjunction with a Shimadzu AIM-8800 infrared microscope (left) was used to analyze each of the melee-size samples set in jewelry. By confirming the analytical site on the monitor, this configuration allows IR spectral analysis of a small area on a small sample (right). Photos by H. Kitawaki.

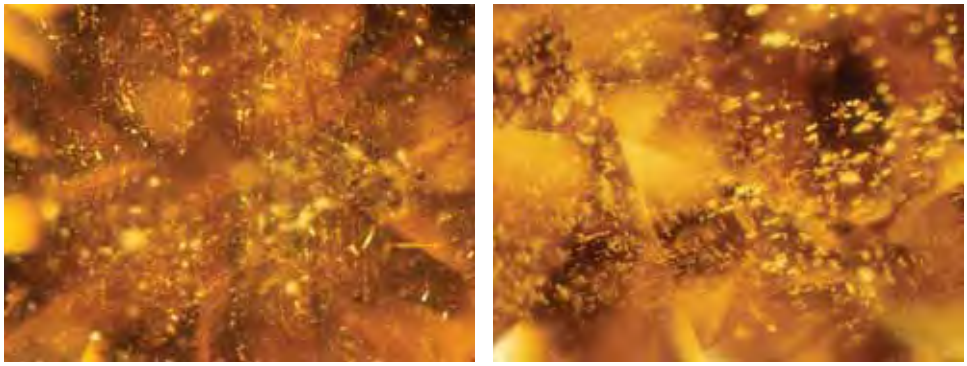

Figure 6. Many of the natural samples revealed the oriented needle-like (left) and highly reflective flake-like (right) inclusions often seen in yellow type Ib natural diamonds. Photomicrographs by H. Kitawaki; magnified 65×.

mechanism of water-rock interactions (Nakashima et al., 1989). However, we do not know of any prior report of its application to gemology. In the present study, we used the Shimadzu IR Prestige-21 spectrometer in conjunction with a Shimadzu AIM-8800 infrared microscope (figure 5).

Again, the measurement range was 4000–400 cm^{-1}, but a resolution between 0.5 and 16 cm^{-1} can be chosen. For routine work, we set the resolution at 4 cm^{-1} with a total of 20 scans per measurement. The IR microscope uses liquid nitrogen to cool the detector, but our sample measurement was done at room temperature. The instrument employs X15 Cassegrain objective/condenser mirrors, and its actual measurement range is 3–400 µm. We set the following positioning range for the sample stage, which can be adjusted automatically: X-axis—70 mm, Y-axis—30 mm, and Z-axis—40 mm. The operator sets the sample on the stage and then, viewing it on a monitor, designates the measurement location; the sample stage automatically moves to the desired spot for the analysis. With this arrangement, we were able to measure each sample set in jewelry individually.

Cathodoluminescence Imaging. We used CL imaging to test a number of stones in 15 items of jewelry and 250 loose samples that either were suspected of being synthetic or did not display positive proof of natural origin with standard gemological tests and micro-IR analysis. Specifically, we used a Premier American Technologies Corp. ELM-3R cathodo-luminescope, with a vacuum chamber 125 mm deep, 170 mm wide, and 60 mm high. This was large enough to easily hold the jewelry pieces in our sample base, although items with a height over 30 mm may block the electron beam. We were able to test nine loose melee (face up) at one time. The vacuum was 20–40 millitorr, and observations were made under the conditions of 4–6 kV and 0.5 mA at room temperature.

RESULTS

Gemological Observations. Microscopic examination revealed inclusions in all but a few of the samples. About 20% showed the oriented needle-like inclusions with a shiny black luster and the highly reflective flake-like inclusions that are characteristic of natural diamonds (Crowningshield, 1994; figure 6). We could not conclusively identify these inclusions, but we believe they were graphite or a sulfide mineral. The clouds of minute inclusions seen in more than half the samples examined also indicated natural origin. These clusters of white dots occasionally had a wispy appearance (figure 7).

However, we also saw features indicating HPHT synthetic origin. Approximately 85 loose samples

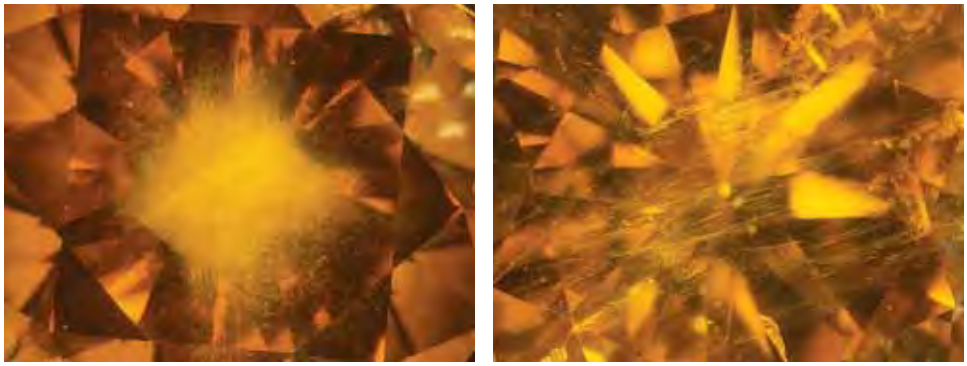

Figure 7. Natural diamonds commonly show minute inclusions in a cloud-like formation (left) that in some stones have a wispy appearance (right). Photomicrographs by H. Kitawaki; magnified 35×.

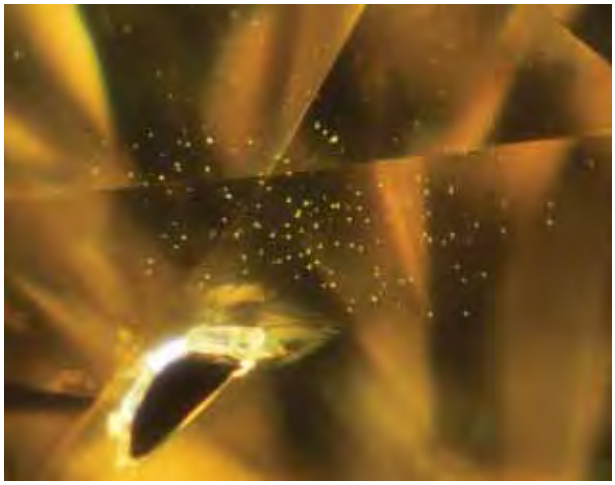

Figure 8. These scattered white pinpoint inclusions indicate that this melee sample is a synthetic diamond. Photomicrograph by H. Kitawaki; magnified 65×.

and several individual pieces of melee in 15 items of jewelry showed pinpoint-like inclusions. In contrast to the clouds of minute inclusions observed in the natural diamonds, these appeared as individual rounded shapes that were scattered irregularly throughout the stones (figure 8). Approximately 10–20% of the samples with pinpoint inclusions also contained metallic inclusions (figure 9), which are obvious indications of HPHT synthesis. A similar proportion of samples with pinpoint inclusions also contained breadcrumb-like inclusions (figure 10). Both the metallic and breadcrumb-like inclusions are typically a solid phase of the flux-metal solvent in which the diamond grew, which was trapped during crystal growth.

The vast majority (over 80%) of the samples showed weak fluorescence to long-wave UV radiation in slightly chalky yellow to orange colors, with a weaker reaction to short-wave UV. In general, these were the same stones that had inclusions of presumably natural origin. The remaining samples were almost or completely inert to both wavelengths. However, this reaction was seen in samples with needle-like inclusions that indicated natural origin as well as in those containing scattered pinpoint-like or metallic inclusions that indicated synthetic origin.

Infrared Spectroscopy. Most of the samples (~70%) were type Ia diamond, with a high nitrogen content; absorptions from the B center (a broad band with peaks at 1332, 1175, 1010, and 775 cm^{-1}) and platelets (1365 cm^{-1}) were detected. Many also showed hydrogen-related absorptions at 1405 cm^{-1} (Davies et al., 1984) or several H-related features in the 3500–3100 cm^{-1} region (figure 11). In addition, a peak at 1430 cm^{-1} is due to C-N absorption. The diamonds showing such spectroscopic features could be identified as natural in origin.

Eighty-five loose samples and about 50 samples in the 15 items of jewelry with synthetic-appearing inclusions showed absorptions only from the C center (i.e., single substitutional nitrogen, 1344 and 1130 cm^{-1}; again, see figure 11). Perfect type Ib stones showing only the C center are very rare among natural diamonds, so IR spectroscopy supported the identification of these samples as synthetic.

Among all the yellow melee tested, 170 loose stones and 100 samples in 15 items of jewelry showed a weak A center (a broad band with peaks at 1282, 1215, 1096, and 472 cm^{-1}) together with the C center. For the most part, these corresponded to stones containing oriented needle-like inclusions or cloud-like inclusions. Natural type Ib yellow diamonds showing the A center are occasionally seen. However, synthetic diamonds produced at extremely high temperatures, or HPHT-treated yellow

Figure 9. Also characteristic of HPHT synthetic diamonds are inclusions of the solidified metallic flux, which were irregular in some of the melee (left) and well formed in others (right). Photomicrographs by H. Kitawaki; magnified 65×.

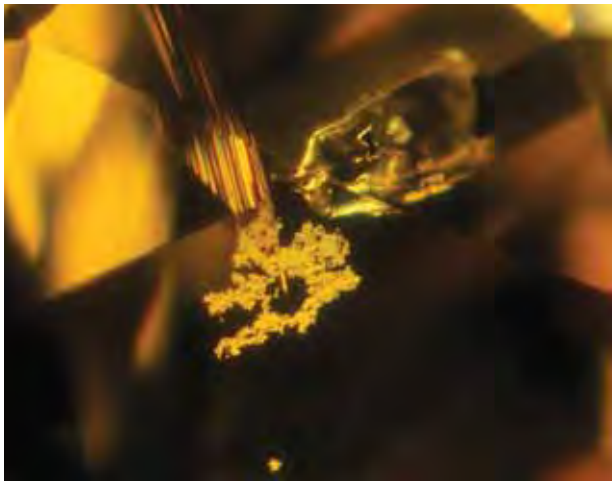

Figure 10. Breadcrumb-like inclusions of metallic flux are clear indicators that this sample is synthetic. Photomicrograph by H. Kitawaki; magnified 65×.

synthetic diamonds, may show similar infrared spectra. Therefore, the combined presence of a weak A center with a C center is not diagnostic for natural or synthetic origin.

Cathodoluminescence Observations. Among the diamonds in the jewelry items, those that were positively identified as natural by IR spectroscopy often showed slightly cloudy orange-yellow to yellow luminescence and a square zonal structure surrounded by octahedral {111} growth horizons, both of which are characteristic of natural diamonds (figure 12). However, some stones showed irregular patterns or an indistinct CL image. For example, a complicated structure may indicate a natural origin, but it is difficult to interpret the growth history (figure 13, left). An indistinct CL image will not help identify the natural or synthetic origin (figure 13, right).

For the most part, samples that showed a weak A center together with a C center in their FTIR spectra also showed linear CL patterns (slip bands; figure 14). This linear pattern with green-to-yellow luminescence originates from the H3 center (Welbourn et al., 1996); each of the fluorescing lines was parallel to octahedral faces and intersected one another. Such linear patterns in yellow diamonds are associated with plastic deformation and thus characterize the stone as natural.

The samples that showed only the C center in FTIR analysis displayed growth zoning characteristic of synthetic diamonds (figure 15). These images were composed of cubic {100} and octahedral growth sectors, among others. The most typical CL image for these samples was a combination of green-yellow cubic sectors, and inert octahedral sectors (again, see figure 15). Adding to this combination, minor sectors that glowed blue-white, such as {110} or {113}, were often recognized (figure 16).

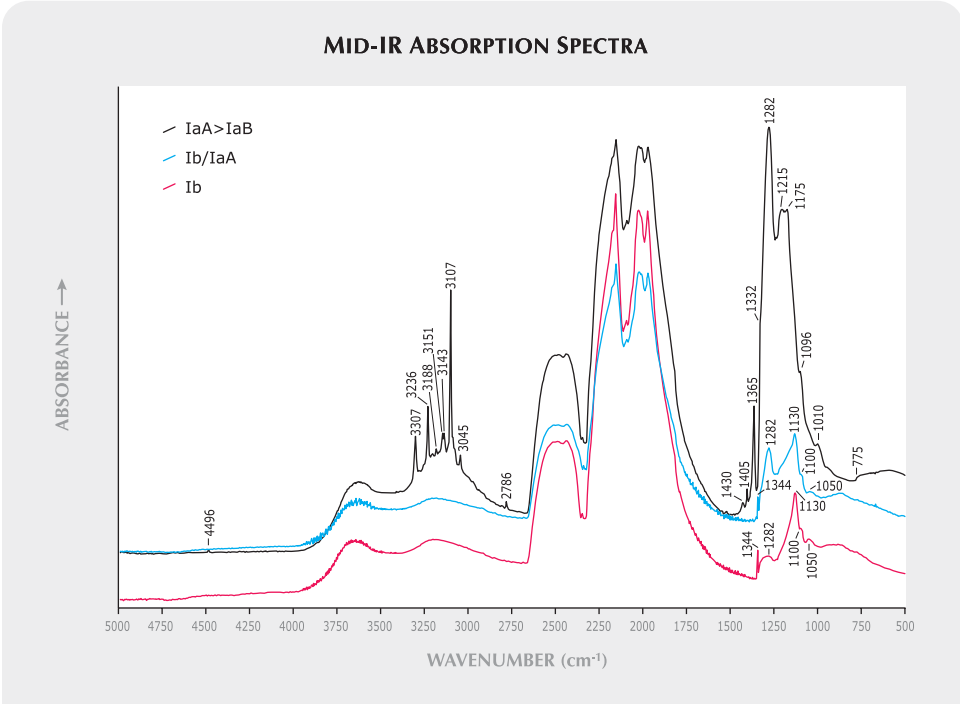

Figure 11. These mid-IR spectra of jewelry-set melee reveal three types of natural and synthetic diamond. The black spectrum is of a natural diamond with a dominant IaA component at 1282, 1215, and 1096 cm^{-1}; a minor IaB component with a sharp peak at 1365 cm^{-1}; and a peak at 1430 cm^{-1} related to C-N absorption. Note also the H-related absorptions at 4496 cm^{-1}, in the 3307–2786 cm^{-1} region, and at 1405 cm^{-1}. The blue spectrum shows a natural diamond that is a mixture of type Ib with IaA. The red spectrum is of a pure type Ib synthetic diamond, characterized by bands at 1344, 1130, and (weaker) ~1282, 1100, and 1050 cm^{-1}.

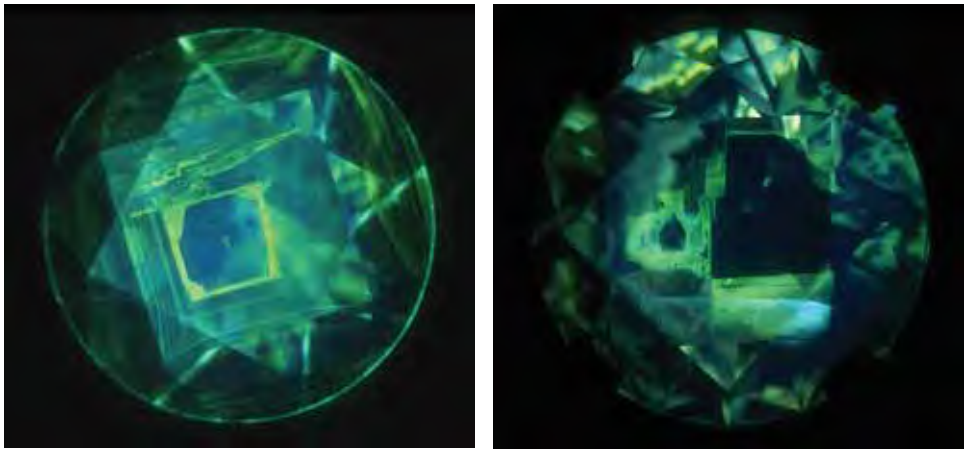

Figure 12. These CL images show the square zonal structure surrounded by octahedral {111} growth horizons characteristic of natural diamonds, as well as changes they undergo during growth. The mantle of the 0.15 ct diamond on the left has a rounded, irregular pattern, suggesting dissolution during crystallization. The ring-set 0.10 ct diamond on the right shows zigzag growth due to small stepped {111} faces. Photos by H. Kitawaki.

Also, though in small quantity, some stones showed orange-yellow luminescence in octahedral sectors and were inert in cubic sectors (figure 17).

The luminescence color seen with a CL image is usually the same as that observed with UV radiation, although it is typically more intense with CL. However, the CL image and fluorescence to UV radiation sometimes may differ due to the lower penetration depth of CL (1–2 µm; Ponahlo, 1992) in comparison with UV radiation (such as that from the DiamondView; Simon Lawson, pers. comm., 2008).

DISCUSSION

At the GAAJ-Zenhokyo Laboratory, yellow synthetic diamonds in melee sizes have been documented since 2005, as loose stones and set in jewelry. The identification of melee-size synthetic diamonds also was reported by Simic and Burnett (2007), but for the most part their methods could not be applied to mounted stones.

Today, it is very unusual for us to find synthetics among all the diamonds identified at our laboratory, and it is unlikely that synthetic diamonds have flooded the gem market. As described above, however, the results of this study suggest that almost 10% of 870 loose yellow melee diamonds that came in over this four-month period were synthetic, and 15 out of the 30 jewelry items studied each contained on average about 10% HPHT-grown diamonds. The diamonds confirmed as HPHT synthetic at our laboratory were reported individually to the clients. For the jewelry items, the clients elected to replace the synthetic stones with natural diamonds after learning our testing results.

Identification of melee-sized yellow diamonds at the GAAJ-Zenhokyo Laboratory is performed in three steps:

1. All diamonds are examined with a gemological microscope and their inclusions studied.
2. All diamonds undergo micro-FTIR spectroscopic analysis.

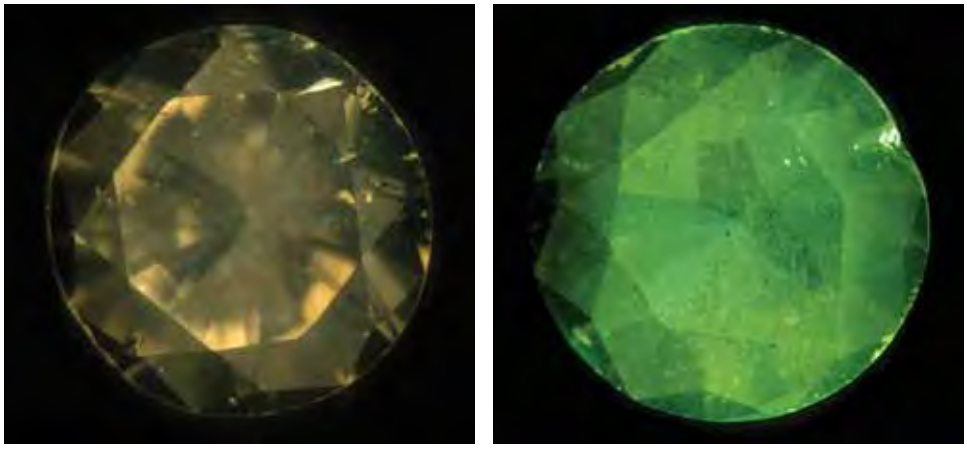

Figure 13. Irregular patterns or unclear CL images were observed in some of the samples. Zoning parallel to an octahedral face at the center of the stone may indicate a natural origin (left). However, an indistinct CL image, such as that seen on the right, is not helpful in establishing a natural or synthetic origin. Photomicrographs by Hideaki Fukushima; magnified 20×.

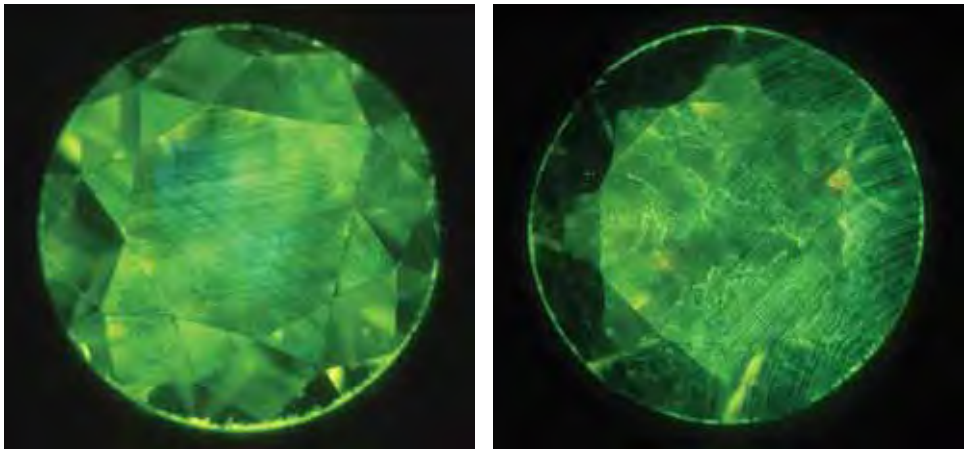

Figure 14. The linear slip bands parallel to the {111} plane in these two CL images of yellow melee are associated with plastic deformation, which identifies the diamonds as natural. The yellowish green color of the growth bands is due to the H3 center. Photomicrographs by A. Abduriyim; magnified 20×.

3. Diamonds for which the origin is still in question are examined by CL.

In the first step, we look for characteristic inclusions, such as the oriented black needle-like inclusions and cloud-like clusters of minute inclusions that are typical of natural diamonds, or the irregularly distributed pinpoint-like inclusions that are seen in synthetics. The presence of metallic inclusions is proof of synthetic origin.

In the second step, the use of an infrared microscope makes it possible to analyze several loose melee-size diamonds at one time, or those set in jewelry that could not be measured by normal FTIR analysis. The samples are observed on a computer monitor, and each can be identified as to its diamond type individually in a matter of seconds. Those stones that show the B center or platelets, or that show absorption related to hydrogen, are identified as natural. Those that contain only the C center (i.e., single substitutional nitrogen) are likely to be synthetic.

In the third step, the CL images of natural diamonds are differentiated by rectangular banding that is parallel to octahedral sectors, or slip bands parallel to octahedral sectors that intersect one another. The former pattern was observed in the type Ia stones, and the latter in type Ib. In contrast, HPHT-grown diamonds show sector zoning that is mainly composed of a combination of cubic and octahedral sectors.

In many of the CL images of synthetic diamonds observed in this study, the center of the original crystal was located on or near the center of the table of the faceted sample. This means that these melee were not cut from remnants of larger pieces, but rather were cut from small as-grown crystals (that is, almost as small as the melee).

Using the procedures described, we can identify most natural and synthetic melee diamonds relatively quickly, a matter of a few minutes for loose samples. Examination of jewelry items with micro-FTIR may require more time to position and focus the individual stones, but nevertheless an item set with 10 melee can be analyzed in about 30 minutes.

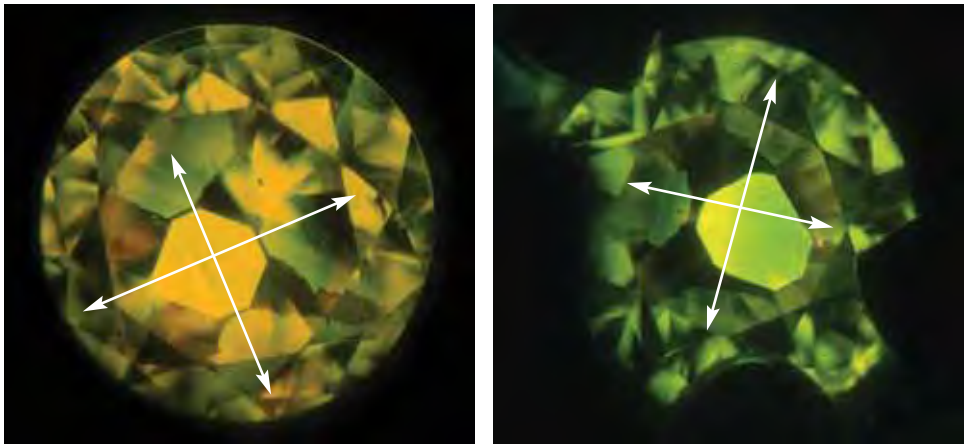

Figure 15. CL imaging identified these yellow melee (left, loose; right, set in a pendant) as synthetic diamonds. Cross-shaped growth patterns were seen in most synthetics, from the presence of cubic (yellowish green) and octahedral (inert) sectors. These zonal structures are distinctly different from those seen in natural diamond. Photomicrographs by H. Kitawaki; magnified 20× (left) and 18× (right).

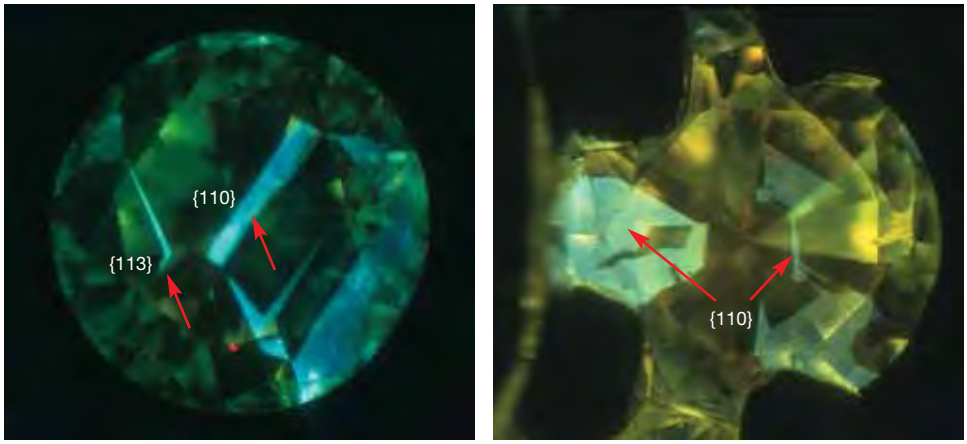

Figure 16. CL imaging revealed blue-white dodecahedral {110} and/or trapezohedral {113} sectors in some of the melee synthetic diamonds (left). The threefold CL pattern displayed by the other synthetic diamond is related to its cubic growth sectors; the dodecahedral {110} sector luminesced a weak blue-white (right). Photomicrographs by H. Kitawaki; magnified 20× (left) and 18× (right).

Figure 17. A characteristic cross-shaped pattern is displayed in this CL image of a loose synthetic diamond. The orange-yellow and inert regions are related to octahedral and cubic growth sectors, respectively. Photomicrograph by H. Kitawaki; magnified 20×.

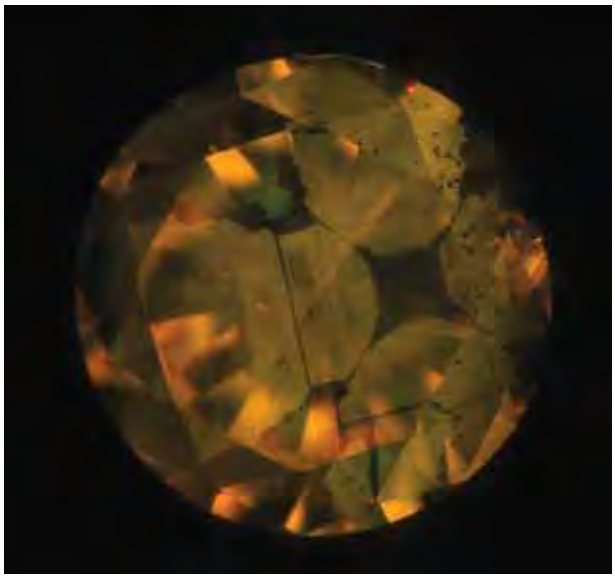

Additional time may be needed to determine if a natural diamond has been treated, but that is beyond the scope of this article.

CONCLUSION

Synthetic diamonds in various colors such as yellow, blue, and pink have been circulated in the gem market although in relatively small quantities. Those identified as synthetic to date in our laboratory were produced by the HPHT method, and they were identified by standard gem testing methods combined with more advanced spectroscopic and cathodoluminescence imaging techniques.

As more melee-size yellow synthetic diamonds are set in jewelry together with natural stones, their identification poses a new challenge for gemological labs. The three-step approach described in this study—examination with a microscope, micro-FTIR spectroscopy (to obtain the spectra of individual melee mounted in jewelry), and CL imaging—is effective in conclusively separating natural from synthetic diamonds.

ABOUT THE AUTHORS
Mr. Kitawaki is director, Dr. Abduriyim is chief research scientist, and Mr. Okano is a research gemologist in the Research Laboratory at the Gemmological Association of All Japan (GAAJ)-Zenhokyo, in Tokyo.

ACKNOWLEDGMENTS
The authors are grateful to gem dealers in Tokyo for information and samples that made this study possible. Thanks to our technical staff members at Zenhokyo for assistance with this work. We are also grateful to Dr. James E. Shigley of GIA in Carlsbad, California, for critically reading and improving the manuscript.

REFERENCES

Allen B.P., Evans T. (1981) Aggregation of nitrogen in diamond, including platelet formation. *Proceedings of the Royal Society*, Vol. A375, pp. 93–104.

Bangert U., Barnes R., Hounsome L.S., Jones R., Blumenau A.T., Briddon P.R., Shaw M.J., Öberg S. (2006) Electron energy loss spectroscopic studies of brown diamonds. *Philosophical Magazine*, Vol. 86, No. 29-31, pp. 4757–4779.

Chalain J.P., Fritsch E., Hänni H.A. (2000) Identification of GE POL diamonds: A second step. *Journal of Gemmology*, Vol. 27, No. 2, pp. 73–78.

Crowningshield G.R. (1994) Gem Trade Lab Notes: Characteristic

inclusions in fancy-color diamonds. *Gems & Gemology*, Vol. 30, No. 1, pp. 41–42.
Davies G., Collins A.T., Spear P. (1984) Sharp infra-red absorption lines in diamond. *Solid State Communications*, Vol. 49, No. 5, pp. 433–436.
Eaton-Magaña S., Post J.E., Walters R.A., Heaney P.J., Breeding C.M., Butler J.E. (2007) Fluorescence spectra of colored diamonds using a rapid, mobile spectrometer. *Gems & Gemology*, Vol. 43, No. 4, pp. 332–351.
Fritsch E., Waychunas G.A. (1994) Gemstones. In M. Robbins, *Fluorescence*, Geoscience Press, Phoenix, AZ, pp. 163–165.
Kiflawi I., Lawson S.C. (2001) Aggregates of nitrogen in diamond. In M. H. Nazaré and A. J. Neves, Eds., *Properties, Growth and Applications of Diamond*, Inspec, London, pp. 130–133.
Kirkley M.B., Gurney J.J., Levinson A.A. (1991) Age, origin, and emplacement of diamonds: Scientific advances in the last decade. *Gems & Gemology*, Vol. 27, No. 1, pp. 2–25.
Lang A.R. (1967) Cause of birefringence in diamond. *Nature*, Vol. 213, January 21, pp. 248–251.
Lawson S.C., Kanda H. (1993) An annealing study of nickel point defects in high-pressure synthetic diamond. *Journal of Applied of Physics*, Vol. 73, No. 8, pp. 3967–3973.
MacMillan R.G., Hofmeister A.M. (1988) Infrared and Raman spectroscopy. In F. C. Hawthorne, Ed., *Spectroscopic Methods in Mineralogy and Geology*, Reviews in Mineralogy, Vol. 18, Mineralogical Society of America, pp. 99–159.
Miyata T., Kitawaki H., Kitamura M. (1999) Cathodoluminescence method and its applications to gemmology. *Journal of the Gemmological Society of Japan*, Vol. 20, No. 1/4, pp. 63–78.
Nakashima S., Ohki S., Ochiai S. (1989) Infrared microspectroscopy analysis of the chemical state and spatial distribution of hydrous species in minerals. *Geochemical Journal*, Vol. 23, pp. 57–64.
Ponahlo J. (1992) Cathodoluminescence (CL) and CL spectra of De Beers' experimental synthetic diamonds. *Journal of Gemmology*, Vol. 23, No. 1, pp. 3–17.
Shigley J.E., Fritsch E., Stockton C.M., Koivula J.I., Fryer C.W., Kane R.E. (1986) The gemological properties of the Sumitomo gem-quality synthetic yellow diamonds. *Gems & Gemology*, Vol. 22, No. 4, pp. 192–208.
Shigley J.E., Fritsch E., Koivula J.E., Sobolev N.V., Malinovsky I.Y., Palyanov Y. (1993) The gemological properties of Russian gem-quality synthetic diamonds. *Gems & Gemology*, Vol. 29, No. 4, pp. 228–248.
Shigley J.E., Abbaschian R., Clarke C. (2002) Gemesis laboratory-created diamonds. *Gems & Gemology*, Vol. 38, No. 4, pp. 301–309.
Shigley J.E., McClure S.F., Breeding C.M., Shen A.H., Muhlmeister S.M. (2004) Lab-grown colored diamonds from Chatham Created Gems. *Gems & Gemology*, Vol. 40, No. 2, pp. 128–145.
Simic D., Burnett L. (2007) Identification of fancy color lab-grown diamonds smaller than 0.09 ct with EGL USA CIS method. *EGL USA Newsletter*, Spring, pp. 2–3.
Sunagawa I., Yasuda T., Fukushima H. (1998) Fingerprinting of two diamonds cut from the same rough. *Gems & Gemology*, Vol. 34, No. 4, pp. 270–280.
Wang W., Moses T., Linares R., Hall. M., Shigley J.E., Butler J. (2003) Gem-quality synthetic diamonds grown by a chemical vapor deposition (CVD) method. *Gems & Gemology*, Vol. 38, No. 4, pp. 268–283.
Wang W., Hall M.S., Moe K.S., Tower J., Moses T.M. (2007) Latest-generation CVD-grown synthetic diamonds from Apollo Diamond Inc. *Gems & Gemology*, Vol. 43, No. 4, pp. 294–312.
Welbourn C.M., Cooper M., Spear P.M. (1996) De Beers natural versus synthetic diamond verification instruments. *Gems & Gemology*, Vol. 32, No. 3, pp. 156–169.

AQUAMARINE, MAXIXE-TYPE BERYL, AND HYDROTHERMAL SYNTHETIC BLUE BERYL: ANALYSIS AND IDENTIFICATION

Ilaria Adamo, Alessandro Pavese, Loredana Prosperi, Valeria Diella,
David Ajò, G. Diego Gatta, and Christopher P. Smith

Aquamarine, Maxixe-type (irradiated) beryl, and two types of hydrothermally grown synthetic blue beryl currently available in the marketplace were investigated by classical gemological methods, chemical analysis, and UV-Vis-NIR and mid-IR spectroscopy. These materials may be conclusively identified by a combination of these techniques. The Maxixe-type beryl (like natural-color Maxixe beryls) is distinguishable by its unusual dichroism, green UV fluorescence (when present), Fe-free chemical composition, and distinctive UV-Vis-NIR spectrum. The hydrothermal synthetic blue beryls can be discriminated from their natural counterparts on the basis of microscopic features, chemical composition, and visible and infrared spectroscopic features.

Aquamarine has been one of the most popular gem materials for centuries, prized for its beauty and rarity. The color of aquamarine ranges from the familiar light blue to blue-green hues, to a rarer highly saturated dark blue (e.g., Rohtert et al., 2003; Laurs, 2005). However, a deep blue color is more typically associated with the color variety known as Maxixe beryl, discovered for the first time in Brazil in 1917 (Roebling and Tromnau, 1935; Schlossmacher and Klang, 1935), which typically fades on exposure to light. Similar beryl specimens appeared in the market around 1973, but such material was artificially irradiated and was thus called *Maxixe-type* beryl (Nassau et al., 1976).

Synthetic blue beryl has been produced by hydrothermal growth techniques since the late 1980s (Koivula and Kammerling, 1988, 1991; Nassau, 1990, 1997). Tairus, a Thai/Russian joint venture, produces synthetic blue beryl in Russia and markets it out of Bangkok (Smirnov et al., 1999). A new hydrothermal synthetic blue beryl was unveiled by Malossi Gemme Create, Milan, Italy, during the 2006 Las Vegas JCK Show (A. Malossi, pers. comm., 2007).

This article presents a full characterization of a suite of aquamarines and other blue beryls of different origins by classic gemological and contemporary analytical techniques, in order to determine those features that may be diagnostic for their identification.

MATERIALS AND METHODS

We examined a total of 25 natural, treated, and synthetic blue beryl specimens (see, e.g., figure 1): four faceted Brazilian aquamarines (0.18 to 1.54 ct); one faceted and one rough aquamarine from Nigeria (1.81 and 54.02 ct, respectively); three faceted (0.08–0.13 ct) and two rough (7.30 and 8.20 ct) aquamarines (marketed as "True Blue" beryl) from the Yukon Territory, Canada; one faceted Maxixe-type (irradiated) blue beryl (1.77 ct); three faceted Tairus hydrothermal synthetic blue beryls (2.03–3.50 ct);

See end of article for About the Authors and Acknowledgments.
GEMS & GEMOLOGY, Vol. 44, No. 3, pp. 214–226.

Figure 1. This study examined three varieties of blue beryl: aquamarine, Maxixe-type (irradiated) blue beryl, and hydrothermally grown synthetic blue beryl. Shown here are some of those samples: two aquamarines from Brazil (far left, 1.54 and 1.33 ct), one from Nigeria (bottom, 1.81 ct), one Maxixe-type beryl (center, 1.77 ct), two Tairus synthetics (top center, 2.03 ct and center right, 3.50 ct), and one Malossi synthetic (top right, 2.92 ct). Composite photo by Fred Kahn and Sun Joo Chung.

and eight faceted (2.70–5.12 ct) and two unfashioned (61.05 and 64.85 ct) Malossi hydrothermal synthetic blue beryls.

All the faceted samples were examined by standard gemological methods to determine their optical properties (refractive indices, birefringence, and pleochroism), specific gravity, UV fluorescence, and microscopic features.

Quantitative chemical analyses were performed on eight faceted samples (three aquamarines from Canada, one Maxixe-type beryl, and one Tairus and three Malossi synthetic blue beryls) using a JEOL JXA-8200 electron microprobe in wavelength-dispersive mode. The following elements were measured: Na, Mg, Al, Si, Cl, K, Ca, Ti, V, Cr, Mn, Fe, Cu, Rb, and Cs. The raw data were processed for matrix effects using a conventional ZAF routine from the JEOL series of programs.

Unpolarized spectroscopic measurements over the near-infrared (9000–4000 cm^{-1}) and mid-infrared (4000–400 cm^{-1}) ranges were carried out on all but the Nigerian samples using a Nicolet Nexus Fourier-transform infrared (FTIR) spectrometer equipped with a diffuse reflectance accessory (DRIFT) and operating with a resolution of 4 cm^{-1}.

Mid-IR spectra were also collected in transmission mode using KBr pellets (2 mg sample mixed with 200 mg KBr), confining the related sampling to portions of two unfashioned specimens (one Canadian aquamarine and one Malossi synthetic beryl).

Polarized ultraviolet-visible–near infrared (UV-Vis-NIR) spectroscopic measurements covering the 250–3300 nm range were performed with a Perkin Elmer Lambda 950 spectrometer using a calcite polarizer (1 nm scan interval) on all samples except the Canadian and Nigerian aquamarines.

RESULTS

Visual Appearance. Natural aquamarine typically ranges from greenish blue to (a purer) blue of low-to-moderate saturation with a light to medium-dark tone. The natural samples in this study varied in hue, tone, and saturation (again, see figure 1). The Canadian samples were darker and more saturated than either the Brazilian or Nigerian samples. The color of our Maxixe-type beryl was significantly more intense than that typically associated with aquamarine and had a slightly violet modifier. The Tairus and Malossi synthetic blue beryls were also significantly more saturated and much darker in tone than most aquamarine. The Malossi samples also had a distinct violet component.

Standard Gemological Properties. The standard gemological properties of the samples included in this study are summarized in table 1.

All the samples, with the exception of the Maxixe-type beryl, exhibited their stronger pleochroic color perpendicular to the c-axis (e-ray). As noted by

Figure 2. Multi-phase fluid inclusions are a common feature in natural aquamarine. Photomicrograph by C. P. Smith; magnified 65×.

Figure 3. The fine, parallel growth channels in this Maxixe-type beryl indicate the natural origin of the host. Photomicrograph by Giulio Chiodi; magnified 50×.

previous researchers, the stronger pleochroic color for Maxixe-type beryl is observed parallel to the c-axis (o-ray). The Maxixe-type beryl was also the only sample that was not inert to both long- and short-wave UV radiation.

Microscopy. The natural aquamarines and Maxixe-type beryl in this study had a wide variety of internal features indicative of their natural origin: single- and multi-phase fluid inclusions (figure 2), various patterns of healed fractures, crystalline inclusions, and growth tubes (figure 3), as

TABLE 1. Gemological properties of the natural and synthetic blue beryls investigated in this study.

Property	Natural				Synthetic	
	Aquamarine			Maxixe-type (irradiated)	Malossi	Tairus
	Brazil	Nigeria	Canada			
Color	Medium blue	Medium greenish blue	Dark grayish blue	Dark slightly violetish blue	Dark violetish blue	Dark grayish blue
Diaphaneity	Transparent	Transparent	Semitransparent to translucent	Transparent	Transparent	Transparent
Refractive indices	n_o = 1.586–1.590 n_e = 1.580–1.582	n_o = 1.586 n_e = 1.578	n_o = 1.601 n_e = 1.592–1.593	n_o = 1.588 n_e = 1.580	n_o = 1.590 n_e = 1.582	n_o = 1.586 n_e = 1.580
Birefringence	0.006–0.008	0.008	0.008–0.009	0.008	0.008	0.006
Specific gravity	2.76	2.67	2.80–2.87	2.75	2.75–2.77	2.71
Pleochroism[a]						
o-ray	Pale greenish blue	Pale greenish blue	Pale greenish blue	Dark blue	Pale blue	Pale greenish blue
e-ray	Medium blue	Medium blue	Dark blue	Colorless	Dark violetish blue	Dark blue
UV fluorescence						
Long-wave	Inert	Inert	Inert	Mod. deep green[b]	Inert	Inert
Short-wave	Inert	Inert	Inert	Mod. yellowish green	Inert	Inert
Internal features	Crystals, two-phase and liquid inclusions, "fingerprints," growth tubes, growth lines, fractures	Crystals, multi-phase inclusions, growth tubes, fractures	Crystals, multi-phase inclusions, "fingerprints," growth tubes, growth lines, fractures, evidence of clarity enhancement	Growth tubes, two-phase and liquid inclusions	Irregular growth structures, "fingerprints," fractures	Irregular growth structures, pinpoints, "fingerprints," fractures, seed plates

[a] *All samples were uniaxial negative, and they showed strong dichroism.*
[b] *Mod. = moderate.*

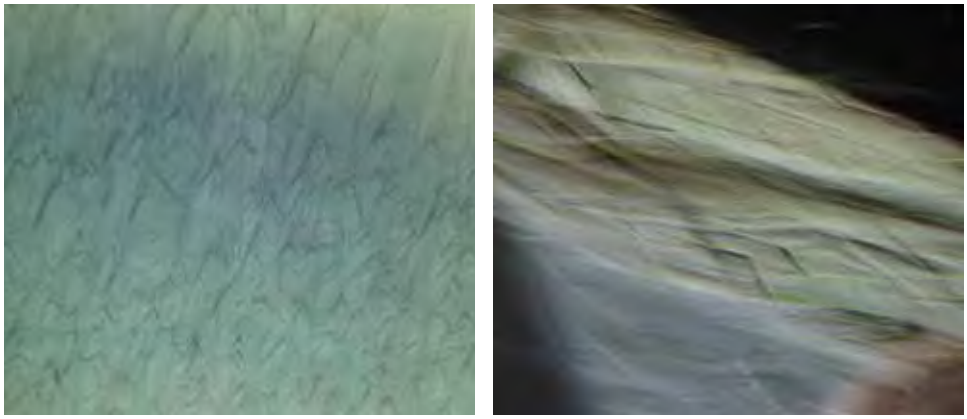

Figure 4. This Malossi hydrothermal synthetic blue beryl exhibits irregular growth features with a step-like shape that provide evidence of the sample's synthetic origin. Photomicrographs by Giulio Chiodi (left, in immersion, magnified 40×) and I. Adamo (right, magnified 35×).

well as straight and angular internal growth structures. Unhealed fractures were also observed in many of the aquamarine samples. However, the Canadian samples also revealed a blue and yellow "flash effect," as is commonly observed in gems that have been clarity enhanced (refer to the "Discussion" of the mid-infrared spectroscopy results below).

The Tairus and Malossi synthetic beryls also revealed several diagnostic internal features. Most notably, these consisted of distinctive irregular internal growth structures (figures 4 and 5). Present in samples from both sources, but more common in those from Tairus, were healed-fracture "fingerprints" (figure 6), as well as open fractures. In addition, all the Tairus synthetic samples contained groups of black pinpoint inclusions (figure 7), with remnants of the seed plates (in two out of the three Tairus samples; e.g., figure 8) that are indicative of the artificial growth process. We did not observe any of these black inclusions or seed-plate remnants in our Malossi synthetic samples.

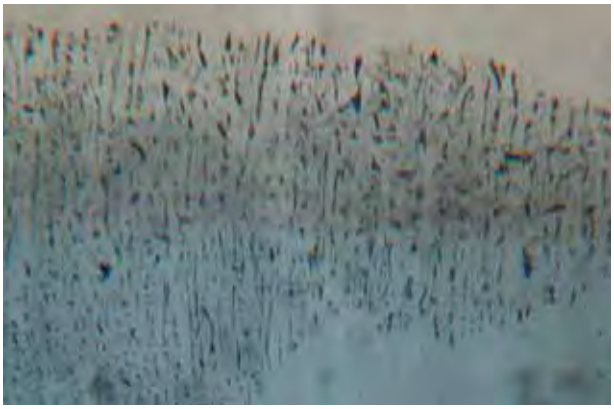

Figure 6. "Fingerprints" (healed fractures) such as this one in a Tairus sample were seen in both types of synthetics. Photomicrograph by Giulio Chiodi, in immersion; magnified 40×.

Figure 5. The Tairus hydrothermal synthetic samples also showed widespread irregular growth structures that demonstrate they are synthetic. Photomicrographs by I. Adamo (left, magnified 20×) and C. P. Smith (right, magnified 32×).

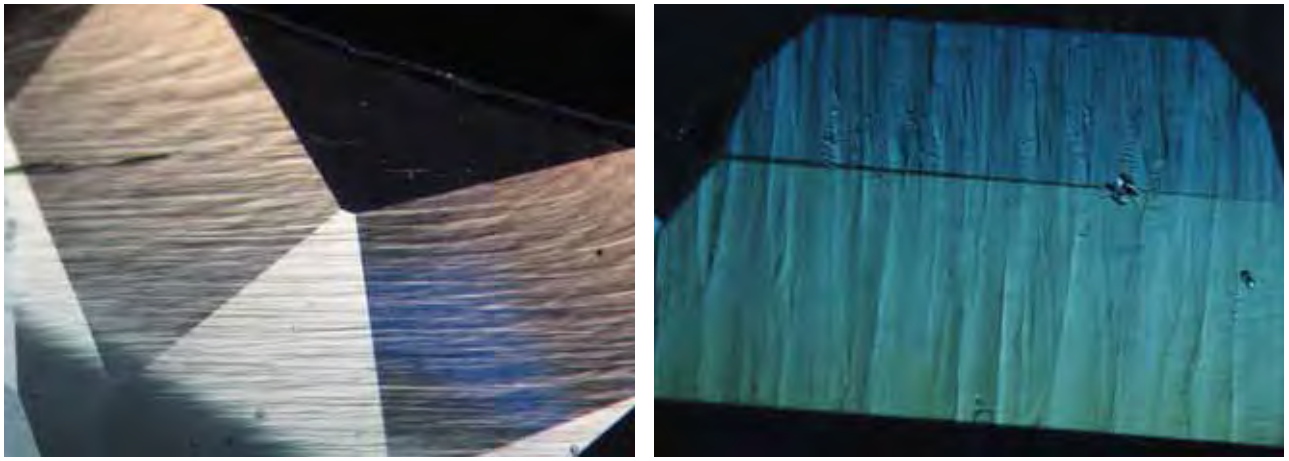

Figure 7. The Tairus synthetic beryls also contained numerous small, irregular black pinpoint inclusions. Photomicrographs by C. P. Smith (left, magnified 32×) and Giulio Chiodi (right, in immersion; magnified 50×).

Chemical Composition. The chemical compositions of three Canadian aquamarines, one Maxixe-type beryl, and one Tairus and three Malossi hydrothermally grown synthetic blue beryls are presented in table 2 and plotted in figure 9. The low totals can be ascribed to the presence of water in both natural and hydrothermal synthetic beryls (e.g., Wood and Nassau, 1968; Deer et al., 1986). Totals can also be affected by variable amounts of lithium, which—like H_2O—is undetectable by electron microprobe.

TABLE 2. Average electron-microprobe analyses for the natural and synthetic blue beryls investigated in this study.[a]

Chemical composition	Natural				Synthetic			
	Canada			Maxixe-type (irradiated)	Malossi			Tairus
Sample	1	2	3		A	B	C	
No. analyses	5	4	5	8	10	4	4	8
Oxides (wt.%)								
SiO_2	62.60	63.11	62.68	65.44	64.22	64.06	63.80	64.56
Al_2O_3	11.75	11.63	11.58	17.70	16.75	16.56	16.52	16.48
FeO[b]	5.04	5.03	4.96	bdl	1.96	1.95	2.50	2.75
MnO	bdl	bdl	bdl	bdl	0.15	0.13	0.10	bdl
K_2O	bdl	bdl	bdl	0.06	bdl	bdl	bdl	bdl
Na_2O	2.24	2.40	2.24	0.47	0.07	0.12	0.13	bdl
MgO	1.76	1.80	1.69	bdl	0.12	0.21	0.22	bdl
Cs_2O	bdl	bdl	bdl	0.70	bdl	bdl	bdl	bdl
CuO	bdl	bdl	bdl	bdl	2.95	1.69	1.57	bdl
BeO[c]	12.91	12.99	12.88	13.56	12.40	12.76	12.79	13.37
Total	96.30	96.96	96.03	97.93	98.62	97.48	97.63	97.16
Ions calculated on 18 oxygens								
Si	6.058	6.068	6.079	6.028	6.018	6.021	6.002	6.032
Al	1.340	1.318	1.323	1.922	1.850	1.835	1.831	1.814
Fe	0.408	0.404	0.402	bdl	0.154	0.153	0.197	0.215
Mn	bdl	bdl	bdl	bdl	0.012	0.011	0.008	bdl
K	bdl	bdl	bdl	0.007	bdl	bdl	bdl	bdl
Na	0.420	0.448	0.422	0.084	0.013	0.022	0.023	bdl
Mg	0.254	0.258	0.244	bdl	0.017	0.030	0.030	bdl
Cs	bdl	bdl	bdl	0.028	bdl	bdl	bdl	bdl
Cu	bdl	bdl	bdl	bdl	0.209	0.120	0.112	bdl

[a] *Instrument operating conditions: accelerating voltage = 15 kV, beam current = 15 nA, count time = 20 seconds on peaks and 5 seconds on background. Standards: natural wollastonite (for Si, Ca), anorthite (for Al), fayalite (for Fe), olivine (for Mg), rhodonite (for Mn), omphacite (for Na), ilmenite (for Ti), K-feldspar (for K), pollucite (for Cs), and sodalite (for Cl); pure V, Rb, Cr, and Cu for those elements. Abbreviation: bdl = below detection limit (in wt.%): 0.05 FeO, 0.08 CuO, 0.04 MnO, 0.04 K_2O, 0.05 Na_2O, 0.05 MgO, 0.04 Cs_2O. Chlorine, calcium, titanium, vanadium, chromium, and rubidium were below the detection limit (0.05 wt.%) in all analyses.*

[b] *Total iron is calculated as FeO.*

[c] *Calculated assuming (Be+Cu)/Si=0.5.*

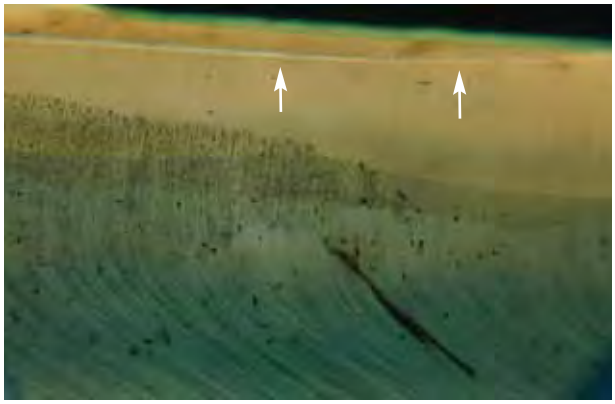

Figure 8. Two of the Tairus synthetic beryls had remnants of the seed plate (see arrows). When present, this provides proof of synthetic origin. Note the widespread irregular growth structures, pinpoint inclusions, and "fingerprints." Photomicrograph by Giulio Chiodi, in immersion; magnified 15×.

Consistent with the chemical formula of beryl ($Be_3Al_2Si_6O_{18}$), all the samples contained Si, Al, and Be as major elements. Minor but significant contents of Fe, Na, and Mg were recorded in the Canadian samples, whereas Na, Cs, and traces of K were recorded in the Maxixe-type sample. The Malossi synthetic blue beryls contained high amounts of Cu and Fe, as well as traces of Mg, Mn, and Na; however, Fe was the only minor element detected in the Tairus synthetic sample.

Figure 9. The average contents of Na_2O, MgO, MnO, FeO, CuO, and Cs_2O are shown for the various types of blue beryl investigated in the present study.

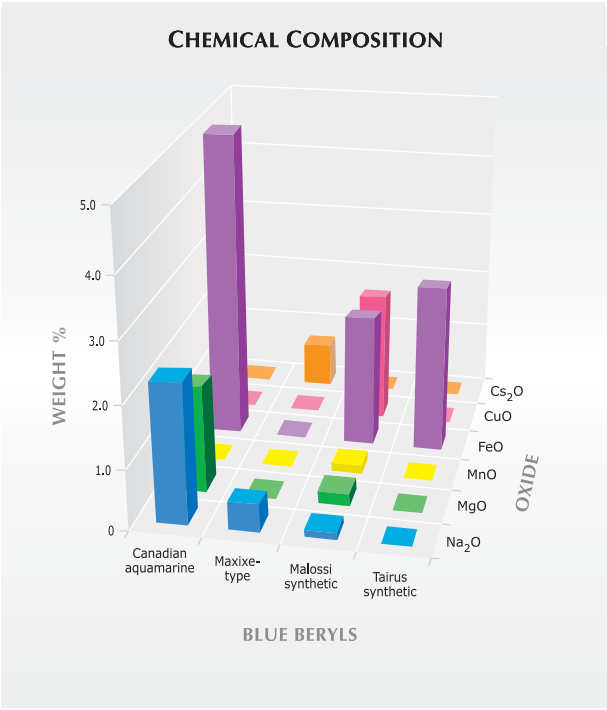

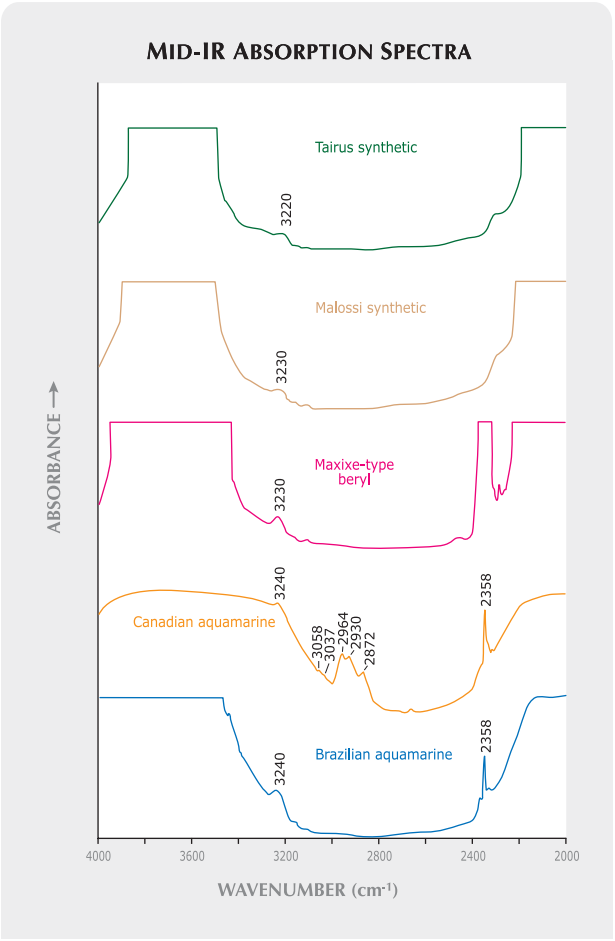

Figure 10. Representative mid-infrared spectra, taken in diffuse reflectance, showed features between 4000 and 3400 cm^{-1} (and to 3200 cm^{-1} in the Canadian material) related to their water contents. The CO_2-related signal at 2358 cm^{-1} in the aquamarines and Maxixe-type beryl have thus far never been found with this strength in synthetics. The peaks between 3000 and 2800 cm^{-1} in the Canadian aquamarine are related to the presence of a filler (for clarity enhancement).

Spectroscopy. Table 3 summarizes the most significant spectroscopic features of the natural, treated, and synthetic blue beryl samples we studied, which are described below.

Mid-Infrared. The mid-infrared spectra revealed a multitude of absorption bands (figure 10). For all the samples, two dominant areas of absorption saturated the detector in the 4000–3400 cm^{-1} (extending to 3200 cm^{-1} in the case of the Canadian aquamarines)

and 2250–400 cm^{-1} regions. A broad band centered between 3240 and 3220 cm^{-1} was also present in all samples. Another area of significant absorption was found at approximately 2400–2250 cm^{-1} (again, see figure 10). In addition, we observed a series of bands in the Canadian samples in the region between ~3000 and 2800 cm^{-1} (the most dominant were at 2964, 2930, and 2872 cm^{-1}).

The presence of water in the beryl structure may be determined by careful analysis of mid-IR spectra collected in transmission mode on powdered material in KBr pellets. This eliminates the total absorption that otherwise occurs in significant regions of that spectrum, although it does require some damage to the original specimen. The IR pattern of a Malossi synthetic beryl that we acquired by this

TABLE 3. Main spectroscopic features of the natural and synthetic blue beryls investigated in this study.

Spectral region	Natural			Synthetic	
	Aquamarine				
	Brazil	Canada		Malossi	Tairus
Mid-IR (4000–2000 cm^{-1})	Total absorption between 4000 and 3400 cm^{-1}, and a band at about 3240 cm^{-1}, related to water content	Total absorption between 4000 and 3200 cm^{-1}, with a band at 3240 cm^{-1}, related to water content (in transmission mode, resolved as 3591 and 3655 cm^{-1} due to type II H_2O) Peaks at 3058, 3037, 2964, 2930, and 2872 cm^{-1}, due to an artificial resin	Total absorption between 4000 and 3400 cm^{-1}, and a band at about 3230 cm^{-1}, related to water content	Total absorption between 4000 and 3400 cm^{-1}, and a band at 3230 cm^{-1}, related to water content (in transmission mode, resolved as 3595 and 3663 cm^{-1} due to type II H_2O, and 3698 cm^{-1} due to type I H_2O)	Total absorption between 4000 and 3400 cm^{-1}, and a band at about 3220 cm^{-1}, related to water content
	Sharp peak at about 2358 cm^{-1}, attributed to structural CO_2	Sharp peak at 2358 cm^{-1}, attributed to structural CO_2	Strong band at about 2358 cm^{-1}, attributed to structural CO_2		
Near-IR (9000–4000 cm^{-1})	Combination bands and overtones of types I and II water molecules	Combination bands and overtones of type II water molecules	Combination bands and overtones of types I and II water molecules	Combination bands and overtones of types I and II water molecules Total absorption between 9000 and 6500 cm^{-1}, likely due to the high Cu^{2+} content	Combination bands and overtones of types I and II water molecules
UV-Vis-NIR (250–850 nm)	Strong absorption band at 825 nm (o- and e-ray), due to Fe^{2+}; broad absorption band at about 640 nm (e-ray), assigned to a $Fe^{2+} \leftrightarrow Fe^{3+}$ charge process or to Fe^{2+} in the channels Peaks at 370 nm (o-ray) and 427 nm (e- and o-ray), associated with Fe^{3+}	Not tested	Set of bands over the 500–700 nm range (573, 588, 605, 625, 645, and 690 nm), related to a radiation-induced color center; also present were bands at 311 nm (e-ray) and 320 nm (o-ray)	Strong absorptions below 360 nm and beyond 580 nm (o-ray) and 610 nm (e-ray), due to a combination of Cu and Fe absorption features Peaks at 370 nm (o-ray) and 428 nm (e- and o-ray), associated with Fe^{3+} Bands at 475 and 540 nm (o-ray) and 568 nm (e-ray), probably due to Mn^{3+} (Ni^{3+} could contribute to the 475 nm absorption feature)	Strong absorption band at 825 nm (o- and e-ray), due to Fe^{2+}; broad absorption band at about 580 nm (e-ray), assigned to a $Fe^{2+} \leftrightarrow Fe^{3+}$ charge process or to Fe^{2+} in the channels Peaks at 370 nm (o-ray) and 428 nm (e- and o-ray) associated with Fe^{3+}

method revealed two dominant absorption bands at 3698 and 3595 cm^{-1}, with a weaker third band positioned at ~3663 cm^{-1}, while the Canadian aquamarine was characterized by two dominant bands at ~3655 and 3591 cm^{-1} (figure 11).

Near-Infrared. As illustrated in figure 12, the significant near-infrared absorption features—strong individual bands and a number of weaker bands—occurred in the regions of ~7300–6800 cm^{-1} and 5650–5000 cm^{-1}. Only the Malossi synthetic beryl exhibited total absorption beyond 6500 cm^{-1}.

UV-Vis-NIR. Polarized UV-Vis-NIR spectra in the 280–850 nm range for four samples are shown in figure 13. In general, all except the Maxixe-type blue beryl shared similar spectral features, characterized by a dominant absorption band at ~825 nm. In the spectra oriented perpendicular to the c-axis direction (e-ray), this band was modified by a side band at ~640 nm in the Brazilian aquamarine and ~580 nm in the Tairus synthetic samples. An additional band positioned at 427/428 nm was evident in spectra recorded for both the e-ray and o-ray, whereas a band at 370 nm was only present in spectra oriented along the o-ray, and a weak band at ~358 nm was recorded only along the e-ray.

In contrast, the absorptions recorded for the Maxixe-type sample consisted of a series of narrow

Figure 11. Alkali-rich Canadian aquamarine and low-alkali Malossi synthetic beryl show different mid-infrared absorption spectra taken in transmission mode on KBr pellets, because of different configurations of the water molecules hosted by the structural channels. Spectra offset vertically for clarity.

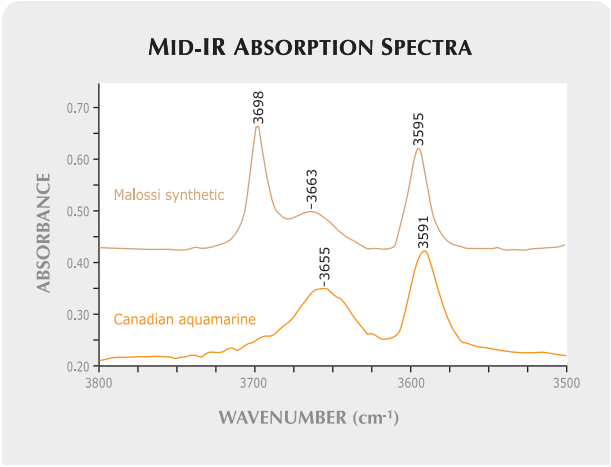

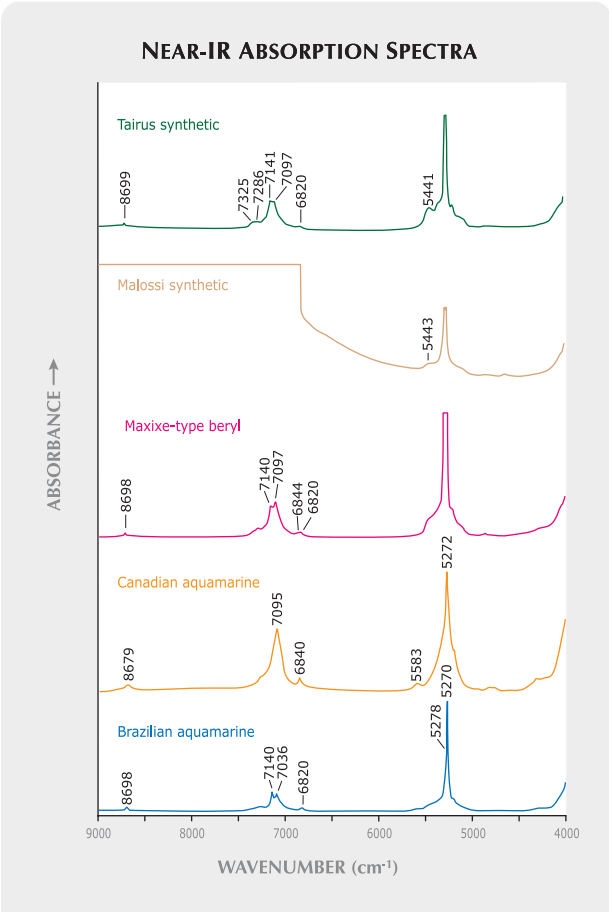

Figure 12. Near-infrared spectra in diffuse reflectance are shown for two aquamarines, a Maxixe-type beryl, and Malossi and Tairus synthetic blue beryls. All except the Canadian aquamarine (which is characterized by the absence of type I water molecules) exhibit somewhat similar combination bands and overtones of type I and II water molecules. Note that the Malossi sample exhibits total absorption between 9000 and 6500 cm^{-1}, most likely due to its high Cu^{2+} content.

bands between 500 and 700 nm, with the primary band positioned at ~690 nm, and a series of associated weaker bands at ~573, 588, 605, 625, and 645 nm (figure 13B). The stronger of this combined absorption was oriented along the c-axis direction (o-ray). Two additional, independent bands that also exhibited strongly pleochroic orientations were positioned at ~311 nm (e-ray) and 320 nm (o-ray).

The Malossi synthetic blue beryl was characterized by two strong absorptions, below about 360 nm and beyond ~580 nm (o-ray) and 610 nm (e-ray). A series of broad bands were also present, positioned at approximately 568 nm in the e-ray and at 475 and 540 nm in the o-ray orientations. The band at ~428 nm was evident in the spectra taken for both the

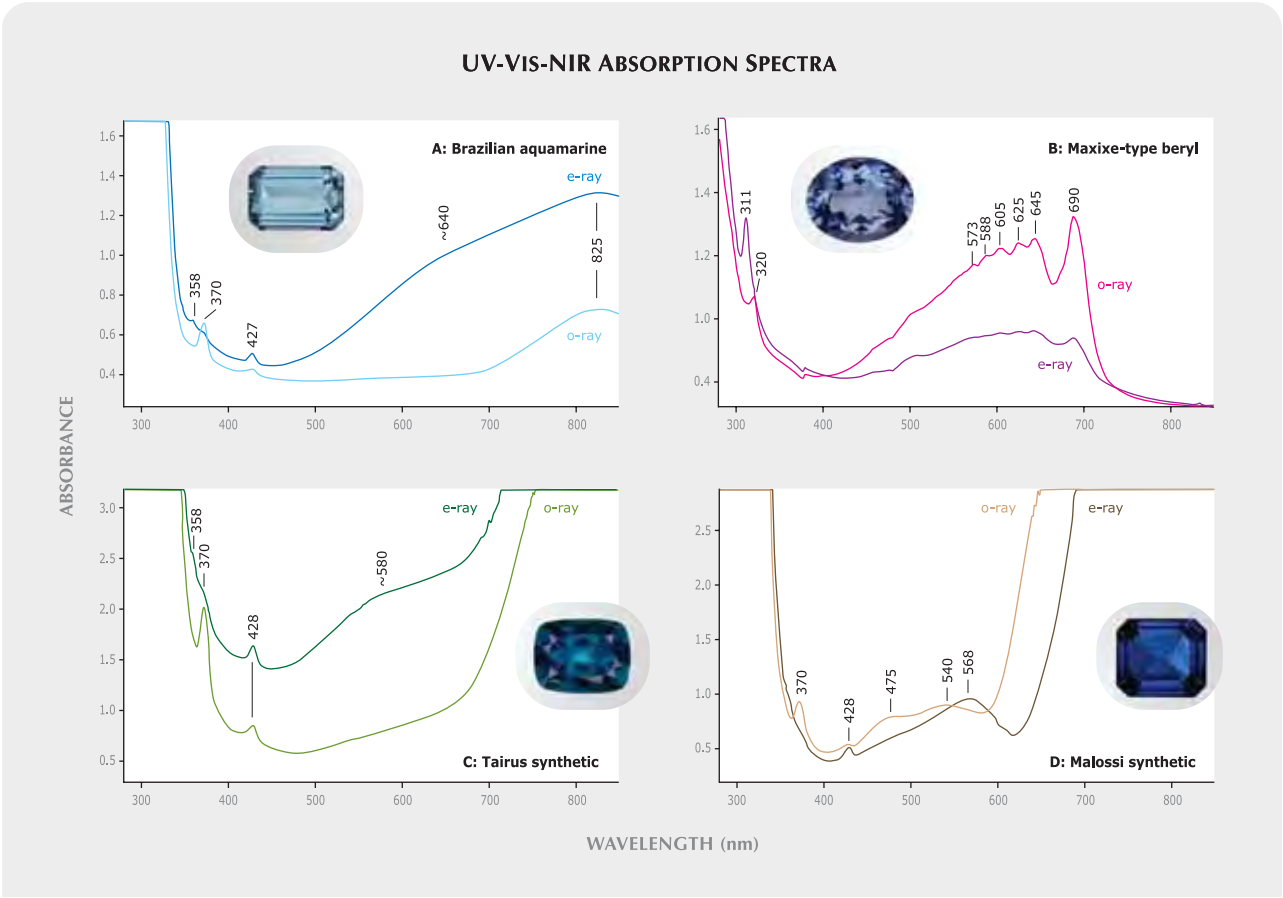

Figure 13. Polarized UV-Vis-NIR spectra are shown for four samples. The aquamarine and Tairus synthetic blue beryl exhibit absorption features associated with iron, whereas the pattern of the Malossi synthetic is mainly a combination of copper and iron absorptions. Manganese may be responsible for the broad bands at 475, 540, and 568 nm in the Malossi synthetic. The spectra of the Maxixe-type beryl are characterized by signals due to radiation-induced color centers.

e- and o-ray orientations, whereas the band at 370 nm was only present along the o-ray.

DISCUSSION

Standard Gemological Properties. The RI and SG values of the Brazilian and Nigerian samples were within the ranges reported for aquamarine (RI: 1.572–1.590; SG: 2.66–2.80; O'Donoghue, 2006). However, the Canadian samples had higher values, as previously reported by Rohtert et al. (2003). These differences are presumably related to the chemical composition (higher Fe, Mg, and Na) and denser inclusions of the Canadian beryls. The Maxixe-type (irradiated) sample had RI and SG values that are in agreement with the literature (e.g., Brown, 1993; Reinitz and Moses, 1997; Wentzell and Reinitz, 1997) and are virtually identical to those of natural Maxixe beryl (Brown, 1993). The RI and SG values of the Tairus synthetic specimens were similar to those reported by Schmetzer (1990) and Smirnov et al. (1999), whereas the Malossi synthetics had slightly higher values, owing to their compositional differences (notably, the presence of Cu). However, the overlap in the ranges of RI and SG values means that these properties cannot be used reliably to discriminate these materials from one another.

The anomalous dichroism of Maxixe-type, as well as Maxixe, beryls is a diagnostic marker (Brown, 1993; Nassau, 1996; Reinitz and Moses, 1997; Wentzell and Reinitz, 1998). As reported by Brown (1993), the green UV fluorescence shown by the Maxixe-type sample is indicative of irradiation treatment.

Microscopy. Magnification can provide important information for the separation of natural and synthetic blue beryl. Aquamarine and other natural blue beryls may be identified by a wide range of multi-

phase fluid inclusions; some mineral inclusions such as apatite, epidote, goethite, hematite, ilmenite, limonite, mica, quartz, spessartine, and tourmaline; as well as internal growth structures (see, e.g., Sinkankas, 1981; Lindt et al., 1986; Gübelin and Koivula, 2005).

All the synthetic blue beryls studied exhibited diagnostic internal features that proved their artificial nature and were distinctive of hydrothermal growth. These included strongly undulating, step- and chevron-like growth structures, which were similar to those that have been reported for hydrothermal synthetic emeralds (see, e.g., Schmetzer, 1988; Schmetzer et al., 1997; Sechos, 1997; Adamo et al., 2005; Gübelin and Koivula, 2005; Schmetzer et al., 2006). Residues of seed plates, when present, are also diagnostic of synthetic origin.

Chemical Composition. Our samples could be readily separated on the basis of their chemical composition. The Canadian aquamarines had the highest FeO contents ever reported in the literature for a blue gem beryl, which were consistent with values reported for Canadian blue beryl by other researchers (Rohtert et al., 2003; Turner et al., 2007). Aquamarine specimens from other localities (e.g., Brazil, Mozambique, Nigeria, Arizona, and Italy) are also characterized by the presence of iron (e.g., Schaller et al., 1962; Graziani and Di Giulio, 1979; Deer et al., 1986; Lind et al., 1986; Aurisicchio et al., 1988; Viana et al., 2002; Neiva and Neiva, 2005). Li, Na, Mg, K, Ca, and Cs are the most common minor elements usually present in aquamarine. Although the distinction of natural aquamarine from alkali-poor synthetic beryl was straightforward for most of the samples in our study, some natural stones—such as those from Nigeria (Lind et al., 1986)—have low alkali contents, so chemical composition alone should not be considered proof of origin. The absence of Fe, as well as of other chromophores, in irradiated Maxixe-type beryl and in untreated Maxixe beryl (Schlossmacher and Klang, 1935) will easily separate them from aquamarine.

The presence of copper (CuO average 2.07 wt.%) is diagnostic of Malossi synthetic beryl. This well-known chromophore produces an intense blue coloration in hydrothermal synthetic beryl (Koivula and Kammerling, 1988; Schmetzer et al., 2006). It is also present as a trace element in some hydrothermally grown synthetic emeralds (Schmetzer, 1988; Mashkovtsev and Smirnov, 2004; Adamo et al., 2005; Schmetzer et al., 2006). However, it has never been reported in any natural aquamarine, Maxixe-type beryl, or Maxixe beryl. For information on the position of Cu in the crystal structure of synthetic beryl, see Adamo et al. (2008).

Tairus synthetic blue beryl may be separated from alkali-rich natural aquamarines by its lower Fe content and absence of any significant Cu, Na, Mg, Mn, K, and Cs (see table 2 and Schmetzer et al., 2006). Again, though, for Na/Mg-poor natural aquamarines such as those from Nigeria (see, e.g., Lind et al., 1986), chemical composition alone does not provide a clear distinction.

Spectroscopy. *Mid-Infrared.* All the samples revealed total absorption in the region of ~2250–400 cm^{-1}, which is intrinsic to beryl, as well as ~4000–3400 cm^{-1}, which is related to the incorporation of water (see, e.g., Stockton, 1987; Adamo et al., 2005).

The strong 2358 cm^{-1} band found in natural aquamarines and Maxixe-type beryl is attributed to structural CO_2, which is commonly present in many natural and synthetic materials (Wood and Nassau, 1967, 1968; Stockton, 1987; Aines and Rossman, 1984; Charoy et al., 1996; Gatta et al., 2006; Andersson, 2006). In beryl, however, only the natural material can show a strong 2358 cm^{-1} peak; this feature is generally weak or absent in the synthetic beryl reported to date (Stockton, 1987; Koivula et al., 1996; Mashkovtsev and Smirnov, 2004; Choudhary and Golecha, 2007). We did not observe any of the characteristic bands attributed to chlorine and ammonium that are often found in hydrothermally grown synthetic emeralds (Schmetzer et al., 1997; Mashkovtsev and Solntsev, 2002; Mashkovtsev and Smirnov, 2004; Adamo et al., 2005).

The absorption features in the ~3000–2800 cm^{-1} range in the aquamarines from Canada indicate the presence of an organic, polymer-type filler (e.g., Johnson et al., 1999; Kiefert et al., 1999), in agreement with our microscopic observations.

The two dominant absorption bands at 3698 and 3595 cm^{-1} in the transmittance powder FTIR spectrum of the Malossi synthetic blue beryl indicate the occurrence of water molecules in two different configurations [type I and type II (Wood and Nassau, 1967, 1968; Schmetzer and Kiefert, 1990; Charoy et al., 1996; Mashkovtsev and Smirnov, 2004)]. The third, weaker and structured absorption band at approximately 3663 cm^{-1} is usually also associated with type II H_2O (Wood and Nassau, 1967, 1968; Farmer, 1974; Aines and Rossman, 1984; Charoy et al., 1996; Viana et al., 2002; Mashkovtsev and Smirnov, 2004),

BOX A: IDENTIFICATION

SEPARATION BETWEEN NATURAL AND SYNTHETIC BLUE BERYL

We found that the Malossi and Tairus synthetic blue beryls could be separated from their natural counterparts on the basis of the following characteristics:

Microscopic Features. The strongly irregular and distinctive growth pattern we observed in all the synthetic samples provides clear evidence of hydrothermal synthesis. When present, the tiny black inclusions and seed-plate residues seen in the Tairus synthetic beryls are also diagnostic of hydrothermal growth in a laboratory. Natural blue beryl may be identified by a wide range of multi-phase fluid inclusions, various mineral inclusions, as well as internal growth structures.

Chemical Composition. All aquamarines are characterized by the presence of iron, which acts as the primary chromophore. Li, Na, Mg, K, Ca, and Cs also can be present in variable amounts. In the case of high and moderate alkali-bearing aquamarines, separation from the alkali-poor Tairus synthetics is possible, but this fails in the case of some Na/Mg-poor aquamarines, such as Nigerian material. The presence of copper (average 2.07 wt.% CuO) in Malossi synthetic blue beryl allows a rapid distinction from natural beryl.

Spectroscopic Measurements. Infrared spectroscopy can be diagnostic if one is able to establish the type of water molecules: If type I H_2O is absent, the beryl specimen may be classified as natural; otherwise, the IR pattern is not distinctive. The detection of Cu by Vis-NIR is typical of the Malossi material.

SEPARATION OF AQUAMARINE FROM MAXIXE AND MAXIXE-TYPE BERYL

We believe the following features provide means to distinguish between aquamarine and Maxixe/Maxixe-type beryl:

Optical Properties: Dichroism. Both Maxixe and Maxixe-type beryls show pleochroic behavior with the dominant blue color parallel to the c-axis (i.e., down the o-ray), which is the opposite of natural aquamarine and the hydrothermally grown synthetics.

Other Gemological Properties. Most Maxixe/Maxixe-type beryls fade on exposure to light and/or heat. A green UV fluorescence reaction, when present, provides an additional indicator that the material is Maxixe-type beryl.

Chemical Composition. The Fe chromophore is absent in Maxixe and Maxixe-type beryls, but it is abundant in all aquamarine from various localities. This confirms that the cause of color in Maxixe and Maxixe-type beryl is a radiation-induced color center.

Spectroscopic Measurements. In keeping with their chemistry, no evidence of iron-related features occurs in the UV-Vis-NIR spectra of Maxixe and Maxixe-type beryls. A visible spectrum with a series of bands positioned between 500 and 700 nm will readily identify them. Color centers associated with the different impurities in Maxixe and Maxixe-type beryls result in slightly different UV-Vis-NIR spectra for these two materials.

although it may also be related to hydroxyl ions (Schmetzer and Kiefert, 1990; Aurisicchio et al., 1994) and/or to a third type of water molecule (Andersson, 2006). Such a combination of type I and II water in beryl is typical of low-alkali-content synthetic and natural beryl (Schmetzer and Kiefert, 1990). In contrast, the IR spectrum of the Canadian aquamarine is distinctive in its absence of the 3698 cm^{-1} absorption feature (type I H_2O), and it is generally diagnostic of an alkali-rich beryl (Schmetzer and Kiefert, 1990).

Near-Infrared. The near-infrared spectra (9000–4000 cm^{-1}) of all our samples revealed several absorption features that can be attributed to combination bands and overtones of water molecules incorporated into the beryl structure. These spectral features are related to the presence of both type I and II water molecules (Wood and Nassau, 1967; Mashkovtsev and Smirnov, 2004), except for the Canadian aquamarine, which has no features related to type I H_2O, as highlighted by mid-IR spectroscopy in transmission mode. The occurrence of total absorption beyond ~6500 cm^{-1}, attributable to the presence of Cu^{2+} (Mashkovtsev and Smirnov, 2004; Adamo et al., 2005; Schmetzer et al., 2006), is typical of the Malossi synthetic material.

UV-Vis-NIR. The Brazilian aquamarines and the Tairus synthetic blue beryls revealed a typical aquamarine spectrum, with a dominant absorption band positioned at ~825 nm (with polarization both parallel and perpendicular to the o-ray) due to Fe^{2+} on two different lattice positions (Wood and Nassau, 1968; Goldman et al., 1978; Schmetzer, 1990; Burns, 1993; Taran and Rossman, 2001; Viana et al., 2002). A side band positioned at ~640 nm in the natural aquamarine and ~580 nm in the Tairus synthetic material (with polarization perpendicular to the o-ray) is also present. This absorption feature has been assigned by some to an $Fe^{2+} \leftrightarrow Fe^{3+}$ charge-transfer process (e.g., Goldman et al., 1978; Schmetzer, 1990; Burns, 1993; Taran and Rossman, 2001), whereas others (e.g., Wood and Nassau, 1968; Viana et al., 2002) have suggested that it arises from Fe^{2+} in the structural channels. The peaks at 370 and 428 nm are related to Fe^{3+} (Goldman et al., 1978; Schmetzer, 1990; Burns, 1993; Viana et al., 2002; Adamo et al., 2005).

Distinctive of the Malossi synthetic blue beryl was a very strong absorption (even more intense than in other samples) starting at ~610 nm (e-ray) and 580 nm (o-ray) and extending to 1500 nm in the near-IR region, which may result from a combination of copper and iron absorptions (see, e.g., Mashkovtsev and Smirnov, 2004; Adamo et al., 2005; Schmetzer et al., 2006). The 370 and 428 nm Fe^{3+} absorption features were also present. The broad bands centered at 475, 540, and 568 nm are probably related to Mn^{3+}, a chromophore known to produce pink, red, and violet hues in beryl (Burns, 1993; Shigley et al., 2001). Ni^{3+} might also contribute to the broad absorption feature at about 475 nm (o-ray; Schmetzer, 1990), in agreement with its presence among the trace elements measured by LA-ICP-MS in one Malossi sample (see data in Adamo et al., 2008).

The presence in the Maxixe-type beryl of narrow absorption features in the 500–700 nm range, with the dominant band at ~690 nm, as well as the vibronic structure that extends toward 400 nm, has been attributed to color centers associated with carbonate impurities that have been activated by irradiation (Nassau et al., 1976; Edgar and Vance, 1977; Andersson, 1979; Nassau and Prescott, 1981; Nassau, 1996; Mathew et al., 1998; Andersson, 2006). In the original Maxixe beryl, these color centers are associated instead with nitrate impurities, causing a slightly different visible spectrum (Andersson, 1979, Nassau, 1996). Thus, the UV-Vis-NIR spectra for both Maxixe and Maxixe-type beryls provide reliable means to distinguish these gem materials from aquamarine.

CONCLUSIONS

Aquamarine, Maxixe-type beryl, and hydrothermally grown synthetic blue beryl may be readily distinguished using a combination of gemological, chemical, and spectroscopic features (see box A). Careful observation of pleochroism, fluorescence, and internal features (with magnification) can provide useful indicators for gemologists with basic equipment. More-sophisticated techniques such as UV-Vis-NIR and mid-infrared spectroscopy, as well as chemical analysis, can provide clear proof of the identification.

ABOUT THE AUTHORS

Dr. Adamo (ilaria.adamo@unimi.it) is a postdoctoral fellow, Dr. Pavese is professor of mineralogy, and Dr. Gatta is a researcher in the Earth Sciences Department of the University of Milan, Italy. Dr. Prosperi is director of the Italian Gemological Institute (IGI) laboratory, Milan. Dr. Diella is a senior researcher of the Environmental Processes Dynamics Institute (IDPA), National Research Council (CNR), Section of Milan, to which Dr. Pavese and Dr. Gatta also belong. Dr. Ajò is director of the Inorganic and Surface Chemistry Institute (ICIS), National Research Council (CNR), Padua, Italy, and is responsible for the CNR coordination group for Gemological Materials Research. Mr. Smith is vice president and chief gemologist at American Gemological Laboratories (AGL) in New York City.

ACKNOWLEDGMENTS

The authors would like to thank Greg Davison (True North Gems, Vancouver, Canada) for providing the blue beryl specimens from the True Blue property in the Yukon Territory, Canada; the Italian Gemological Institute for providing aquamarine samples from Brazil, the Maxixe-type blue beryl specimen, and the Tairus hydrothermal synthetic blue beryls; Alberto Malossi (Malossi Gemme Create, Milan) for providing the Malossi synthetic blue beryl samples; and C. R. "Cap" Beesley (AGL) for providing the aquamarine samples from Brazil and Nigeria. Dr. Giulio Chiodi (Vicenza, Italy), Fred Kahn, and Sun Joo Chung (AGL) are gratefully acknowledged for some photos. The authors are indebted for technical assistance to: Dr. Vanda Rolandi (University of Milan—Bicocca, Italy) and Stefano Villa (IGI, Milan) for collaboration in the collection of photomicrographs; Dr. Marcello Picollo, Bruno Radicati (CNR, Florence), and Franco De Zuane (CNR, Padua) for preliminary nonpolarized UV-Vis-NIR spectroscopy; and Dr. Nicola Rotiroti (University of Milan) for collaboration in X-ray single-crystal data collection and structure refinement. Dr. Karl Schmetzer (Petershausen, Germany) is thanked for his useful suggestions. The manuscript benefited considerably from the critical reviews of Dr. Lee A. Groat and Dr. Michael S. Krzemnicki. This study was supported through the Ingenio Global Grant project by the European Social Fund, the Italian Ministry of Labour and Welfare, and the Lombardy Region.

REFERENCES

Adamo I., Gatta G.D., Rotiroti N., Diella V., Pavese A. (2008) Gemmological investigation of a synthetic blue beryl: A multi-methodological study. *Mineralogical Magazine* (in press).

Adamo I., Pavese A., Prosperi L., Diella V., Merlini M., Gemmi M., Ajò D. (2005) Characterization of the new Malossi hydrothermal synthetic emerald. *Gems & Gemology*, Vol. 41, No. 4, pp. 328–338.

Aines R.D., Rossman G.R. (1984) The high temperature behavior of water and carbon dioxide in cordierite and beryl. *American Mineralogist*, Vol. 69, No. 3/4, pp. 319–327.

Andersson L.O. (1979) The difference between Maxixe beryl and Maxixe-type beryl: An electron paramagnetic resonance investigation. *Journal of Gemmology*, Vol. 16, No. 5, pp. 313–317.

Andersson L.O. (2006) The position of H^+, Li^+ and Na^+ impurities in beryl. *Physics and Chemistry of Minerals*, Vol. 33, No. 6, pp. 403–416.

Aurisicchio C., Fioravanti G., Grubessi O., Zanazzi P.F. (1988) Reappraisal of the crystal chemistry of beryl. *American Mineralogist*, Vol. 73, No. 7/8, pp. 826–837.

Aurisicchio C., Grubessi O., Zecchini P. (1994) Infrared spectroscopy and crystal chemistry of the beryl group. *Canadian Mineralogist*, Vol. 32, No. 1, pp. 55–68.

Brown G. (1993) Maxixe-type beryls. Ghost from the past. *Australian Gemmologist*, Vol. 18, No. 7, pp. 215–221.

Burns R.G. (1993) *Mineralogical Applications of Crystal Field Theory*, 2nd ed. Cambridge Topics in Mineral Physics and Chemistry, Cambridge University Press, Cambridge, UK.

Charoy B., De Donato P., Barres O., Pinto-Coelho C. (1996) Channel occupancy in an alkali-poor beryl from Serra Branca (Goiás, Brazil): Spectroscopic characterization. *American Mineralogist*, Vol. 81, No. 3/4, pp. 395–403.

Choudhary G., Golecha C. (2007) Gem News International: New Tairus synthetic beryl simulating "Paraíba" tourmaline. *Gems & Gemology*, Vol. 43, No. 4, pp. 385–387.

Deer W.A., Howie R.A., Zussman J. (1986) *Disilicates and Ring Silicates. Rock-Forming Minerals*, Vol. 1B, Geological Society of London, UK, pp. 373–409.

Edgar A., Vance E.R. (1977) Electron paramagnetic resonance, optical absorption, and magnetic circular dichroism studies of the CO_3^- molecular-ion in irradiated natural beryl. *Physics and Chemistry of Minerals*, Vol. 1, No. 2, pp. 165–178.

Farmer V.C. (1974) *The Infrared Spectra of Minerals*. Mineralogical Society, London.

Gatta G.D., Nestola F., Bromiley G.D., Mattauch S. (2006) The real topological configuration of the extra-framework content in alkali-poor beryl: A multi-methodological study. *American Mineralogist*, Vol. 91, No. 1, pp. 29–34.

Goldman D.S., Rossman G.R., Parkin K.M. (1978) Channel constituents in beryl. *Physics and Chemistry of Minerals*, Vol. 3, No. 3, pp. 225–235.

Graziani G., Di Giulio V. (1979) Growth of aquamarine crystal from Brazil. *Neues Jahrbuch für Mineralogie—Monatshefte*, Vol. 3, pp. 101–108.

Gübelin E.J., Koivula J.I. (2005) *Photoatlas of Inclusions in Gemstones*, Vol. 2. Opinio Publishers, Basel, Switzerland.

Johnson M.L., Elen S., Muhlmeister S. (1999) On the identification of various emerald filling substances. *Gems & Gemology*, Vol. 35, No. 2, pp. 82–107.

Kiefert L., Hänni H.A., Chalain J-P., Weber W. (1999) Identification of filler substances in emeralds by infrared and Raman spectroscopy. *Journal of Gemmology*, Vol. 26, No. 8, pp. 501–520.

Koivula J.I., Kammerling R.C. (1988) Gem News: Unusual synthetic beryls from the Soviet Union. *Gems & Gemology*, Vol. 24, No. 4, pp. 252–253.

Koivula J.I., Kammerling R.C. (1991) Gem News: More Soviet synthetics. *Gems & Gemology*, Vol. 27, No. 1, pp. 55.

Koivula J.I., Kammerling R.C., DeGhionno D., Reinitz I., Fritsch E., Johnson M.L. (1996) Gemological investigation of a new type of Russian hydrothermal synthetic emerald. *Gems & Gemology*, Vol. 32, No. 1, pp. 32–39.

Laurs B.M. (2005) Gem News International: Saturated blue aquamarine from Nigeria. *Gems & Gemology*, Vol. 41, No. 1, p. 56.

Lind T., Schmetzer K., Bank H. (1986) Blue and green beryls (aquamarines and emeralds) of gem quality from Nigeria. *Journal of Gemmology*, Vol. 20, No. 1, pp. 40–48.

Mashkovtsev R.I., Smirnov S.Z. (2004) The nature of channel constituents in hydrothermal synthetic emerald. *Journal of Gemmology*, Vol. 29, No. 3, pp. 129–141.

Mashkovtsev R.I., Solntsev V.P. (2002) Channel constituents in synthetic beryl: Ammonium. *Physics and Chemistry of Minerals*, Vol. 29, No. 1, pp. 65–71.

Mathew G., Karanthy R.V., Gundu Rao T.K., Deshpande R.S. (1998) Maxixe-type colour centre in natural colourless beryl from Orissa, India: An ESR and OA investigation. *Journal of Gemmology*, Vol. 26, No. 4, pp. 238–251.

Nassau K. (1990) Synthetic gem materials in the 1980s. *Gems & Gemology*, Vol. 26, No. 1, pp. 50–63.

Nassau K. (1996) On the identification and fade testing of Maxixe beryl, golden beryl and green aquamarine. *Journal of Gemmology*, Vol. 25, No. 2, pp. 108–115.

Nassau K. (1997) The chronology of synthetic gemstones. *Journal of Gemmology*, Vol. 25, No. 7, pp. 453–516.

Nassau K., Prescott B.E. (1981) Nonfading Maxixe-type beryl? *Gems & Gemology*, Vol. 17, No. 4, pp. 217–219.

Nassau K., Prescott B.E., Wood D.L. (1976) The deep blue Maxixe-type color center in beryl. *American Mineralogist*, Vol. 61, No. 1/2, pp. 100–107.

Neiva A.M.R., Neiva M.C.J. (2005) Beryl from the granitic pegmatite at Nativo, Alto Ligonha, Mozambique. *Neues Jahrbuch für Mineralogie, Abhandlungen*, Vol. 181, No. 2, pp. 173–182.

O'Donoghue M. (2006) *Gems*, 6th ed. Butterworth-Heinemann, Oxford, UK.

Reinitz I., Moses T. (1997) Lab Notes: Beryl, treated color. *Gems & Gemology*, Vol. 33, No. 4, p. 293.

Roebling W., Tromnau H.W. (1935) Maxixeberyll. II. *Zentralblatt für Mineralogie, Geologie und Paläontologie*, Vol. A, pp. 134–139.

Rohtert W.R., Quinn E.P., Groat L.A., Rossman G.R. (2003) Gem News International: Blue beryl discovery in Canada. *Gems & Gemology*, Vol. 39, No. 4, pp. 327–329.

Schaller W.T., Stevens R.E., Jahns R.H. (1962) An unusual beryl from Arizona. *American Mineralogist*, Vol. 47, No. 5/6, pp. 672–699.

Schlossmacher K., Klang H. (1935) Der Maxixeberyll. I. *Zentralblatt für Mineralogie, Geologie und Paläontologie*, Vol. A, pp. 37–44.

Schmetzer K. (1988) Characterization of Russian hydrothermally grown synthetic emeralds. *Journal of Gemmology*, Vol. 21, No. 3, pp. 145–164.

Schmetzer K. (1990) Hydrothermally grown synthetic aquamarine manufactured in Novosibirsk, USSR. *Gems & Gemology*, Vol. 26, No. 3, pp. 206–211.

Schmetzer K., Kiefert L. (1990) Water in beryl—A contribution to the separability of natural and synthetic emeralds by infrared spectroscopy. *Journal of Gemmology*, Vol. 22, No. 4, pp. 215–223.

Schmetzer K., Kiefert L., Bernhardt H-J., Beili Z. (1997) Characterization of Chinese hydrothermal synthetic emerald. *Gems & Gemology*, Vol. 33, No.4, pp. 276–291.

Schmetzer K., Schwarz D., Bernhardt H-J, Häger T. (2006) A new type of Tairus hydrothermally-grown synthetic emerald, coloured by vanadium and copper. *Journal of Gemmology*, Vol. 30, No. 1/2, pp. 59–74.

Sechos B. (1997) Identifying characteristics of hydrothermal synthetics. *Australian Gemmologist*, Vol. 19, No. 9, pp. 383–388.

Shigley J.E., McClure S.F., Cole J.E., Koivula J.I., Lu T., Elen S., Demianets L.N. (2001) Hydrothermal synthetic red beryl from the Institute of Crystallography, Moscow. *Gems & Gemology*, Vol. 37, No. 1, pp. 42–55.

Sinkankas J. (1981) *Emerald and Other Beryls*. Chilton Book Co., Radnor, PA.

Smirnov S., Mashkovtsev R., Thomas V., Maltsev V., Alexey I., Anastasiya B. (1999) New hydrothermal synthetic gemstones from Tairus, Novosibirsk, Russia. *Gems & Gemology*, Vol. 35, No. 3, pp. 175–176.

Stockton C.M. (1987) The separation of natural from synthetic emerald. *Gems & Gemology*, Vol. 23, No. 2, pp. 96–99.

Taran M.N., Rossman G.R. (2001) Optical spectroscopy study of tuhualite and a re-examination of the beryl, cordierite, and osumilite spectra. *American Mineralogist*, Vol. 86, No. 9, pp. 973–980.

Turner D., Groat L.A., Hart C.J.R., Mortensen J.K., Linnen R.L., Giuliani G., Wengzynowski W. (2007) Mineralogical and geochemical study of the True blue aquamarine showing, southern Yukon. *Canadian Mineralogist*, Vol. 45, No. 2, pp. 203–227.

Viana R.R., Jordt-Evangelista H., Magela da Costa G., Stern W.B. (2002) Characterization of beryl (aquamarine variety) from pegmatites of Minas Gerais, Brazil. *Physics and Chemistry of Minerals*, Vol. 29, No. 10, pp. 668–679.

Wentzell C.Y., Reinitz I. (1998) Lab Notes: Maxixe beryl, faded and fading. *Gems & Gemology*, Vol. 34, No. 4, pp. 284–285.

Wood D.L., Nassau K. (1967) Infrared spectra of foreign molecules in beryl. *Journal of Chemical Physics*, Vol. 47, No. 7, pp. 2220–2228.

Wood D.L., Nassau K. (1968) The characterization of beryl and emerald by visible and infrared absorption spectroscopy. *American Mineralogist*, Vol. 53, No. 5/6, pp. 777–800.

Call for Abstracts

2ND GEMOLOGICAL RESEARCH CONFERENCE

AUGUST 21–23, 2009 ◆ TOWN & COUNTRY RESORT AND CONVENTION CENTER ◆ SAN DIEGO, CALIFORNIA

To explore the latest technical developments in the field, the Gemological Institute of America is organizing its second Gemological Research Conference (GRC). The GRC is designed to provide a platform for sharing expertise and ideas. The event will feature:

- World-renowned keynote speakers
- Cutting-edge oral and poster presentations and panel discussions
- Two parallel tracks emphasizing technical gemology and jewelry/business issues
- International, multi-disciplinary participation, including a session co-organized by the Mineralogical Society of America
- Photography contest and workshops
- Field trips to historic gem pegmatites in San Diego County

CALL FOR ABSTRACTS

Prospective oral and poster presenters should submit their abstracts (up to 400 words plus one figure or table) via the conference website by March 1, 2009. All abstracts will be reviewed for appropriateness and scientific merit by members of the GRC Advisory Committee. Abstracts for all presentations given at the conference will be published in a proceedings volume.

IMPORTANT DATES

March 1, 2009	Abstract submission deadline
May 1, 2009	Notice of acceptance/rejection of abstracts
May 15, 2009	Travel grant application deadline
June 1, 2009	Early (discounted) registration deadline
June 1, 2009	Oral/poster presenter registration deadline

FIELD TRIPS

Optional field trips will take a limited number of GRC participants to the gem pegmatite mines of San Diego County.

The poster session and cocktail reception are sponsored by the Gem & Jewellery Export Promotion Council, India

GRC

hosted by:

TECHNICAL PROGRAM

The 2009 GRC will feature invited keynote speakers and submitted oral and poster presentations, in two parallel tracks. An opening plenary presentation will be given by noted California Institute of Technology mineralogist Dr. George Rossman. Following are the main session themes and keynote speakers:

Track 1: Gemology

Colored Stone Identification
Keynote: Dr. Michael Krzemnicki, SSEF Swiss Gemmological Institute

Diamond Identification
Keynote: Dr. Alexander Zaitsev, City Univ. of New York

Gem Characterization Technology and Instrumentation
Keynote: Dr. Alan Koenig, U.S. Geological Survey

Gem Treatment and Synthesis
Keynote: Dr. Robert Linares, Apollo Diamond Inc.

Gemstone Inclusions
Keynote: John Koivula, GIA

General Gemology
Keynote: Shane McClure, GIA

Geology of Gem-Forming Environments
(co-organized by the Mineralogical Society of America)
Keynote: Dr. Thomas Stachel, University of Alberta

New Gem Localities
Keynote: Dr. Dietmar Schwarz and Vincent Pardieu, Gübelin Gem Lab

Track 2: Jewelry/Business/Pearls

Color Description and Appraising of Gems
Keynote: Gail Brett Levine, National Assn. of Jewelry Appraisers

Fair Trade and Environmental Issues in Gemology
Keynote: Dr. Saleem Ali, University of Vermont

Gem Market Research, Economics, and Legal Issues
Keynote: David Hargreaves, New African Mining AG

Jewelry History, Gems in Cultural Heritage, and Museum Studies
Keynote: Cigdem Lule-Whipp, GIA London

Jewelry Manufacturing Technology
Keynote: Jeff High, Gemvision Inc.

Pearls and Organic Gems
Keynote: Kenneth Scarratt, GIA Thailand

CONTACT US

For more information, visit www.grc2009.gia.edu, e-mail grc2009@gia.edu, or contact:

Dr. James E. Shigley
(Conference Co-Chair)
Tel: 760-603-4019
Fax: 760-603-4021
E-mail: jshigley@gia.edu

Brendan M. Laurs
(Conference Co-Chair)
Tel: 760-603-4503
Fax: 760-603-4595
E-mail: blaurs@gia.edu

Dona M. Dirlam
(Poster Session)
Tel: 760-603-4154
Fax: 760-603-4256
E-mail: ddirlam@gia.edu

A NEW TYPE OF SYNTHETIC FIRE OPAL: MEXIFIRE

Gagan Choudhary and Rajneesh Bhandari

Synthetic opals have been produced and used in jewelry for more than three decades, and various imitation opals have been introduced in the trade. This article describes a new type of synthetic fire opal marketed as "Mexifire." Some of the gemological properties of this synthetic are similar to those of natural fire opal. However, a low SG value (<1.77) offers strong evidence of synthetic origin, and further indications are provided by a relatively low RI value (<1.40) and the presence of scattered pinpoints when examined with magnification.

Natural fire opal is known mainly from Mexico (see, e.g., Spencer et al., 1992). Other locations include Kazakhstan, Turkey (O'Donoghue, 2006), Ethiopia (Johnson et al., 1996), Oregon (Laurs and Quinn, 2003), and Java (Sujatmiko et al., 2005). The high value and commercial interest in fire opal from various locations has stimulated the production of synthetic counterparts.

Natural opal is hydrated silica, amorphous to microcrystalline, with the chemical formula $SiO_2 \cdot nH_2O$ (Webster, 2002). Soon after the structure of opal was determined, in 1964, the first attempt at manufacturing synthetic opal was reported; it was introduced commercially in 1975 (see, e.g., Smallwood, 2003).

See end of article for About the Authors.
GEMS & GEMOLOGY, Vol. 44, No. 3, pp. 228–233.

Synthetic opal is produced by a number of sources, including Gilson, Kyocera/Inamori, and some Russian manufacturers (e.g., Quinn, 2003; Smallwood, 2003). Several varieties are available, with or without play-of-color, ranging from white and black to pink, orange, or brown. This article describes the properties of a new type of synthetic fire opal (figure 1) developed by one of the authors (RB) and manufactured by Rhea Industries, which is marketed as "Mexifire."

Most of the synthetic opal produced in the past showed distinct play-of-color, which was caused by a three-dimensional array of uniformly sized particles (Nassau, 1980; Schmetzer, 1984; Smallwood, 2003). These synthetic play-of-color opals can be achieved by: (1) producing suitably uniformly sized silica spheres; (2) settling these spheres into a close-packed structure; and then (3) solidifying, aggregating, dehydrating, and compacting the array into a stable product. The Mexifire synthetic opals do not exhibit play-of-color and are made using a different process (modified sol gel). Under specific conditions, silica precursors (tetraethyl orthosilicate [TEOS] in this case) are used to produce a matrix of silica, which is similar to the structure of natural fire opal. As in natural fire opal (Fritsch et al., 1999, 2006), the orange color is caused by traces of iron. Unlike natural opal, these synthetic opals do not craze (see below).

MATERIALS AND METHODS

We examined 38 faceted fire opals: 26 synthetic (0.23–3.50 ct; again, see figure 1) and 12 natural that were said to be from Mexico (0.30–4.00 ct; e.g., figure 2). Only a limited range of sizes for synthetic samples is reported here, but larger pieces may become available in the future.

Figure 1. These samples (0.23–3.50 ct) of synthetic fire opal, marketed as "Mexifire," were studied for this report. Photo by G. Choudhary.

Standard gemological tests were performed on all samples. Refractive index was measured using a GemLED refractometer. Hydrostatic specific gravity was determined using a Mettler Toledo CB 1503 electronic balance. A polariscope was used to check for strain patterns. Fluorescence was checked with exposure to long-wave (365 nm) and short-wave (254 nm) UV radiation. Absorption spectra were observed with a desk-model GIA Prism 1000 spectroscope. We examined the internal features of the samples using both a binocular gemological microscope (with fiber-optic and other forms of lighting, including darkfield and brightfield) and a horizontal microscope with the samples immersed in water.

Energy-dispersive X-ray fluorescence (EDXRF) qualitative chemical analyses of all 38 samples were performed using a PANalytical Minipal 2 instrument under two different conditions: Elements with low atomic number (e.g., Si) were measured at 4 kV tube voltage and 0.850 mA tube current; transition and heavier elements were measured at 15 kV and 0.016 mA.

Infrared spectra of all 38 samples were recorded in the 6000–400 cm^{-1} range at a standard resolution of 4 cm^{-1} and 50 scans per sample using a Nicolet Avatar 360 Fourier-transform infrared (FTIR) spectrometer at room temperature with a transmission accessory. Multiple IR spectra were collected to find the orientation of best transmission, which was greatly affected by the cut of the samples.

Several tests for possible crazing were conducted over a period of one year. A total of 20 additional

Figure 2. Among the natural fire opals studied for a comparison to the Mexifire synthetics are these brownish orange (left, 0.30–0.86 ct) and orangy yellow samples (right, 0.67–0.81 ct), all of which are reportedly from Mexico. Photos by G. Choudhary.

Mexifire synthetic opals and 10 additional natural fire opals were placed under a 100 watt lamp for 240 hours. The samples were observed at regular intervals for signs of crazing.

RESULTS AND DISCUSSION

Visual Characteristics. The 26 Mexifire synthetic opals ranged from medium-to-dark brownish orange to orangy yellow (again, see figure 1). The 12 natural fire opals tested for comparison fell into two color groups: One was a brownish orange similar to the Mexifire product (again, see figure 2, left), while the other was a brighter orangy yellow (figure 2, right). All the synthetics were evenly colored when viewed from the table. When viewed from the side, one of them was darker in the girdle area than in the pavilion (figure 3). This color variation also has been seen in natural fire opal (see Gübelin and Koivula, 2005, p. 498). All the samples appeared transparent under normal viewing conditions, but they displayed a slight haziness when observed with a fiber-optic light. In addition, all the synthetic samples took a good-quality polish, but a few of the natural samples appeared to have a duller luster as a result of their regular use in research and educational activities in the laboratory (which caused some abrasions and scratches).

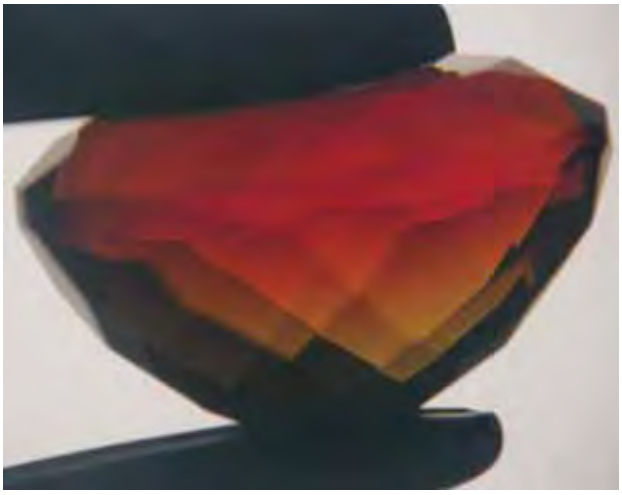

Figure 3. One of the synthetic fire opals displayed variations in bodycolor when viewed from the side. The girdle area appears darker than the pavilion. Photomicrograph by G. Choudhary, brightfield illumination; magnified 15×.

Gemological Properties. The gemological properties of the 38 synthetic and natural fire opal samples are described below and summarized in table 1.

TABLE 1. Properties of Mexifire synthetic opal and natural fire opal.

Property	Mexifire synthetic fire opal	Natural fire opal
Color	Brownish orange to orangy yellow	Brownish orange to orangy yellow
Color distribution	Typically even	Often color zoned; flow-like or wavy pattern
Diaphaneity	Transparent under normal viewing conditions; translucent/turbid with fiber-optic light	Transparent to translucent
Quality of polish	Good	Dull to good
Refractive index	1.380–1.405	1.400–1.435 (this study) 1.420–1.430 (O'Donoghue, 1988)
Specific gravity	1.63–1.77	1.92–2.06 (this study) 2.00 (Webster, 2002)
Polariscope reaction	Strong strain pattern with snake-like bands	Weak strain pattern; no snake-like bands seen
Long- and short-wave UV fluorescence	Inert	Inert
Desk-model spectroscope	No features	No features
Internal features	1. Turbidity following zones (with fiber-optic light) 2. Scattered pinpoints 3. Whisker-like inclusion (in one sample)	1. Turbidity following zones (in one sample) 2. Scattered inclusions of pyrite or some flake-like inclusions 3. Dendritic inclusions common 4. Flow patterns, cloudy zones, fluid inclusions, and a feather-like feature; whisker-like inclusion (in one sample)
EDXRF analysis	Presence of Si, Fe, and Ca	Presence of Si, Fe, and Ca
FTIR spectroscopy	Absorption band in the 5350–5000 cm^{-1} region; hump ranging from 4600 to 4300 cm^{-1}; detector saturated at wavenumbers below 4000 cm^{-1}	Absorption band in the 5350–5000 cm^{-1} region ; hump ranging from 4600 to 4300 cm^{-1} (absent from some natural stones); detector saturated at wavenumbers below 4000 cm^{-1}
Stability to crazing	No crazing seen in 20 samples	Three of the 10 samples crazed within a week to a month

Figure 4. Turbid zones were observed in almost all the synthetic samples (left; magnified 20×) and in one of the natural opals (right, magnified 15×). Also note the scattered pinpoints throughout the sample on the left. Photomicrographs by G. Choudhary, fiber-optic illumination.

Refractive Index. All the synthetic fire opals gave RI readings in the range of 1.380–1.405 (four at 1.380, one at 1.382, one at 1.385, and 11 at 1.390, while four displayed a shadow edge at 1.395, three at 1.400, and two at 1.405). All the natural fire opals tested for comparison displayed RIs of 1.400–1.435. O'Donoghue (1988) stated that the typical refractive index value of Mexican opal falls in the range of 1.420–1.430, but on rare occasions it may go as low as 1.37. Expanding the range of color to include "smoky" opal with play-of-color, however, O'Donoghue (2006) gave a different value of 1.4625 for Mexican opal, and a range of 1.44–1.46 for opal in general. Measuring a refractive index below 1.400 in a material that looks like fire opal should create suspicion.

Specific Gravity. The Mexifire samples had SG values in the range of 1.63–1.77. These values are low for synthetic opal. Although Smallwood (2003) reported SGs down to 1.74 for a Russian product, and Gunawardene and Mertens (1984) measured an SG of 1.91 for Gilson polymer "Mexican fire opal," some synthetic opals have shown SG values up to 2.27 (e.g., Kyocera: Quinn, 2003). The SGs for the tested natural opals varied from 1.92 to 2.06. Therefore, specific gravity values that are significantly below this range provide an excellent indication that an opal is synthetic. During the SG measurements, the synthetic specimens did not show any signs of porosity; this also was reflected in the quality of polish they displayed.

Polariscope Reaction. All the synthetic samples gave a strong strain pattern with snake-like bands. By contrast, the strain pattern in the natural opals was much weaker and did not exhibit snake-like bands.

Fluorescence. All samples, natural and synthetic, were inert to long- and short-wave UV radiation.

Spectroscope Spectrum. In both the synthetic and natural samples, no absorption features were seen with the desk-model spectroscope.

Internal Features. Examination of the Mexifire samples with the gemological and horizontal microscopes revealed the following features:

1. *Turbidity:* Most exhibited moderate-to-strong turbidity when illuminated with a fiber-optic light. In darkfield illumination, however, they appeared transparent. The turbidity was somewhat zonal (figure 4, left), as seen in one of the natural samples examined for this study (figure 4, right) and in some other natural fire opals (Choudhary and Khan, 2007).
2. *Pinpoints:* All synthetic samples exhibited scattered pinpoints throughout the stones (again, see figure 4, left). These pinpoints were best seen when the samples were illuminated with fiber-optic light; only a weak effect was visible in darkfield. Even at higher magnification, the exact nature of these pinpoints could not be resolved. Although similarly scattered flake-like inclusions have been seen previously in natural opals, and Gübelin and Koivula (2005) mentioned tiny grains of pyrite scattered throughout a stone, we did not find any reports of such "pinpoint" inclusions in a natural opal.
3. *Whisker-like Inclusion:* One of the synthetic fire opals displayed a whisker-like inclusion (figure 5, left) that broke the surface. Its exact nature could not be determined, but it looked like a hollow tube filled with an epigenetic material. One of the natural opals displayed a similar inclusion (figure 5, right). Johnson et al. (1996) reported similar-shaped inclusions in fire opal from Ethiopia.

Over the years, synthetic and imitation opals have been differentiated from natural material by the

Figure 5. One of the synthetic samples contained the whisker-like inclusion on the left (magnified 75×), which appears to be a hollow tube filled with an epigenetic material. A similar feature was seen in one of the natural fire opals (right, magnified 80×). Photomicrographs by G. Choudhary, fiber-optic illumination.

presence of a "lizard skin" or "chicken wire" effect and/or a columnar growth pattern (see, e.g., Gübelin and Koivula, 1986, 2005; O'Donoghue, 2006, 2007). Detailed examination of the inclusions and growth patterns in the Mexifire samples was conducted using various types of illumination and techniques, but no lizard skin or chicken-wire effect was observed. This effect is visible only in synthetic opals made of uniformly sized silica spheres with a close-packed structure, which serves as further evidence that the structure of these new synthetic opals is different from that of most synthetic or imitation opals described previously. One exception involves some Russian synthetic opals that also do not show a lizard skin effect (Smallwood, 2003).

Some additional internal features seen in the natural opals that were studied for comparison are shown in figure 6. See Gübelin and Koivula (2005) for detailed illustrations of inclusions in natural opals.

EDXRF Analysis. Qualitative EDXRF spectroscopy of all the samples, synthetic as well as natural, revealed the presence of Si as the major element, which is expected for opal. In addition, the samples in both groups contained traces of Fe and Ca. We did not detect any Zr, which has been used for impregnating and stabilizing opal (Webster, 2002; Smallwood, 2003).

FTIR Analysis. The infrared spectra recorded for the synthetic and natural samples displayed similar features in the range 6000–400 cm^{-1} (e.g., figure 7; also compare to Johnson et al., 1995). Slight differences in the intensity and appearance of the absorption pattern were caused by variations in the amount of transmission; better transmission revealed sharper absorption features. All samples had an absorption band in the region of 5350–5000 cm^{-1}; this feature also consisted of sharp peaks, depending on the transmission. A hump was observed in the 4600–4300 cm^{-1} range, often with small peaks, in all of the synthetic samples and in seven of the 12 natural opals in this study. The absence of the absorption feature at 4600–4300 cm^{-1} may provide a useful identification criterion for determining natural origin. The detector was saturated by strong absorption at wavenumbers below approximately 4000 cm^{-1}.

Some Inamori/Kyocera products are regarded as imitations rather than synthetics because they use polymers as binding agents. Although the low SG values of the Mexifire products are consistent with the presence of polymers, this could not be confirmed with IR spectroscopy due to complete absorption in that region of

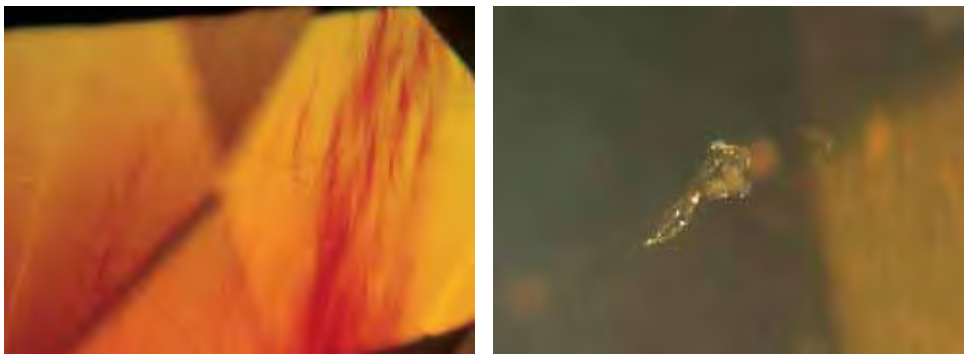

Figure 6. Some of the natural fire opals studied for comparison displayed internal features such as wavy flow patterns with color concentrations (left, magnified 45×) and a feather-like inclusion (right, fiber-optic illumination, magnified 80×) that were not seen in their Mexifire synthetic counterparts. Photomicrographs by G. Choudhary.

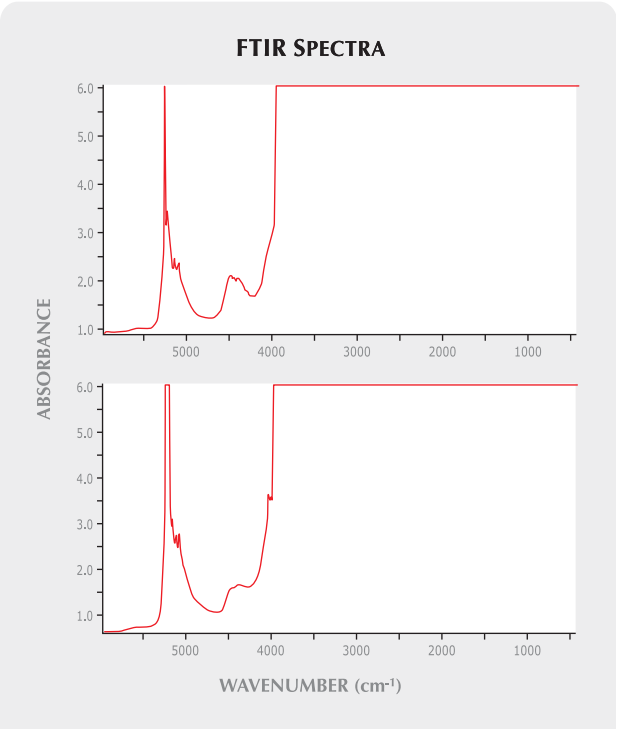

Figure 7. These representative IR spectra of Mexifire synthetic opal (top) and natural fire opal (bottom) exhibited similar features: an absorption band in the 5350–5000 cm^{-1} region, a hump in the 4600–4300 cm^{-1} range (which was absent from the spectra of some of the natural samples), and total absorption below approximately 4000 cm^{-1}.

the spectrum. Nevertheless, the manufacturer claims that no polymer is present in these Mexifire opals.

Stability to Crazing. None of the 20 Mexifire pieces exhibited any signs of crazing during these experiments, but three of the natural fire opals crazed within a week to a month. The seven other natural samples did not exhibit any signs of crazing.

CONCLUSION

Similarities in some of the gemological properties, as well as in the chemical composition and IR spectral features, were noted between Mexifire synthetic opals and their natural fire opal counterparts. However, a low SG value (<1.77) is an excellent indication that a fire opal is not natural, and additional evidence is provided by a relatively low RI value (<1.40) and internal features such as scattered pinpoints. In addition, the absence of a hump at 4600–4300 cm^{-1} in the IR spectrum suggests that the sample is natural.

ABOUT THE AUTHORS

Mr. Choudhary is assistant director of the Gem Testing Laboratory, Jaipur, India. Mr. Bhandari is a chemical engineer and owner of Rhea Industries, Jaipur.

REFERENCES

Choudhary G., Khan M. (2007) Gem News International: A remarkably large fire opal carving. *Gems & Gemology*, Vol. 43, No. 3, pp. 258–259.

Fritsch E., Rondeau B., Ostrooumov M., Lasnier B., Marie A.M., Barrault A., Wery J., Connoué J., Lefrant S. (1999) Découvertes récentes sur l'opale [Recent discoveries about opal]. *Revue de Gemmologie a.f.g.*, No. 138/139, pp. 34–40.

Fritsch E., Gaillou E., Rondeau B., Barreau A., Albertini D., Ostrooumov M. (2006) The nanostructure of fire opal. *Journal of Non-Crystalline Solids*, Vol. 352, No. 38–39, pp. 3957–3960.

Gübelin E.J., Koivula J.I. (1986) *Photoatlas of Inclusions in Gemstones*, Vol. 1. ABC Edition, Zurich, Switzerland.

Gübelin E.J., Koivula J.I. (2005) *Photoatlas of Inclusions in Gemstones*, Vol. 2. Opinio Publishers, Basel, Switzerland.

Gunawardene M., Mertens R. (1984) Gilson created fire opal imitation with play-of-color. *Journal of Gemmology*, Vol. 19, No. 1, pp. 43–53.

Johnson M.L., Kammerling R.C., McClure S.F. (1995) Gem Trade Lab Notes: Glass imitation "Mexican" opal. *Gems & Gemology*, Vol. 31, No. 3, pp. 201–202.

Johnson M.L., Kammerling R.C., DeGhionno D.G., Koivula J.I. (1996) Opal from Shewa Province, Ethiopia. *Gems & Gemology*, Vol. 32, No. 2, pp. 112–120.

Laurs B.M., Quinn E.P. (2003) Gem News International: Fire opal from Juniper Ridge, Oregon. *Gems & Gemology*, Vol. 39, No. 1, pp. 55–56.

Nassau K. (1980) *Gems Made by Man*. Gemological Institute of America, Santa Monica, CA.

O'Donoghue M. (1988) *Gemstones*. Chapman and Hall Ltd., London.

O'Donoghue M., Ed. (2006) *Gems—Their Sources, Description, and Identification*, 6th ed. Butterworth-Heinemann, Oxford, UK.

O'Donoghue M. (2007) Synthetic, color enhanced and imitation opal. In J. Clifford et al., Eds., *Opal—The Phenomenal Gemstone*. Lithographie LLC, East Hampton, CT, pp. 100–103.

Quinn E.P. (2003) Gem News International: New synthetic opal varieties. *Gems & Gemology*, Vol. 39, No. 4, p. 340.

Schmetzer K. (1984) An investigation of the synthetic products of Gilson showing a play-of-color. *Journal of Gemmology*, Vol. 19, No. 1, pp. 27–42.

Smallwood A. (2003) 35 years on: A new look at synthetic opal. *Australian Gemmologist*, Vol. 21, No. 11, pp. 438–447.

Spencer R.J., Levinson A.A., Koivula J.I. (1992) Opal from Querétaro, Mexico: Fluid inclusion study. *Gems & Gemology*, Vol. 28, No. 1, pp. 28–34.

Sujatmiko H., Einfalt H.C., Henn U. (2005) Opals from Java. *Australian Gemmologist*, Vol. 22, No. 6, pp. 254–259.

Webster R. (2002) *Gems—Their Sources, Descriptions and Identification*, 5th ed. Rev. by P.G. Read, Butterworth-Heinemann, Oxford, UK.

THE COLOR DURABILITY OF "CHOCOLATE PEARLS" BY BALLERINA PEARL CO.

Garry Du Toit, Andy H. Shen, and Christopher M. Breeding

Treated-color brown Tahitian cultured pearls, known in the trade as "Chocolate Pearls," have become increasingly prevalent in the market. As a result, it is important that the durability of the color treatment is well understood. Seven Chocolate Pearls supplied by Ballerina Pearl Co. and 12 untreated Tahitian cultured pearls (for comparison) were exposed to conditions of consumer care and wear—heat, household chemicals, daylight, and some typical cosmetics—to determine their effects on the color. The results were similar for both groups: They did not change color when exposed to daylight, cosmetics, and some chemicals; subtle changes were noticed after exposure to heat; and more significant changes were observed when the samples were exposed to chemically reactive household cleaning solutions.

The Ballerina Pearl Co. produces attractive brown pearls from off-color "black" Tahitian cultured pearls using a bleaching process (Wang et al., 2006); these are now known in the trade as "Chocolate Pearls" (see, e.g., Sanchez, 2004; Zachovay, 2005).

See end of article for About the Authors and Acknowledgments.
GEMS & GEMOLOGY, Vol. 44, No. 3, pp. 234–241.

The increasing availability of such "chocolate" cultured pearls in the marketplace likewise creates a need for better understanding of any durability issues involving their treated color. Under normal wearing conditions, these treated cultured pearls could be subjected to situations such as unintentional exposure to heat in a domestic kitchen, contact with typical household chemicals, and prolonged exposure to daylight; most will be exposed to common cosmetics. All of these situations could affect the color of Chocolate Pearls, just as they can affect untreated pearls (e.g., Nassau, 1984; Nassau and Hanson, 1985; Martin, 1987; Overton and Elen, 2004; CIBJO, 2007). Through a series of carefully controlled exposure experiments involving heat, standard household chemicals, daylight, and certain cosmetics, we examined the durability of the color of several Ballerina Chocolate Pearls as compared to their untreated Tahitian counterparts.

MATERIALS AND METHODS

We studied seven treated Tahitian "chocolate" cultured pearls provided by Ballerina Pearl Co. (figure 1). They ranged from 8.44 to 12.57 ct (10.50–12.53 mm; see table 1). The colors were dark orangy brown, orangy brown, and pinkish brown, according to the GIA pearl grading color reference charts (Gemological Institute of America, 2000), as determined by experienced gemologists. All had high luster.

For comparison, we also examined 12 untreated "black" Tahitian cultured pearls ranging from 6.42 to

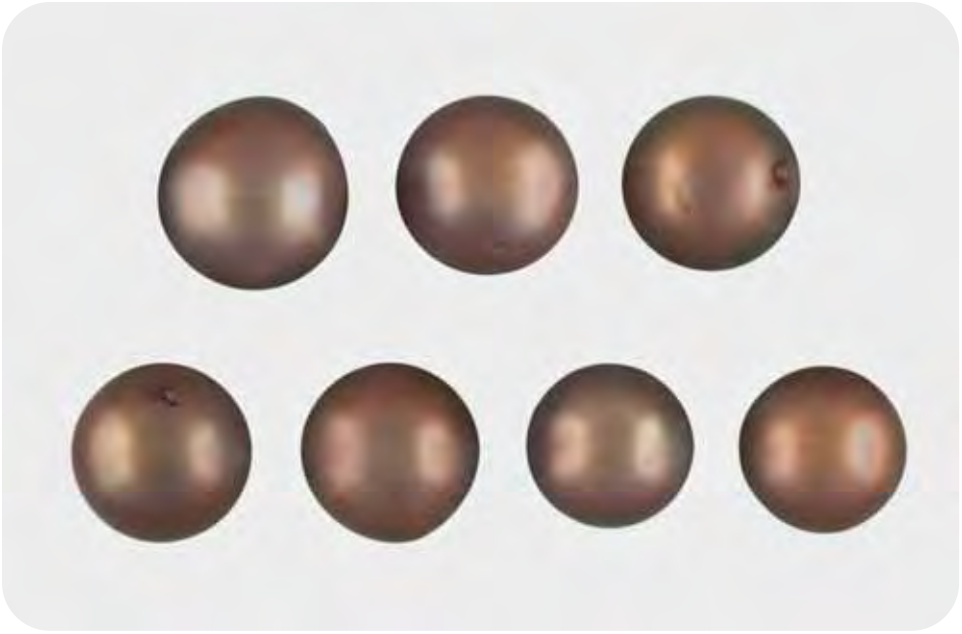

Figure 1. These seven Tahitian cultured Chocolate Pearls (10.50–12.53 mm), treated by Ballerina Pearl Co. using a proprietary bleaching method, were studied to evaluate their durability to various conditions of consumer wear. The samples are in order (CCP-1 to CCP-7) from left to right, top to bottom. Composite photo by Suchada Kittayachaiwattana.

30.62 ct (9.81–25.94 mm in longest dimension; again, see table 1). The dominant colors were gray, brown, and black with green, pink, and purple modifiers (see table 1), again based on the GIA color reference charts (e.g., figure 2). One sample showed orient and one showed green and rosé overtones. All but one of the untreated Tahitian cultured pearls had good to very good luster.

We identified two broad types of durability concerns: (1) jewelry manufacturing or repair processes, and (2) daily use by consumers. Pearls are well known to be fragile gems, so informed jewelers are careful not to expose them to adverse conditions during setting and repair and to clean them using only mild soap and water, never with ultrasonic or steam cleaners. In addition, pearl nacre consists mainly of the mineral aragonite with organic materials, which are very soft (Mohs hardness = 2.5–3.5; Sinkankas, 1972). Most household scrubbing cleansers contain particles of quartz (hardness = 7) or marble (hardness = 3) or other materials that will inevitably damage pearl nacre, whether or not the pearl has been treated. Thus, we focused our study on durability issues involved with the nonabrasive interaction between the jewelry of an average consumer and that consumer's daily activities. The following experiments were performed using a group of potentially adverse conditions designed with these everyday interactions in mind (table 2).

The reader is cautioned that not all pearls marketed as Chocolate Pearls have been treated in the same manner as the Ballerina product (see, e.g., Hänni,

TABLE 1. Characteristics of the seven "chocolate" cultured pearls from Ballerina Pearl Co. and 12 natural-color Tahitian cultured pearls used for the various durability tests.

Sample	Weight (ct)	Measurements (mm)	Color	Luster
"Chocolate" Cultured Pearls				
CCP-1	12.57	11.97–12.53	Pinkish brown	High
CCP-2	11.78	11.76–11.84	Pinkish brown	High
CCP-3	10.20	11.27–11.43	Dark orangy brown	High
CCP-4	10.56	11.35–11.42	Orangy brown	High
CCP-5	9.85	11.17–11.55	Pinkish brown	High
CCP-6	8.44	10.50–10.60	Dark orangy brown	High
CCP-7	8.52	10.58–10.67	Pinkish brown	High
Natural-Color Tahitian Cultured Pearls				
PE-1	6.53	9.29–11.37	Dark greenish gray	Good
PE-2	6.69	9.42–12.01	Dark green-gray	Very good
PE-3	10.96	11.50–11.99	Gray with green and rosé overtones	Good
PE-4	7.32	9.94–10.93	Dark gray	Very good
PE-5	8.83	10.65–12.84	Gray with orient	Very good
PE-6	9.40	10.76–14.40	Pinkish brown and greenish gray with orient	Good
PE-12	27.64	14.54–18.78	Dark gray	Good
PE-13	13.28	11.87–14.25	Purplish gray	Good
PE-14	12.38	11.15–15.57	Dark greenish gray	Very good
PE-15	11.49	11.51–13.38	Greenish black	Good
PE-16	6.42	9.69–9.81	Dark green-gray	Good
PE-17	30.62	14.35–25.94	Gray	Fair

Figure 2. These six untreated "black" Tahitian cultured pearls are part of the sample group tested using similar methods to serve as a reference for any color changes observed in the treated Chocolate Pearls. Again the samples are in order (PE-1 to PE-6) from left to right, top to bottom. Composite photo by Wuyi Wang (not scaled to size).

2006); therefore, some may react differently to the tests conducted in this study. It should also be noted that these experiments were performed with a small number of undrilled samples and for limited durations (up to 40 hours), so they may not predict the long-term durability of the treatment in all cases. Likewise, we tested specific products within a category, not the range of products that are available in each category (e.g., only one ammonia solution and one each perfume, hair spray, and facial cream). We examined the results visually with the unaided eye as well as with a gemological microscope using 10–70× magnification throughout the course of the tests.

Controlled Heating. To examine the effects of accidental exposure to heat in the kitchen (e.g., placement of a ring near a hot burner or electric frying pan), we performed controlled heating experiments using a Lindberg/Blue M Moldatherm box furnace. We heated two treated Chocolate Pearls and two untreated Tahitian samples at 90°C (194°F) and 150°C (302°F), respectively, in air for 0.5, 1.5, and 2.5 hours (treated samples) and 2 and 2.75 hours (untreated). Target temperatures were reached prior to placing the samples in the oven. Temperature variations at each targeted temperature were within 10°C.

Prolonged Exposure to Common Household Chemicals. Because pearls set in a ring or bracelet have a good possibility of being exposed to household cleaners and other products when worn by the consumer, we tested five common chemicals: rubbing alcohol (isopropyl), acetone (reagent grade, commonly used as fingernail polish remover), ammonia (5–10% ammonium hydroxide solution), and two kinds of bleach—undiluted liquid Clorox (5.25% sodium hypochlorite solution) and undiluted liquid Clorox 2 (chlorine-free or "color safe" version; 5–25% sodium perborate tetrahydrate). One treated and one untreated sample were immersed in each solution for various periods of time to evaluate the effects of exposure (again, see table 2). We used a clear polyethylene bottle to facilitate observation and assessed the samples visually every five minutes during the first hour and every hour for the following four hours. For the isopropyl alcohol and acetone tests, we immersed the Chocolate Pearls for five hours and the untreated pearls for 18 hours. For the Clorox test, we immersed both samples for only 50 minutes (due to observation of rapid surface damage). For the ammonia and Clorox 2 solutions, we immersed the samples for a total of 18 hours in each. If any change in color or texture was observed prior to the planned end of the immersion time, we stopped the experiment and documented the changes. Otherwise, experiments were run to completion and documented immediately thereafter.

Effects of Daylight. To evaluate the effects of exposure to daylight, we placed two "chocolate" cultured pearls and two untreated Tahitian samples in direct sunlight on a window sill at room temperature in Bangkok (13°27′ N) in March 2008, for a period of five days with a total sunlight exposure time of 40 hours.

Contact with Cosmetics. For this test, we used typical cosmetics: YSL Paris perfume by Yves Saint Laurent, TRESemmé European Tres Two Extra Hold hair spray, and L'Oréal Transformance face cream. We immersed one treated and one untreated sample in the perfume for 2.5 hours and a second untreated and second treated sample in the hair spray for 3.5 hours. After these tests were completed, and no changes were observed with either the unaided eye or a gemological microscope, we thoroughly cleaned all four samples and immersed them in the face cream for 26 hours.

TABLE 2. Durability testing of Ballerina treated "chocolate" cultured pearls and of untreated Tahitian cultured pearls for comparison.

Testing method	Conditions	"Chocolate" cultured pearls			Untreated Tahitian cultured pearls		
		Sample(s)	Duration (hours)	Results	Sample(s)	Duration (hours)	Results
Controlled heating	90°C	CCP-1 & CCP-2	0.5, 1.5, 2.5	Color appeared slightly lighter with increasing heating duration (fig. 3)	PE-5 & PE-6	2.75	Very subtle color fading noted in one of two pearls tested
	150°C		0.5, 1.5, 2.5	Color appeared slightly lighter with increasing heating duration (fig. 3)		2	Showed slightly lighter tones with much of the greenish overtone becoming browner (fig. 4)
Bleach (Clorox)	Immersed in 5.25% sodium hypochlorite (bottled, undiluted chlorine bleach)	CCP-5	0.83	After 30 min., slight color fading observed; after 50 min., whitish spots and etched, flaky texture observed on the surface with white discoloration rings concentrated near natural indentations (figs. 5 and 6)	PE-15	0.83	After 30 min., slight color fading observed; after 50 min., whitish spots and etched, flaky texture observed on the surface with white discoloration rings concentrated near natural indentations
Acetone	Immersed in reagent grade acetone	CCP-7	5	No visible changes	PE-13 & PE-17	18	After 4 hours, the hue became noticeably darker and the stone appeared browner (fig. 7)
Isopropyl alcohol	Immersed in standard rubbing alcohol	CCP-6	5	No visible changes	PE-12	18	No visible changes
Ammonia	Immersed in 5–10% ammonium hydroxide	CCP-6	18	No change after 2 hours; after 18 hours, significant color fading noted and distinct irregular zones of light and dark color observed (figs. 8 and 9)	PE-14	18	No change after 2 hours; after 18 hours, some color fading and distinct irregular zones of light and dark color observed
"Color safe" bleach (Clorox 2)	Immersed in 5–25% sodium perborate tetrahydrate (bottled, undiluted chlorine-free bleach)	CCP-7	18	No change after 2 hours; after 18 hours, slight color fading noted and faint mottled whitish appearance (fig. 8)	PE-16	18	No change after 2 hours; after 18 hours, slight color change noted (darker tone in general), but no obvious damage observed
Daylight	Exposed to direct sunlight	CCP-3 & CCP-4	40	No visible changes	PE-3 & PE-4	40	No visible changes
Cosmetics	Immersed in perfume	CCP-1	2.5	No visible changes	PE-1	2.5	No visible changes
	Immersed in hair spray	CCP-2	3.5	No visible changes	PE-2	3.5	No visible changes
	Immersed in face cream	CCP-1 & CCP-2	26	No visible changes	PE-1 & PE-2	26	No visible changes

RESULTS

Exposure to Heat. Heating the Chocolate Pearls at 90°C and 150°C produced similar results. The pinkish brown color appeared slightly lighter in tone (figure 3), but we detected no variation in hue. The reference untreated samples showed little reaction at 90°C, but at 150°C they also appeared to have slightly lighter tones with much of the greenish overtone becoming browner (figure 4).

Exposure to Household Chemicals. Exposure of the samples to various chemical solvents produced dramatically different results. After immersion in concentrated Clorox chlorine bleach for 30 minutes, sample CCP-5 became slightly lighter in tone (figure 5B). After 50 minutes, noticeable whitish spots developed on its surface and an etched, flaky texture (figure 5C) was apparent. Discoloration was especially prominent around natural indentations on the surface, as white, ring-like patterns (figure 6). The untreated Tahitian sample had a similar reaction. In contrast, the Chocolate Pearls immersed in acetone (CCP-7) and isopropyl alcohol (CCP-6) showed no significant changes after five hours. While untreated

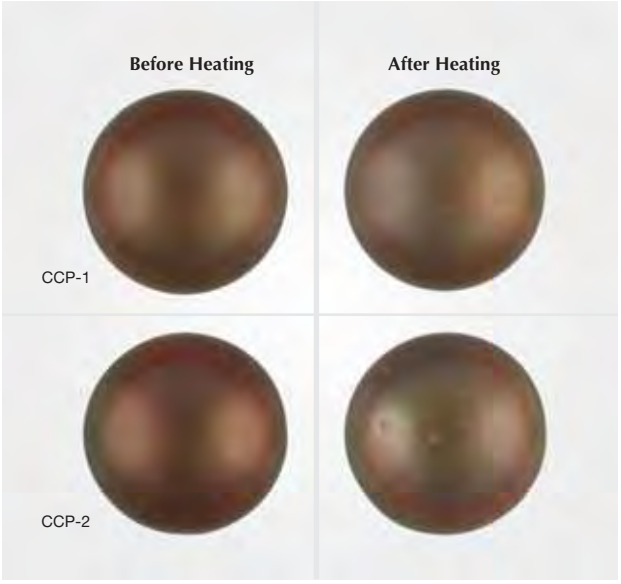

Figure 3. The pinkish brown color of these samples (CCP-1 and CCP-2) appeared lighter after heating at either 90°C or 150°C, but no variation in hue was detected. Top: CCP-1 before heating (left) and after heating at 90°C for 2.5 hours (right). Bottom: CCP-2 before heating (left) and after heating at 150°C for 2.5 hours (right). Photos by Wuyi Wang.

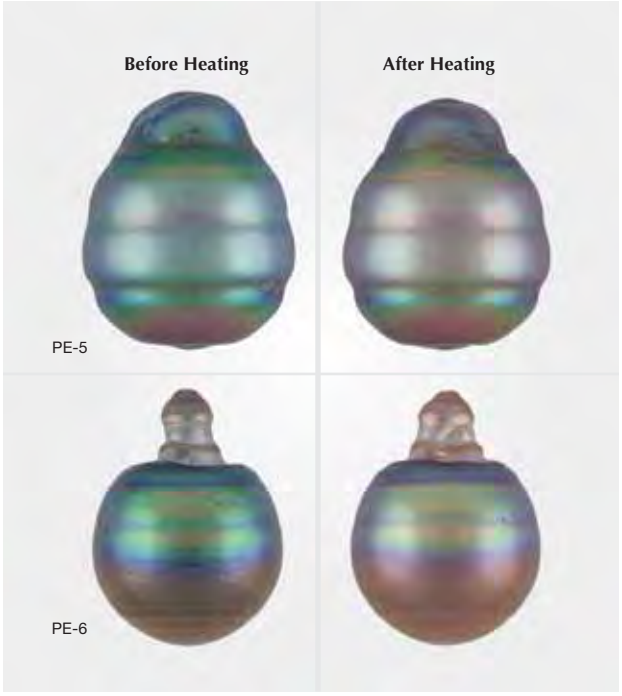

Figure 4. The untreated Tahitian cultured pearls (PE-5 and PE-6) showed little reaction at 90°C, but at 150°C they also developed slightly lighter tones with much of the greenish overtone becoming browner in color. Left: before heating; right: after heating at 150°C for 2 hours. Photos by Wuyi Wang.

sample PE-12 also did not react to isopropyl alcohol (after a total of 18 hours of immersion), acetone caused untreated samples PE-13 and PE-17 to become noticeably darker with a more brownish hue (see, e.g., figure 7), starting after four hours of immersion.

The apparently unaffected Chocolate Pearl samples, CCP-6 and CCP-7, were then cleaned in water and immersed in concentrated ammonia and "color safe" Clorox 2 bleach, respectively. After two hours of exposure, neither sample showed any changes; after 18 hours, however, both showed color fading. The sample exposed to Clorox 2 bleach became lighter in color with faint, irregular whitish patches (figure 8). In contrast, large sections of the surface of the treated sample exposed to ammonia became discolored, with distinct light regions mixed with remnant zones of darker color (figures 8 and 9). The degree of color fading caused by ammonia over an 18-hour period was substantially more than that

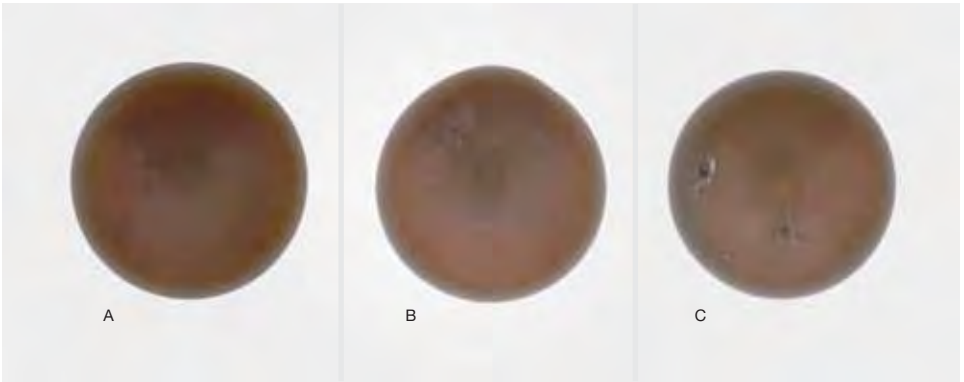

Figure 5. After immersion in concentrated Clorox chlorine bleach for 30 minutes, sample CCP-5 (A, before immersion) showed slight changes in color appearance (B), with noticeable changes apparent after immersion for 50 minutes (C). Photos by Robison McMurtry.

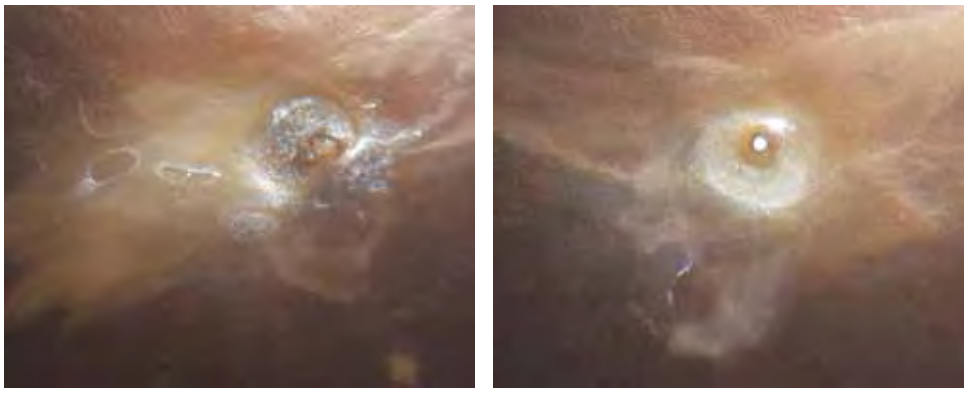

Figure 6. On areas of the surface where natural indentations were present, immersion in concentrated Clorox bleach for 50 minutes produced prominent discoloration—seen as white, ring-like patterns around the indentations (here, on sample CCP-5). Photomicrographs by A. H. Shen; fields of view 5.2 mm (left) and 3.1 mm (right).

observed from both types of bleach; however, the damage produced by the chlorine bleach occurred in a much shorter time period (less than one hour). Similar reactions were seen in the untreated Tahitian samples.

Exposure to Daylight. Prolonged daylight exposure appeared to have little, if any, effect on the color of the Chocolate Pearls or the untreated samples. After 40 hours of cumulative exposure to direct near-equatorial sunlight, no noticeable change in tone, hue, or saturation was observed.

Exposure to Cosmetics. In the course of daily wear by a consumer, cosmetics are the chemicals with which pearls are most likely to come into contact. After extended exposure to perfume, hair spray, and face cream, both the color and luster of the Chocolate Pearls tested remained unchanged. Likewise, the untreated samples also showed no changes. Although it is commonly stated that consumers should avoid having pearls come into contact with cosmetics, we found no detrimental effects when the pearls in this experiment were exposed to cosmetics. It should be noted, however, that we used relatively short exposure times compared to a lifetime of wearing pearl jewelry.

DISCUSSION

From our data, it appears that the Ballerina Chocolate Pearls are no less durable than their untreated Tahitian counterparts. Neither should be subjected to high temperatures or exposed to a strong cleaner such as chlorine bleach or concentrated ammonia for any extended period of time. "Color safe" bleach can also cause damage with prolonged exposure. Although milder solvents such as acetone and isopropyl alcohol did not appear to cause noticeable damage to the Chocolate Pearls under the test conditions, the untreated Tahitian sample began to change color in acetone after four hours of immersion. Therefore, prolonged exposure to acetone is inadvisable in either the treated or untreated material.

Again, it should be noted that these experiments were performed with a small number of undrilled samples and for limited durations. Drilled samples would have allowed access to the interior, so the samples might have experienced different reactions. Likewise, we tested specific products

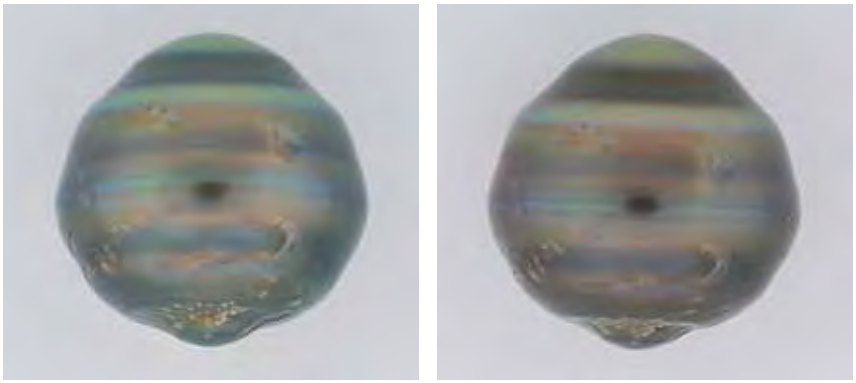

Figure 7. Unlike Ballerina Chocolate Pearl CCP-7, untreated sample PE-13 (left, before immersion) became noticeably darker and browner when placed in acetone for four hours (right, after immersion). Photos by C. D. Mengason.

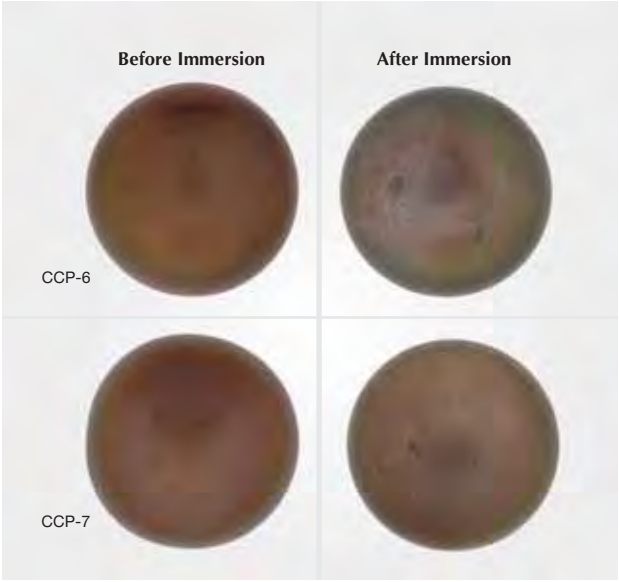

Figure 8. Samples CCP-6 and CCP-7 both showed color fading after 18 hours of immersion in concentrated ammonia and "color safe" Clorox 2 bleach, respectively. Top: CCP-6 before immersion in ammonia (left) and after immersion for 18 hours (right). Bottom: CCP-7 before immersion in Clorox 2 bleach (left) and after immersion for 18 hours. Photos by Robison McMurtry.

within a category, but not the range of products available in that category. Therefore, the results of these experiments may not predict the long-term durability of the treatment in all cases.

Figure 9. Large sections of the pearl surface exposed to ammonia (CCP-6) for 18 hours became discolored, with distinct light regions mixed with remnant zones of darker color. Photomicrograph by A. H. Shen; field of view 2.6 mm.

CONCLUSIONS

The recent popularity of Chocolate Pearls requires that we better understand their durability under typical conditions of consumer wear, especially in the household. Our experiments revealed that, in most situations tested, the durability of the color of Ballerina "chocolate" cultured pearls is comparable to that of untreated Tahitian cultured pearls. When exposed to daylight and cosmetics such as perfume, hair spray, and a facial cream, our samples showed no noticeable changes in color. Only relatively prolonged exposure to heat, ammonia, or bleach caused significant alterations to the surface texture and color of the treated and untreated cultured pearls. The wearer should also be reminded that, because of the relative softness of pearls, abrasive household cleansers (many of which consist of particulate ingredients harder than pearl nacre) represent another danger (not tested here because of known behavior) in the average household.

Although it seems unlikely that most pearl jewelry would be exposed to temperatures as high as 90°C or to harsh chemicals for extended periods of time, such exposure does happen and it is important to understand its effect on this organic gem and inform the consumer accordingly. All cultured pearls are fragile and susceptible to damage by physical contact with harsh chemicals and heat or the application of cosmetics; therefore, the consumer would be well advised to remove pearl jewelry when these possibilities exist. By exercising caution, a consumer can greatly reduce the cumulative effects that such exposure may have.

It is important to note again that treated cultured pearls with similar "chocolate" colors are also present in the market from sources other than Ballerina Pearl Co. Since the treatment process is proprietary, and the starting materials may come from various sources, there is no guarantee that Chocolate Pearls from other companies will show analogous results.

ABOUT THE AUTHORS

Mr. Du Toit is manager of Gem Identification at GIA Research (Thailand). Dr. Shen and Dr. Breeding are research scientists at the GIA Laboratory, Carlsbad.

ACKNOWLEDGMENTS

The authors are grateful to Dr. Wuyi Wang of the GIA Laboratory in New York for acquiring samples for these experiments and for helpful discussions.

REFERENCES

CIBJO (2007) *CIBJO Blue Books - The Pearl Book*, version 2007-6, http://download.cibjo.org/CIBJO_2007-6_draft_pearl-2008.pdf.

Gemological Institute of America (2000) *GIA Pearl Grading Color Reference Charts*, Carlsbad, CA.

Hänni H.A. (2006) Gem News International: Update on "chocolate" Tahitian cultured pearls. *Gems & Gemology*, Vol. 42, No. 4, pp. 284–285.

Martin D.D. (1987) Gemstone durability: Design to display. *Gems & Gemology*, Vol. 23, No. 2, pp. 63–77.

Nassau K. (1984) *Gemstone Enhancement*. Butterworth-Heinemann, Boston.

Nassau K., Hanson A.E. (1985) The pearl in the chicken: Pearl recipes in *Papyrus Holmiensis*. *Gems & Gemology*, Vol. 21, No. 4, pp. 224–231.

Overton T.W., Elen S. (2004) Gem News International: Dyed cultured pearls fading on exposure to heat. *Gems & Gemology*, Vol. 40, No. 3, pp. 267–268.

Sanchez L. (2004) Trade raises questions about chocolate pearls. *Jewellery News Asia*, No. 241, pp. 160, 162.

Sinkankas J. (1972) *Gemstone and Mineral Databook*. Winchester Press, New York.

Wang W., Scarratt K., Hyatt A., Shen A.H.-T., Hall M. (2006) Identification of "Chocolate Pearls" treated by Ballerina Pearl Co. *Gems & Gemology*, Vol. 42, No. 4, pp. 222–235.

Zachovay M. (2005) Gem News International: "Chocolate" Tahitian cultured pearls. *Gems & Gemology*, Vol. 41, No. 2, pp. 183–184.

Gota de Aceite: Nomenclature for the Finest Colombian Emeralds

Ronald Ringsrud

The finest and rarest emeralds are sometimes said to have an optical effect called *gota de aceite*. This term describes an aspect of emerald clarity that is associated with Colombian emeralds. Yet overuse has separated the term from its actual meaning. This article reports on the gemological causes of the *gota de aceite* optical effect and defines the phenomenon.

Made famous by Spanish *conquistadores* nearly five centuries ago, the Colombian emerald mines still produce stones of superb quality and fineness today. Most notable are emeralds from the Muzo region, which encompasses not only the Muzo mine but also the La Pita, Coscuez, and Peñas Blancas mines. The nomenclature that applies to certain Colombian emeralds has specific and useful meaning, but many terms have lost precision over time.

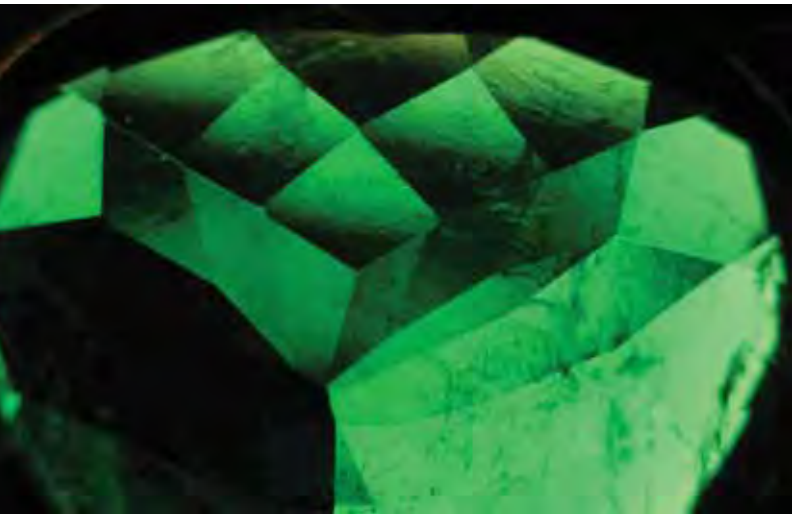

Figure 1. In the six upper facets of this 9.20 ct heart-shaped Colombian emerald, a roiled, softening effect lends texture to the stone. This effect, called gota de aceite, *is a result of transparent growth structures within the emerald. Photomicrograph by R. Ringsrud.*

Figure 2. The approximately 2.15 ct emerald in this ring provides an exceptional example of the gota de aceite *effect. Photo by Thomas Hainschwang.*

Gota de aceite (Spanish for "drop of oil," pronounced "**go**-tuh day ah-**say**-tay") describes a remarkable phenomenon that occurs very rarely and typically only in the finest emeralds (figure 1; see also Hainschwang, 2008). Emeralds with this effect display a roiled appearance (see figures 2 and 3) that is reminiscent of honey or oil—hence the name. The phenomenon has also been called the "butterfly

See end of article for About the Author and Acknowledgments.
Gems & Gemology, Vol. 44, No. 3, pp. 242–245.

Figure 3. In this 2.77 ct emerald, the zones of internal reflection have soft edges that reveal the presence of gota de aceite. *The phenomenon is best appreciated by rocking the emerald back and forth, as shown in these two views. Photomicrographs by R. Ringsrud.*

wing effect" (*efecto aleta de mariposa*). In fact, the term *gota de aceite* has largely fallen from favor in Colombia, perhaps because of the negative connotations associated with the word *oil* in recent decades (due to its use in filling emerald fissures). Yet the expression has been used by at least three generations of Colombian emerald dealers, and the optical effect may increase the value of a stone significantly.

In six years of studying this phenomenon, the author has detected it in only one out of every 1,000 or so fine emeralds, personally viewing about 18 unmistakable examples and 50 muted ones. The contribution of *gota de aceite* to the desirability of such stones is similar to that of the velvety effect in Kashmir sapphires. In both cases, the diffusion of light spreads the area of color, thus reducing extinction (figure 4).

What Is *Gota de Aceite*? The *gota de aceite* effect was first mentioned in an article by E. J. Gübelin in the Winter 1944–45 issue of *Gems & Gemology* (figure 5). At the time, this phenomenon was thought to be a result of calcite grains microscopically "dusting" the interior of the emerald, disrupting the growth structures. Dr. Gübelin described an emerald "exhibiting a great mass of calcite inclusions (presumably precipitation during growth of the host mineral) which is responsible for the slightly oily appearance of some of the most beautiful and highly priced Colombian emeralds" (p. 179). Since then, the term *calcite precipitation* has also been used occasionally to describe this phenomenon (Gübelin and Koivula, 1986).

However, recent microscopic and microprobe studies by John I. Koivula have demonstrated that calcite inclusions are probably not involved with creating the *gota de aceite* effect (pers. comm., 2008). Instead, unusual irregularities in the internal crystal structure are responsible for the roiled dispersion of light. These microscopic features are apparently the result of irregularities in growth conditions during emerald crystallization that gave rise to both raised hexagonal terminations and geometric depressions. After their formation, these growth structures were further overgrown with emerald. When the columnar structure is viewed parallel to the c-axis, the roughly hexagonal forms are visible (figures 6 and 7, left). However, when the emerald is turned 90° and viewed perpendicular to the c-axis (i.e., perpendicular to the table of the faceted emerald), the narrow cross-section of the columnar structure is revealed (figure 7, right). Mr. Koivula also reported that, using Raman spectroscopy, he did not identify any calcite inclusions in two emeralds with *gota de aceite*.

Although this author could find no reference to emeralds with this effect from sources other than Colombia, there is no apparent reason why these growth structures could not occur in emeralds from other localities.

Similar Optical Effects. Some emeralds have an attractive soft appearance that is not caused by true *gota de*

Figure 4. This image dramatically reveals how extinction in an emerald (the dark area at the top of this 3.60 ct stone) can achieve color through the soft diffusion of light caused by the gota de aceite *effect. Photomicrograph by R. Ringsrud; magnified 20×.*

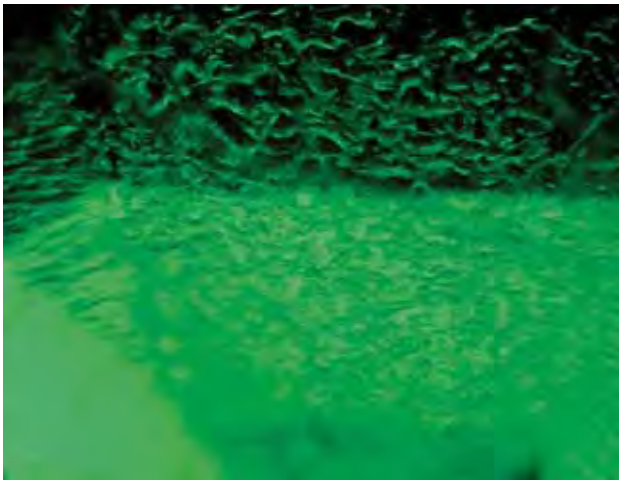

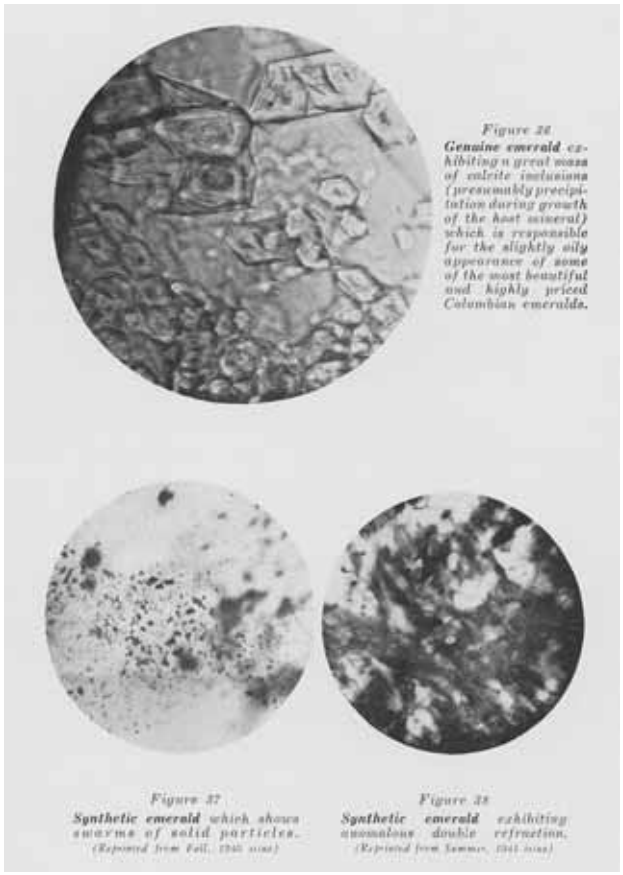

Figure 5. Although Dr. E. J. Gübelin did not specifically use the expression gota de aceite*, his figure 36 caption refers to the "oily appearance" of an emerald he documented in the 1940s (Gübelin, 1944–1945). This is comparable to the roiled appearance (like water in cognac) of a hessonite. Dr. Gübelin recognized that this effect occurs in some of the finest emeralds.*

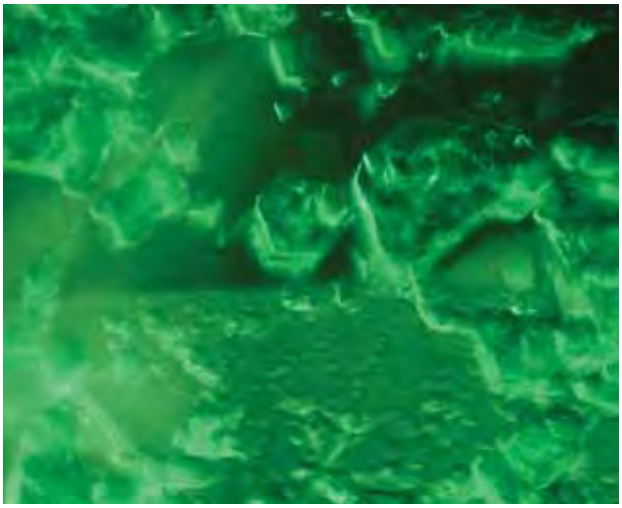

Figure 6. This image shows the geometric growth structures within a gota de aceite *emerald. Note the similarity to the Gübelin image (figure 5, top). Photomicrograph by R. Ringsrud; magnified 30×.*

aceite growth structures. For example, the author saw a 3.07 ct emerald that was initially thought to show *gota de aceite*, but microscopic examination revealed the presence of a large field of two- and three-phase inclusions (figure 8). Because these inclusions were semitransparent, they effectively mimicked *gota de aceite*. Such a phenomenon could be called a pseudo–*gota de aceite* effect.

It should also be noted that the *gota de aceite* effect in fine Colombian emeralds may appear somewhat similar to the roiled growth zoning observed in many hydrothermally grown synthetic emeralds, particularly those from Russia. Therefore, careful examination is important to avoid a potential misidentification.

Figure 7. The growth structures that cause gota de aceite *can be difficult to see or capture on film. In the photo on the left, the shadowing technique was used to reveal the geometric (but not necessarily hexagonal) growth features seen when looking down the c-axis. On the right, the same emerald is shown in a view perpendicular to the c-axis, which reveals the typically narrow band of columnar structures associated with this phenomenon. Photomicrographs by John I. Koivula; fields of view 2.1 mm.*

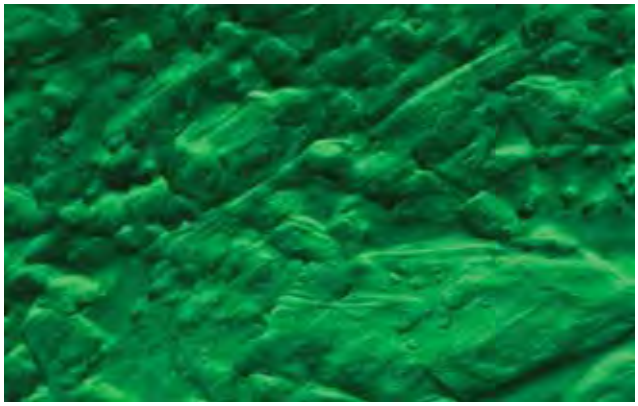

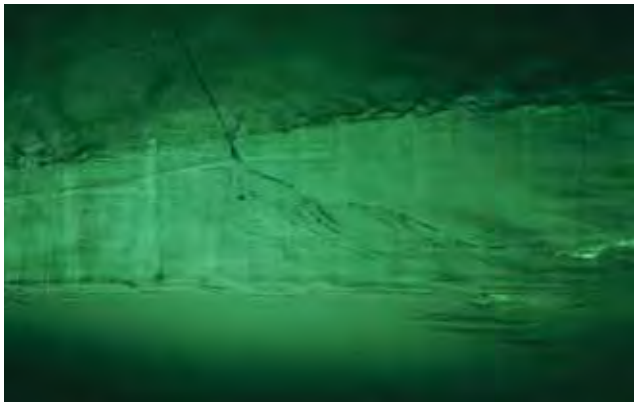

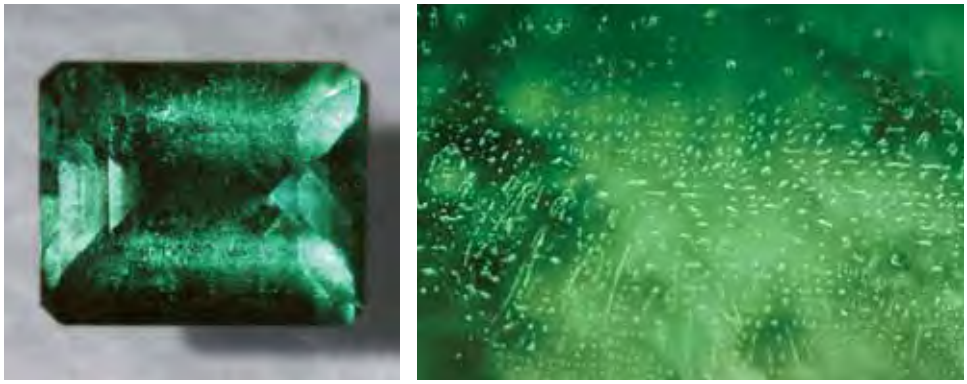

Figure 8. Although this 3.07 ct emerald (left) was initially thought to show gota de aceite, *subsequent microscopic examination revealed that its soft appearance was caused by a field of minute fluid inclusions (right; magnified 22×). Photos by R. Ringsrud.*

***Gota de Aceite*: Use and Misuse of the Term.** Confusion of nomenclature with regard to *gota de aceite* has taken two forms. Because the phrase is typically used only with respect to very fine emeralds, some exceptional stones are labeled with this term even though they do not actually have the effect. The mere fact that the emerald is very fine often inspires the owner or seller of the stone to use *gota de aceite* as a superlative.

There is also confusion relating to "old mine" emeralds. *Old mine* is another term applied to rare and fine emeralds, but it refers to the provenance and age of the emerald. Specifically, it refers to emeralds sent by the Spanish colonies in the New World to Europe and Asia in the 16th, 17th, and 18th centuries, as well as Swat Valley and Habachtal emeralds of the same era (Schwarz and Giuliani, 2002). However, the presence of *gota de aceite* may wrongly inspire the owner or seller to call the stone "old mine."

Conversations with Colombian emerald dealers and connoisseurs reveal common agreement that the traditional definition of *gota de aceite* requires the presence of growth structures, either angular or hexagonal, as seen in figures 6 and 7 (Oscar Baquero, Ray Zajicek, Jimmy Rotlewicz, Roland Schluessel, and Pierre Vuillet, pers. comms., 2007). By definition, the structures causing the effect must be transparent. Because of variations in the size of the hexagonal structures and in the thickness of the zone containing them, the strength of the effect is also quite variable. This author recommends that gemologists classify *gota de aceite* as either "muted," "moderate," or "distinct." To be considered "distinct," the effect should be clearly visible to the naked eye as the stone is rocked back and forth. It is important to move the stone to reveal the liquid-like softening of the texture that is the hallmark of *gota de aceite*.

Conclusion. The term *gota de aceite* refers to a specific optical effect that is seen rarely in Colombian emeralds; it is not meant to be a marketing superlative. It is hoped that this article will call attention to some inconsistencies of nomenclature in a trade full of arcane terms and meanings. Only with careful examination and an understanding of the growth structures that cause the effect can it be determined that an emerald merits the descriptor *gota de aceite*.

ABOUT THE AUTHOR

Mr. Ringsrud owns Ronald Ringsrud Co. in Saratoga, California, and has been importing Colombian emeralds into the United States for 25 years.

ACKNOWLEDGMENTS

The author thanks John I. Koivula (GIA Laboratory, Carlsbad) for sharing his knowledge and experience and for supplying photomicrographs. Ray Zajicek (Equatorian Imports Inc., Dallas, Texas) is thanked for providing emerald samples as well as information. German Sanchez (Universal Emeralds Ltda., Bogotá) and Gabriel Acuña (Esmeralda Gems, Los Angeles) provided emeralds and discussion. For additional insights, the author thanks Roland Schluessel (Pillar & Stone International Inc., Tiburon, California), Pierre Vuillet (Institut de Recherche pour le Développement, Paris), Guillermo Angarita (The Best Emeralds Ltda., Bogotá), and Jimmy Rotlewicz (Gemtec, Bogotá). Oscar Baquero (GemsMetal S.A., Bogotá) is also thanked for introducing the author to gota de aceite *emeralds 12 years ago.*

REFERENCES

Gübelin E.J. (1944–45) Gemstone inclusions. *Gems & Gemology*, Vol. 4, No. 12, pp. 174–179.

Gübelin E.J., Koivula J.I. (1986) *Photoatlas of Inclusions in Gemstones*. ABC Edition, Zurich, Switzerland, p. 252.

Hainschwang T. (2008) Extraordinary "gota de aceite" emerald submitted to the Lab. *GEMLAB Research Newsletter*, June, www.gemlab.net/website/gemlab/fileadmin/user_upload/Research/Gemlab-Newsletter-06-2008.pdf.

Schwarz D., Giuliani G. (2002) Emeralds from Asia. In G. Giuliani et al., Eds., *Emeralds of the World*, Lapis International, East Hampton, CT, pp. 62–63.

COLOR VARIATIONS AND PROPERTIES OF JOHACHIDOLITE FROM MYANMAR

Karen M. Chadwick and Christopher M. Breeding

To learn more about the rare gem material johachidolite, the authors used various analytical techniques to study 15 faceted samples from Myanmar that showed a range of colors: saturated orange, orange, yellow, desaturated yellow, and desaturated green. Both orange/yellow-hued and green samples showed trends for beryllium and the radioactive/radiogenic elements uranium, thorium, and lead. Orange/yellow samples also showed relatively constant rare-earth element (REE) concentrations, but the green samples had higher REE values, especially for the lighter elements.

Johachidolite—$CaAlB_3O_7$—is a rare borate mineral named after the Johachido district, North Korea, which is its type locality. Investigations of the Korean material (grains up to 1 mm) showed that it was transparent and colorless or semitransparent and white (see, e.g., Iwase and Saito, 1942; Aristarain and Erd, 1977). In 1998, Harding et al. reported on a relatively large (14.02 ct) pale yellow faceted specimen from Myanmar. The large size of that stone led to speculation that it could potentially be synthetic; however, a lack of information regarding synthesis of Ca-Al borates resulted in the conclusion that the specimen was probably natural. Kawano and Abduriyim (2007) published a compositional analysis of a bicolored rough sample, and showed that elemental concentrations in the two portions were different. Also in 2007, Peretti et al. published a comprehensive report on johachidolite based on over 500 faceted specimens and 200 rough samples. The purpose of the current article is to present further data and observations on this rare gem material, and offer some new conclusions.

Materials and Methods. In late 2007 and early 2008, Mark Kaufman loaned GIA 14 faceted johachidolites from Myanmar that ranged from 0.11 to 0.95 ct and varied from saturated orange to desaturated green (e.g., figure 1). Two of these specimens exhibited distinct color zoning—orange and desaturated yellow (e.g., figure 1, inset). We also had the opportunity to examine a 0.16 ct faceted stone that was sent to GIA's Carlsbad laboratory for an Identification Report.

Standard gemological testing was conducted on all 15 stones. We also performed energy-dispersive X-ray fluorescence (EDXRF) spectroscopy using a Thermo ARL Quant'X instrument (15 samples), Raman spectroscopy with a Renishaw InVia Raman system (514 nm laser excitation, 2000–100 cm^{-1} scan range, at room temperature; eight samples), and ultraviolet-visible–near infrared (UV-Vis-NIR) absorption spectroscopy using a PerkinElmer Lambda 950 UV/Vis Spectrometer (250–1000 nm scan range; four samples, approximately oriented to alpha and gamma directions using RI values from the table of each stone). Laser ablation–inductively coupled plasma–mass spectrometry (LA-ICP-MS) data were gathered for all 14 of the samples loaned to GIA using a Thermo X-Series II ICP-MS attached to a New Wave 213 nm laser ablation system (~10 J/cm^2 fluence, 40 μm spot, 7 Hz repetition rate, 1.0 liter/min He carrier gas flow rate that mixes with Ar before entering the ICP, and NIST reference standards). One or two random locations on the girdle were sampled by LA-ICP-MS for 12 of the stones, while the two strongly color-zoned stones were each sampled in both the lighter and darker regions. Specimens were separated into five color categories (saturated orange, orange, yellow, desaturated yellow, and desaturated green) for data comparison.

Results and Discussion. Examination of the original 14 stones loaned by Mr. Kaufman showed gemological properties (table 1) that were consistent in RI (n_α=1.717–1.718, n_γ=1.724–1.725) and birefringence (0.006–0.008), but

See end of article for About the Authors and Acknowledgments.
GEMS & GEMOLOGY, Vol. 44, No. 3, pp. 246–251.

Editor's note: Consistent with its mission, GIA has a vital role in conducting research, characterizing gemstones, and gaining knowledge that leads to the determination of gemstone origins. The gemstones studied in this article are not subject to the 2008 Burmese JADE Act, and their import was in accordance with U.S. law.

Figure 1. These seven johachidolites (0.19–0.95 ct) illustrate the range of colors in the samples from Myanmar examined for this study. From left to right, the samples are J15, J04, J01, J12, J02, J13, and J10. Two of the johachidolites analyzed in this study were distinctly color zoned, as shown in the inset (specimen J14, 0.21 ct). The apparent orange zone on the left side of the stone is actually a reflection of the color from the right side. Courtesy of Mark Kaufman; photos by C. D. Mengason and Robert Weldon (inset).

revealed a range in color, pleochroism, and intensity of fluorescence to long- and short-wave UV radiation. The long-wave fluorescence, in particular, showed a strong correlation with color category (see table 1): The orange samples were generally inert, the yellow specimens had weak-to-moderate blue reactions, and the green samples fluoresced strong blue. Our fluorescence observations were generally consistent with those of Peretti et al. (2007). Hydrostatic SG varied (3.23–3.67; mean = 3.46), but the values were reasonably uniform given the small size of some samples. Data collected for the stone sent in for the Identification Report (sample J06 in table 1) were similar to those from the other 14 samples. Characteristics for all 15 specimens were generally comparable with those reported by Peretti et al. (2007)—n_α = 1.716–1.717, n_γ = 1.725–1.728, birefringence = 0.008–0.012, SG = 3.44—although they did not note any pleochroism in their samples. Microscopic examination revealed "fingerprints," clouds of tiny inclusions, and fractures/cavities.

The Raman spectra were consistent with the published results of Harding et al. (1998) and Peretti et al. (2007). All of our Raman spectra contained the seven peaks specifically cited by Harding et al., but with the 684 cm^{-1} feature sometimes only occurring as a shoulder, rather than a defined peak. Similarly, our spectra showed the strongest Raman scattering in the direction perpendicular to the table (as opposed to perpendicular to the girdle); consequently, we observed the peaks at 1191 and 1112 cm^{-1} (the former most often as a shoulder) referenced by Peretti et al. in all of our table analyses, but not in most of our girdle analyses.

EDXRF analysis identified the presence of the following elements: Al, Ca (in major amounts), Fe (minor), Cu, Zn, Ga, Sr, and U (trace). Six of the 15 samples analyzed contained dramatically elevated levels of Th (J08–J13), two showed minor/trace levels (J14, J15), and the remaining seven had none. These results for Th, as well as for the other trace elements detected by EDXRF, later proved to be consistent with the data from LA-ICP-MS measurements.

Our LA-ICP-MS data showed some interesting results for elemental concentration versus color (again, see table 1). For some elements, chemical composition was variable and the data did not show any significant trends. However, the concentration of Be clearly decreased from the saturated orange samples through the desaturated yellow ones (figure 2; note that the color-zoned samples are not included), but the green samples did not show any appreciable trend for Be. Pb, Th, and U all showed a different trend—higher concentrations in the desaturated green and desaturated yellow samples relative to the saturated orange, orange, and yellow samples (figure 3; note that U is not shown, merely for brevity).

A representative subset of the REEs (La through Dy in table 1) all exhibited relatively little variation in the orange- and yellow-hued samples, but elevated levels in the green samples (figure 4; note that just La and Sm are

Figure 2. Be concentration decreased from the saturated orange to the desaturated yellow johachidolite samples.

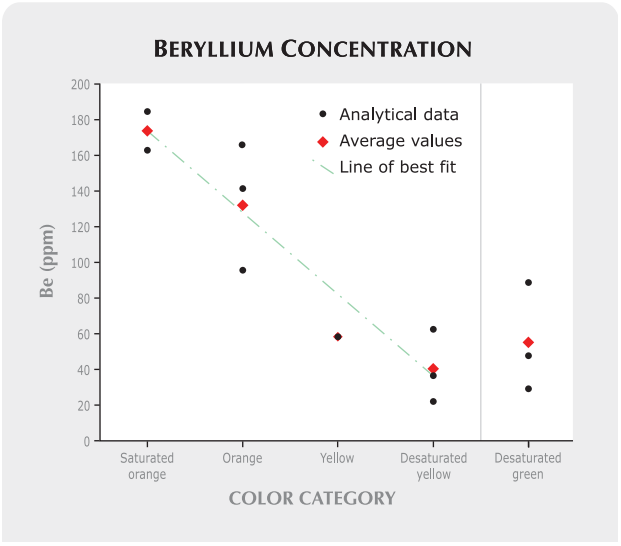

TABLE 1. Gemological properties and trace-element composition of 15 johachidolite samples in five color categories, including two bicolored stones.

Property	Saturated orange		Orange				Yellow
	J01	J02	J03	J04	J05	J06	J07
Weight (ct)	0.21	0.59	0.11	0.19	0.22	0.16	0.17
Color	Medium to medium dark yellowish orange	Medium dark yellowish orange	Medium yellowish orange	Medium orange-yellow	Medium orange-yellow	Medium orange-yellow	Medium light orangy yellow
Color zoning	None	None	None	None	None	None	Minor
Pleochroism	Moderate orange/yellow	Moderate orange/yellow	Moderate orange/yellow	Weak orange/yellow	Moderate orange/yellow	None	Weak orange/yellow
RI							
n_α	1.717	1.717	1.717	1.717	1.717	1.718	1.718
n_γ	1.725	1.725	1.724	1.725	1.725	1.726	1.725
Birefringence	0.008	0.008	0.007	0.008	0.008	0.008	0.007
SG	3.49	3.46	3.26	3.53	3.56	3.47	3.40
UV fluorescence							
Long-wave	Inert	Inert	Inert	Very weak blue	Inert	Inert	Weak blue
Short-wave	Inert	Inert	Inert	Inert	Inert	Inert	Inert
Trace elements (ppm)[a]							
Be	162.7	184.3	141.2	158.6	95.5	na	58.3
Na	40.2	72.5	78.3	31.9	73.4	na	62.4
Mg	366.5	134.5	50.8	298.8	202.8	na	146.8
Si	533.0	231.2	254.7	327.0	199.6	na	222.2
Ti	3.3	bdl	1.7	5.2	1.5	na	2.7
V	3.1	1.8	0.5	2.0	4.6	na	5.7
Cr	5.1	bdl	1.6	0.3	0.5	na	1.3
Fe	289.1	110.7	86.9	214.3	124.1	na	94.0
Zn	6.8	8.9	0.6	6.8	bdl	na	0.6
Ga	68.0	58.8	23.2	61.7	45.3	na	33.7
Y	2.5	1.1	0.8	1.4	2.2	na	0.7
La	7.6	3.1	1.8	8.7	5.6	na	4.6
Ce	17.9	6.2	3.5	15.6	11.3	na	14.8
Pr	1.9	0.7	bdl	1.5	1.4	na	1.7
Nd	5.0	3.4	1.1	5.2	4.8	na	6.7
Sm	0.6	0.6	bdl	1.1	1.1	na	1.8
Gd	0.7	0.3	bdl	1.0	0.9	na	0.8
Dy	bdl	0.3	bdl	bdl	0.5	na	bdl
Pb	1.0	1.0	0.8	1.8	1.0	na	1.5
Th	20.3	2.4	11.9	9.9	12.7	na	3.7
U	1.8	bdl	0.6	0.9	0.9	na	0.6

[a] *Chemical data were collected by LA-ICP-MS using NIST glass references and represent one spot per sample or the average of two spots per sample. Shaded elements show systematic variations between some color categories. Abbreviations: bdl = below detection limit; na = not analyzed.*

shown, again for brevity). Further, when the average rare-earth-element concentration for the green samples was ratioed to the average value for all the orange- and yellow-hued samples, the results (figure 5) clearly indicated an enrichment of the lightest REEs in the green material. Peretti et al. (2007) proposed four different types or generations of johachidolite—based in part on differences in amounts of light and heavy REEs—that varied from light green and light yellow (type 1) to vivid yellow through vivid orange (type 4).

The two distinctly zoned samples (J14 and J15; table 1) showed results consistent with the above observations for the orange and desaturated yellow stones. One of the specimens exhibited a bicolored response to long-wave UV radiation: The desaturated yellow area fluoresced moderate blue, while the orange region was inert; this is in agreement with the fluorescence trend noted for the unzoned samples in those two hues. For both zoned stones, the Be concentration was higher in the orange areas, as opposed to the desaturated yellow areas, while the radioactive elements (i.e., U and Th)

Desaturated yellow			Desaturated green			Orange	Desaturated yellow	Orange	Desaturated yellow
J08	J09	J10	J11	J12	J13	J14		J15	
0.12	0.23	0.95	0.20	0.24	0.60	0.21		0.25	
Extremely light yellow-orange	Extremely light yellow-orange	Light yellow	Extremely light green	Very light yellowish green	Very light yellowish green	Medium orange-yellow	Light yellow-orange	Light-to-medium orange-yellow	Light yellow-orange
None	None	None	None	Minor	None	Distinct		Distinct	
None	None	None	None	None	None	None		None	
1.718	1.718	1.717	1.718	1.718	1.718	1.717		1.717	
1.725	1.724	1.725	1.725	1.725	1.725	1.725		1.725	
0.007	0.006	0.008	0.007	0.007	0.007	0.008		0.008	
3.23	3.43	3.42	3.67	3.60	3.46	3.45		3.44	
Moderate blue	Moderate blue	Moderate blue	Strong blue	Strong blue	Strong blue	Inert	Moderate blue	Weak blue	Weak blue
Inert	Inert	Very weak blue/yellow	Weak blue	Weak blue/yellow	Weak blue/yellow	Inert	Inert	Inert	Inert
36.5	22.0	62.4	29.1	88.6	47.6	109.6	23.5	157.9	46.3
63.8	113.3	31.8	73.3	88.5	25.8	61.6	34.5	19.8	96.1
140.8	103.4	197.0	246.5	603.7	266.6	162.5	54.4	296.9	138.1
255.9	88.4	586.6	212.4	517.0	504.7	242.3	208.9	bdl	139.7
6.1	2.3	bdl	4.0	15.8	2.1	0.6	11.8	bdl	6.0
1.3	3.6	5.9	6.6	5.7	6.9	3.0	3.0	8.1	9.1
1.0	bdl	5.8	0.5	1.6	3.8	0.7	bdl	bdl	bdl
152.7	121.3	273.8	114.9	312.6	240.5	110.3	95.6	57.9	156.9
bdl	0.6	4.9	0.6	5.8	5.4	bdl	bdl	3.0	1.8
59.6	46.8	75.5	45.2	86.3	66.2	40.0	39.1	75.7	85.9
9.1	1.2	4.0	4.3	9.6	4.1	bdl	1.7	1.3	8.1
9.3	3.6	5.5	69.8	19.9	12.3	2.9	6.1	5.2	14.1
17.0	8.0	13.6	131.9	39.6	28.9	6.0	11.6	10.8	25.4
1.5	0.9	1.7	9.6	3.2	3.8	0.6	1.1	1.5	3.2
5.5	3.9	6.2	25.2	10.1	13.0	2.0	3.8	6.7	12.9
1.7	1.4	1.9	5.4	3.4	3.2	bdl	0.7	1.7	3.9
1.6	1.0	1.4	2.8	2.1	2.1	bdl	0.5	1.0	3.9
2.0	bdl	1.1	1.5	2.9	1.4	bdl	bdl	0.8	2.4
2.2	2.2	3.1	4.2	7.4	3.2	bdl	1.0	0.5	2.0
702.3	679.5	1050	1259	3718	1682	2.7	156.7	5.9	488.7
101.5	7.8	28.1	28.2	50.6	31.2	0.7	60.5	1.0	109.0

were less abundant in the orange parts. In addition, the REE concentrations were slightly lower in the orange regions.

Approximately oriented UV-Vis-NIR spectroscopy was performed on four samples from various color categories (orange, yellow, desaturated yellow, and desaturated green); the resultant spectra showed some notable differences in the UV-Vis wavelengths (figure 6). In the visible region, not surprisingly, the transmission windows correlated to sample color. The UV region, however, contained two distinct features: a broad shoulder at ~330–340 nm (visible only in the spectra for the gamma direction; not shown in figure 6) and, more obviously, a peak at ~375 nm. This peak was strongest in the spectrum of the desaturated green specimen, was smaller through desaturated yellow and yellow, and was absent from the spectrum of the orange sample. While this peak has been reported previously in the literature, its cause is unknown. We noted, however, good correlation between the thorium concentrations and this ~375 nm feature in the UV-Vis spectra; there were greatly elevated Th values in the desaturated

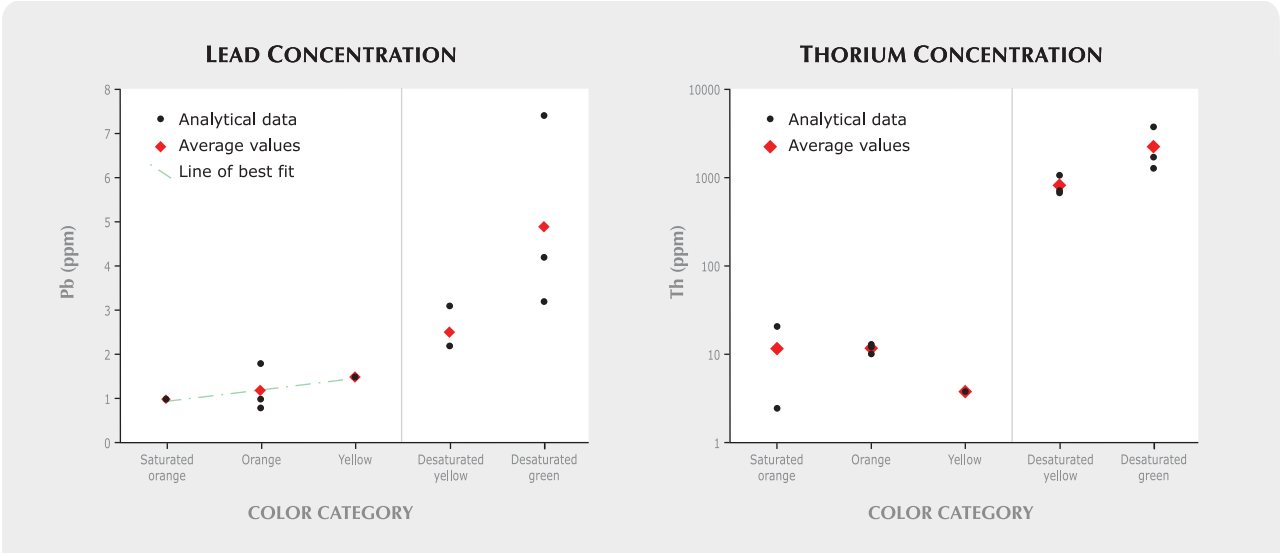

Figure 3. The concentrations of Pb (left) and Th (right; note logarithmic scale) are plotted for johachidolite samples from the various color categories. The desaturated green and desaturated yellow categories show higher concentrations than the others.

green and desaturated yellow samples and much lower Th concentrations in the orange and in most of the yellow stones. Thus, we hypothesize that Th may play an important role in the coloration of johachidolite. More work will be needed to test this observation; other authors have not found a similar correlation between Th and color (Peretti et al., 2007).

The observed trends in our data are in agreement with the results of Kawano and Abduriyim (2007), who performed LA-ICP-MS analysis on a color-zoned rough sample from Myanmar, and with those of Peretti et al. (2007), who performed LA-ICP-MS analyses on multiple samples, including a color-zoned one. Both studies noted higher concentrations of Be in the more saturated (yellow/yellow-orange) part of the rough compared to the colorless part, and correspondingly lower concentrations of Th and U. Kawano and Abduriyim also found higher concentrations of the REEs in the colorless portion; while our analyses generally detected similar levels for the REEs in the saturated orange through desaturated yellow samples, the

Figure 4. The concentrations of rare-earth elements were fairly constant in all johachidolite colors except for the desaturated green samples, which contained higher levels of these elements. Plotted here are the values for La (left) and Sm (right).

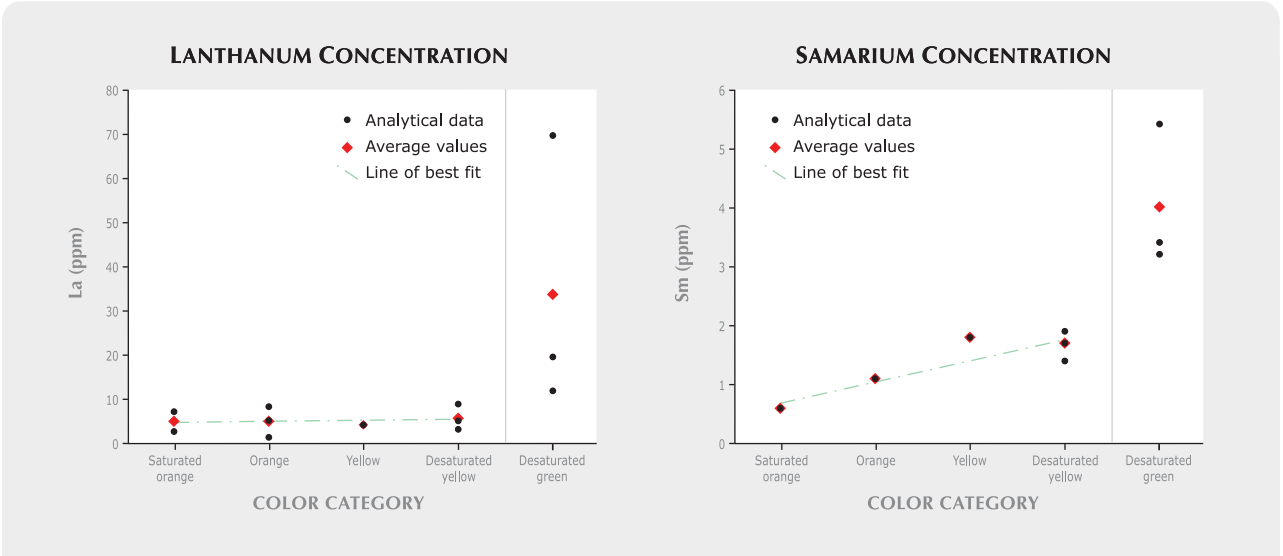

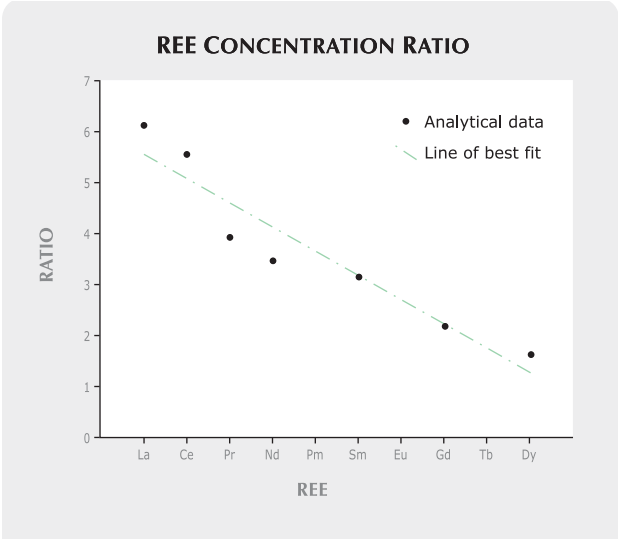

Figure 5. The ratios of average concentrations of REEs in the green samples to those of the orange- and yellow-hued samples show a systematic decrease from the light to the heavy elements. This reflects enrichment of light REEs in the desaturated green material. (Note that data for the rare-earth elements Pm, Eu, and Tb were not included in the analyses.)

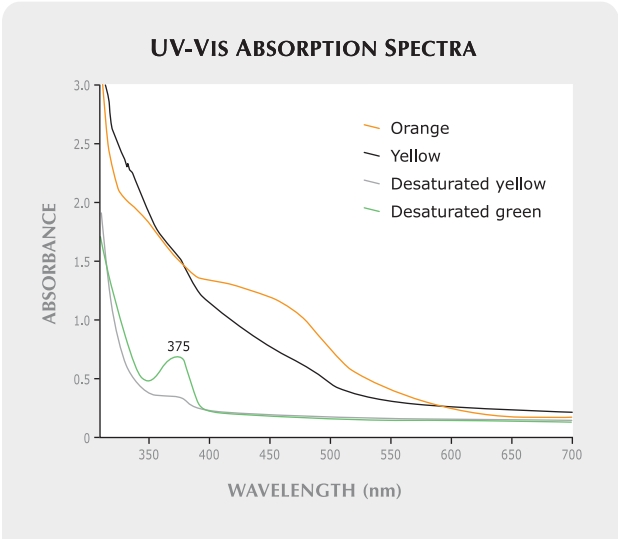

Figure 6. Approximately oriented (alpha direction) UV-Vis spectra for four of the samples—representative of four of the color categories (orange [J03], yellow [J07], desaturated yellow [J09], and desaturated green [J11])—showed different characteristics. The spectrum for the desaturated green sample has a particularly prominent peak at ~375 nm.

desaturated green samples showed clearly elevated concentrations. Also, in our analyses Th showed the greatest variation in concentration from saturated orange (average ~11 ppm) to desaturated green (average ~2220 ppm); similarly, Kawano and Abduriyim (2007) reported Th concentrations ranging from 30 ppm in the yellow part of their zoned sample to 1590 ppm in the colorless part.

Conclusions. In a study of faceted johachidolites from Myanmar, we found trends in UV fluorescence versus color—with the strongest reaction for the green samples—as well as in trace-element concentrations versus color. Gemological properties were generally consistent with those presented by other authors, except that we noted pleochroism in some of our samples. Beryllium values decreased from the saturated orange specimens through the desaturated yellow ones, while Pb, Th, and U values all showed elevated concentrations in the green and desaturated yellow samples relative to the saturated orange, orange, and yellow ones. The REEs showed relatively similar concentrations in the orange/yellow specimens, but distinctly elevated levels in the green samples, and also exhibited fractionation (greater amounts of the lighter REEs). Our UV-Vis data suggested a possible link between Th concentration and color, but the cause of color in johachidolite bears further research.

ABOUT THE AUTHORS

Ms. Chadwick (karen.chadwick@gia.edu) is staff gemologist, and Dr. Breeding is research scientist, in the Identification Department at the GIA Laboratory in Carlsbad, California.

ACKNOWLEDGMENTS

The authors thank Mark Kaufman (Kaufman Enterprises, San Diego, California) for loaning johachidolite samples for this research, and Alethea Inns (staff gemologist, GIA Laboratory, Carlsbad) for help with collecting observations.

REFERENCES

Aristarain L.F., Erd R.C. (1977) Johachidolite redefined: A calcium aluminum borate. *American Mineralogist*, Vol. 62, pp. 327–329.

Harding R.R., Francis J.G., Oldershaw C.J.E., Rankin A.H. (1998) Johachidolite—a new gem. *Journal of Gemmology*, Vol. 26, No. 5, pp. 324–329.

Iwase E., Saito N. (1942) Jōhachidōlite—a new mineral of hydrous fluoborate of sodium, calcium and aluminium. *Scientific Papers of the Institute of Physical and Chemical Research*, Vol. 39, No. 1077, pp. 300–304.

Kawano J., Abduriyim A. (2007) Natural johachidolite. *Gemmology*, Vol. 38, No. 459, pp. 12–14.

Peretti A., Peretti F., Tun N.L., Günther D., Hametner K., Bieri W., Reusser E., Kadiyski M., Armbruster T. (2007) Gem quality johachidolite: Occurrence, chemical composition and crystal structure. *Contributions to Gemology*, Vol. 5, pp. 1–53.

LAB NOTES 2008

EDITORS
Thomas M. Moses and
Shane F. McClure
GIA Laboratory

A CITRINE with Eye-Visible Brazil-Law Twinning

The New York laboratory recently received a dark brownish orange pear shape for identification. The stone, which measured approximately 18.70 × 10.20 × 7.30 mm, was set in a yellow metal brooch with numerous variously colored and shaped transparent stones (figure 1). Standard gemological examination and the presence of mineral inclusions established that the stone was natural citrine. Of particular note was the striking eye-visible Brazil-law twinning decorated by cloud-like inclusions (figure 2, left).

Brazil-law twinning is common in amethyst and citrine, but typically it can only be seen by viewing the stone parallel to the optic axis between crossed polarizers. Finding the optic-axis direction in a faceted stone can be challenging because colored gemstones are usually oriented for maximum weight retention and best color, not crystallographically. Thus, Brazil-law twinning is usually seen only after careful observation using a polariscope and an immersion cell (see, e.g., R. Crowningshield et al., "A simple procedure to separate natural from synthetic amethyst on the basis of twinning," Fall 1986 *Gems & Gemology*, pp. 130–139).

Figure 1. The dark pear-shaped citrine at the far left in this brooch shows eye-visible Brazil-law twinning with fiber-optic light.

However, the twinning in this stone was visible to the unaided eye using only fiber-optic light. Even more unusual, the appearance was stronger with fiber-optic light (again, see figure 2, left) than between crossed polarizers (figure 2, right). In this case, according to GIA chief gemologist John Koivula, the mounting and the faceted shape of the stone both limit the transmission of polarized light through the citrine, although immersion of the piece (even in water) should result in a clearer polarized light pattern. The fact that the

Editors' note: All items are written by staff members of the GIA Laboratory.

GEMS & GEMOLOGY, *Vol. 44, No. 3, pp. 252–260.*

Figure 2. The Brazil-law twinning in this citrine is visible to the unaided eye using only fiber-optic light (left); it is also more easily seen with fiber-optic light than between crossed polarizers (right). Field of view ~7.9 mm.

stone was cut with the table perpendicular to the optic axis was also a factor in the ease of observation, as was the presence of a cloud of minute particles trapped in the Brazil twin lamellae.

Wai L. Win

Figure 3. Sponge coral, because of its porous nature, is often impregnated with plastic to strengthen it. Note the continuous pattern of plastic-filled polyp cavities in this 54.88 ct piece.

COMPOSITE of Coral and Plastic

The Carlsbad laboratory recently began receiving multiple orange beads of various sizes and shapes for identification. These initially appeared to be a plastic-impregnated variety of coral that is often referred to as "sponge coral" because of the numerous natural voids typical of this material. It is a common practice to fill these voids with plastic to strengthen the coral and make it more suitable for jewelry use (figure 3).

Close inspection of these beads revealed, however, that although they contained many of the round- to oval-shaped cavities that are characteristic of sponge coral, there was a lack of continuity in the pattern. There were large areas that had no structure at all and instead were filled with numerous tiny irregular pieces of some other material (figure 4) as well as gas bubbles. It became clear that these samples were in fact a composite of fragments of sponge coral held together with an orange plastic that had been mixed with a ground-up material, probably coral or shell.

To confirm this identification, we soaked a single bead in a bath of methylene chloride for approximately 48 hours. This caused the plastic component to dissolve and the bead to disintegrate into its composite pieces (figure 5).

This is the first time we have encountered such an assemblage with coral, although a similar intent was evident in recent samples of ruby fragments held together with a high-lead-content glass. Therefore, we described the new material on the laboratory report in the same manner, calling it a "coral/plastic composite."

Kimberly M. Rockwell

Figure 4. Unlike the bead in figure 3, this sample (8.65 ct) proved to consist of pieces of coral and other natural materials held together with a plastic binder.

Figure 5. After it was soaked in methylene chloride to remove the plastic, the bead in figure 4 disintegrated into fragments.

DIAMOND

Black Diamonds Colored by Hydrogen Clouds

The vast majority of black diamonds submitted to the laboratory have been treated by high-temperature heating in a vacuum. These stones are usually opaque and heavily fractured. Black graphite inclusions, induced by heating, block light transmission and cause the host diamond to appear black.

Recently at the New York laboratory, we examined two cut-cornered rectangular brilliants, weighing 2.69 and 2.72 ct, that were submitted at the same time. Both were color graded Fancy black (figure 6), but unlike treated black diamonds, these two stones were transparent to fiber-optic illumination and contained numerous dense hydrogen clouds but no evidence of graphite inclusions. A strong 3107 cm^{-1} peak, attributed to hydrogen, was visible in their mid-infrared absorption spectra (figure 7). After nitrogen, hydrogen was the most abundant impurity in these diamonds. The dense hydrogen clouds are responsible for the natural black color.

Figure 6. The black color of these diamonds (2.69 and 2.72 ct) was caused by dense inclusions of hydrogen clouds.

The two diamonds were almost identical, and we suspected that they had originated from the same crystal. This was supported by DiamondView images of the two stones, which showed striking almost-mirror-image butterfly structures in the center of their table facets (figure 8).

Figure 7. The mid-IR absorption spectra of the two Fancy black diamonds show a strong 3107 cm^{-1} peak, attributed to hydrogen.

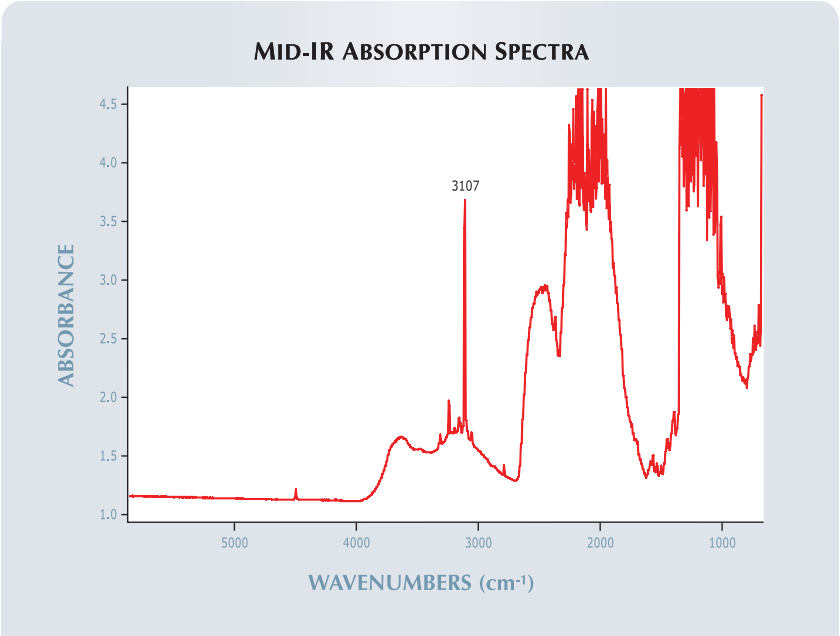

The distribution of these symmetrical hydrogen clouds throughout the crystal was dictated by the {100} growth direction of the diamond lattice (W. Wang and W. Mayerson, "Symmetrical clouds in diamond—the hydrogen connection," *Journal of Gemmology*, Vol. 28, No. 3, 2002, pp. 143–152). The tables of both diamonds were cut and oriented in the {100} crystal face direction, resulting in the butterfly images that indicated their origin from the same piece of rough.

The grading reports we issued for these two stones stated that they had a natural origin of color.

Paul Johnson

Irradiated Diamond: An Easy Call

Given the complexity and variety of diamond treatments these days, it is not often that the nature of a stone can be decided with a relatively quick look through the microscope. Heat, radiation, and pressure are applied and reapplied to both natural and synthetic diamonds; surface-reaching cracks are filled with glass; surfaces are coated; and the geologic origin indicated by mineral inclusions is negated through the application of focused laser energy and acid boiling. The equipment needed to conclusively identify treatment in diamonds is becoming increasingly

Figure 8. The symmetry of the DiamondView images indicates that the two black diamonds were cut from the same crystal. Butterfly ~3 mm wide.

expensive, highly analytical, and fully computerized.

So, though it does not happen often anymore, it is refreshing to encounter a treated diamond that requires only a microscope and gemological training to determine whether and how it was treated. Recently, a 4.06 ct dark orange-brown, marquise-shaped brilliant provided just such an opportunity.

The stone, which was submitted for origin-of-color determination, measured 17.95 × 8.09 × 4.86 mm. Viewed face-up with the unaided eye, it appeared to have an evenly distributed bodycolor. Viewed through the microscope, however, its story was completely different. The orange-brown color of this type IIa diamond was clearly concentrated along the pavilion facet junctions and around the culet (figure 9), creating a slightly distorted version of the so-called umbrella effect that results from irradiation treatment applied in a cyclotron. Bombardment of a diamond in a cyclotron generally produces an "olive" green color. If such a stone is then heated in air to 590–620°C, the color will change to an orange-brown (J. I. Koivula, *The MicroWorld of Diamonds*, Gemworld International, Northbrook, IL, 2000, pp. 64–65), which presumably is what happened to this diamond. Although decades ago many diamonds were treated in cyclotrons, we rarely encounter them in the laboratory today, probably because detecting the treatment is such an "easy call."

John I. Koivula and Laura L. Dale

Figure 9. The obvious orange-brown color zoning along the facet junctions of this cyclotron- and heat-treated diamond makes the treatment determination easy. Field of view ~1.5 mm.

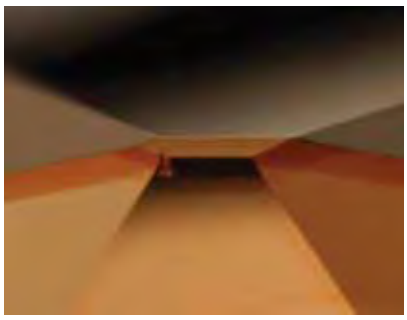

Natural Type Ib Diamond with Unusual Reddish Orange Color

Few natural diamonds contain detectable levels of isolated nitrogen. These stones usually display an orange-yellow color, occasionally with brownish modifiers. The trade refers to some stones in this group as "canary" yellow. In the New York laboratory, however, we recently examined a diamond with isolated nitrogen that was an unusual reddish orange color.

This 1.32 ct round-cornered square brilliant (6.18 × 6.14 × 4.42 mm) was color graded Fancy reddish orange (figure 10), which is very rare in natural-color diamonds. It was inert to conventional long-wave ultraviolet (UV) radiation, but showed very weak orange fluorescence to short-wave UV. With magnification, this diamond revealed clouds of tiny particles that spread out across most of the table facet and exhibited both symmetrical and irregular shapes. Clouds are a very common feature in natural type Ib diamonds, and with this exception the color was distributed evenly. The infrared absorption spectrum revealed that this stone contained a substantial amount of isolated nitrogen (34 ppm). In addition, it contained about 11 ppm of the A aggregate of nitrogen. The occurrence of A aggregates contributed to the formation of the H3 defect, which was distributed along several sets of lamellae and exhibited clear green fluorescence in the strong UV radiation of the DiamondView.

The UV-visible–near infrared (UV-Vis-NIR) absorption spectrum (figure 11), collected at liquid-nitrogen temperature, displayed a very smooth absorption curve with no sharp peaks. The absorption increased dramatically from ~620 nm to the high-energy side, with total absorption at wavelengths below 480 nm. This type of absorption pattern could be attributed to a specific concentration of isolated nitrogen, and created a transparent window in

Figure 10. The unusual color of this 1.32 ct type Ib Fancy reddish orange diamond could be attributed to a specific concentration of isolated nitrogen. Reddish hues are very rare for natural type Ib diamonds.

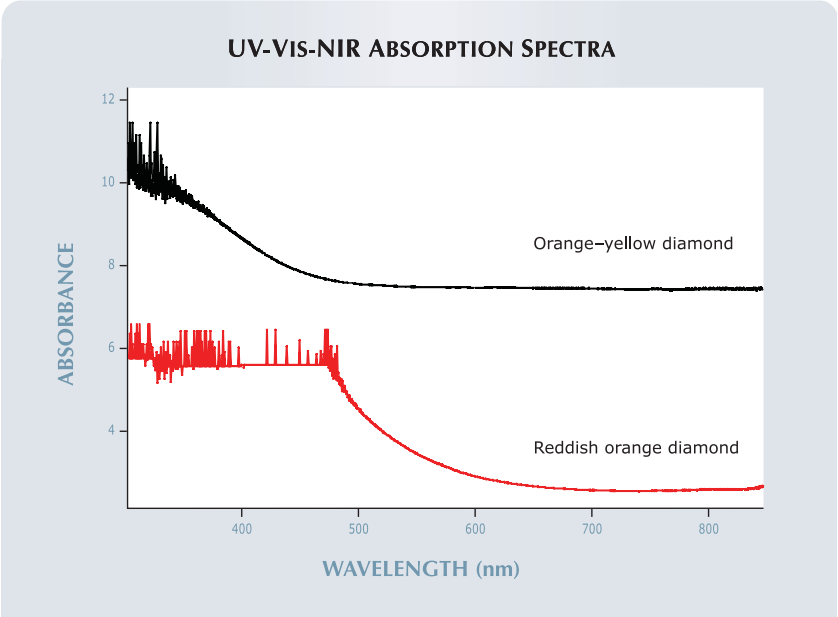

Figure 11. In its UV-Vis-NIR spectrum, the 1.32 ct reddish orange diamond showed much stronger absorption in the yellow-green region than do typical type Ib diamonds colored by isolated nitrogen (e.g., top spectrum). Spectra offset vertically for clarity.

the red-orange region. The color contribution from the H3 defect was trivial, if any. With either higher or lower concentrations of isolated nitrogen, there might not have been a reddish hue.

Examination of this special diamond indicated that reddish hues can be present in some rare type Ib diamonds, in addition to the well-known orange-yellow colorations.

Wuyi Wang

Observed Oddities in Diamond

Occasionally, features we observe in diamond are appreciated for their appearance alone rather than any scientific value they might have (e.g., Lab Notes: Winter 2007, pp. 363–364; Summer 2008, pp. 157–158). Olivine is one of the most common inclusions in diamond, and usually no second thought would be given to such an inclusion beyond its effect on the diamond's clarity grade. At the Carlsbad laboratory, however, we recently observed an olivine inclusion in a diamond that was interesting because it had the appearance of a winged insect (figure 12). The anatomy of the crystal was unusual, consisting of a hexagonal cross-section and a bulbous shape that, when combined with the associated cleavage fracture "wings," reinforced the resemblance to a moth or mayfly.

Burned patches on a diamond are likewise nothing out of the ordinary—normally just a surface feature that can affect the polish grade. Recently, though, a stone submitted to the Carlsbad laboratory was observed to have an unusually deep polish feature with a decidedly "tropical" appearance (figure 13). The burn—on an extra facet—resembled flowers or ferns; similar to ferns, it appeared almost fractal in nature. Covering the entire extra facet (approximately 0.55 mm wide), the burn feature had surprising depth of relief, which was especially evident at the facet edges.

These two features show us, once again, that the seemingly mundane task of grading diamonds can prove interesting with the application of a little imagination.

Karen M. Chadwick

Figure 12. This olivine inclusion and its associated cleavage fracture (left) resemble a winged insect at high magnification (right). Length of the crystal is ~0.56 mm.

Figure 13. The burn on this extra facet resembles ferns or flowers and has surprising depth of relief, readily seen at the facet edges. Field of view ~0.7 mm.

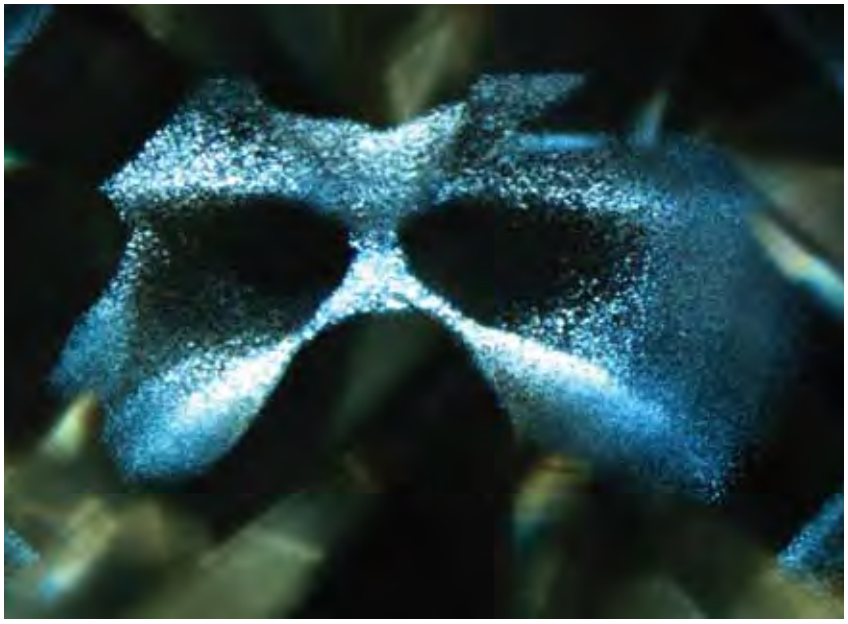

Figure 14. Discovered in a brownish green type Ia diamond, this hydrogen cloud has a unique three-dimensional shape reminiscent of a Venetian party mask. Field of view ~2.9 mm.

"Party" Diamond

In past Lab Notes sections, we have reported on a variety of cloud patterns in diamonds (e.g., Spring 1999, pp. 42–43; Fall 2000, pp. 255–256; Spring 2001, pp. 58–59). Cloud formations in diamonds are actually phantoms mimicking the growth of their hosts. As such, most clouds have stellate or cruciform habits that can be described geometrically by the isometric crystal system that governs the structure of single-crystal diamonds. Of course, there are exceptions to every rule, and the hydrogen cloud pictured in figure 14 definitely fell into that category.

As is typical with hydrogen clouds, this one was hosted by an off-color type Ia diamond, in this case a dull brownish green round brilliant cut that was submitted to the Carlsbad lab for an origin-of-color determination. While this was a routine submission, the pattern shown by the more-or-less centrally located phantom cloud was anything but routine. When examined with fiber-optic illumination from the side, the cloud had the appearance of a Venetian mask, similar to those worn by partygoers at a masquerade ball. Given the cloud's unique and complex appearance, it was impossible to clearly describe its geometry in terms of the known crystal habits of diamond (see, e.g., V. Goldschmidt, *Atlas der Krystallformen*, Vol. 3, C. Winters, Heidelberg, Germany, 1916).

While we thought we recognized both octahedral and dodecahedral structural components, the "eye" holes in the mask-shaped cloud—which were devoid of light-scattering, cloud-forming particles—did not seem to fit either morphology. This cloud's appearance was so unusual in our experience that we felt it worthy of documentation, even though a geometric description was not possible.

John I. Koivula and Laura L. Dale

Pinkish Brown Diamond with Mantle-Mineral Inclusions

Among natural purple-to-pink diamonds, some are distinguished by color concentrations along octahedral {111} glide planes. When the colored glide planes are positioned properly, the otherwise subtle pink hue is intensified. Our observations have revealed that almost all purple-to-pink diamonds with glide planes are type IaA with moderate-to-high concentrations of nitrogen, which indicates a correlation between the formation of glide planes and the nitrogen aggregation state. In the New York laboratory, we recently examined a large diamond of this type. Gemological and spectroscopic analysis revealed some interesting features, including unique mantle-mineral inclusions.

The 4.29 ct diamond was color graded Fancy pinkish brown (figure 15). It had an unusual cutting style: a modified heart brilliant with a wavy top edge in place of the usual lobes. It fluoresced moderate blue to long-wave UV radiation and very weak yellow to short-wave UV. With magnification, sharp parallel glide planes with concentrated pink color were easily observed throughout most of the stone. The strong UV radiation of the DiamondView revealed linear green fluorescence perfectly aligned along the glide planes due to localized

Figure 15. The color of this 4.29 ct Fancy pinkish brown diamond is caused by a broad absorption band at ~550 nm related to internal glide planes. It is also notable for its unusual cutting style and mineral inclusions.

Figure 16. This large octahedron (~1.0 mm long) seen in the pinkish brown diamond is believed to be chromite. The parallel lines on its surface very likely formed simultaneously with the glide planes in the host.

formation of H3 defects. As expected, the infrared and UV-Vis absorption spectra showed that the diamond was type IaA with a high concentration of nitrogen, and that it was colored by absorption at ~550 nm.

An outstanding feature of this diamond was its inclusion of minerals from the earth's mantle. Colorless euhedral inclusions of varying sizes were confirmed to be olivine by Raman spectroscopy. In addition, a large black octahedron was present at the top of the wavy region (figure 16). Based on its color, luster, and morphology, it was probably chromite, though we could not confirm this with Raman analysis. An interesting feature of this inclusion was the presence of parallel lines on its surface (again, see figure 16), which very likely formed simultaneously with the glide planes in the host diamond. This is the first time we have observed glide planes in both the host diamond and its chromite inclusion.

Wuyi Wang

Large EMERALD-in-Quartz Specimen

Laboratory gemologists deal with the identification of treatments, synthetics, and imitations on an almost routine basis. So when the opportunity to examine a truly rare natural gem material arises, it is greeted with a good deal of enthusiasm. Such was the case recently, when we examined a large transparent quartz crystal that contained eye-visible, gem-quality inclusions of emerald (figure 17), a first in our experience. An intergrowth of emerald and quartz was reported in the Summer 2000 Lab Notes section (pp. 164–165), but that faceted stone was essentially half semitransparent white quartz and half low-quality emerald—quite different from the specimen described here.

The 69 g quartz crystal (74.05 × 31.91 × 20.41 mm) was reported by emerald dealer Ron Ringsrud (Ronald Ringsrud Co., Saratoga, California) to have been recovered from the La Pita mine in Boyacá, Colombia. He submitted the specimen for gemological examination with the permission of the owner, German Sanchez (Universal Emerald CI Ltda., Bogotá).

As seen in figure 17, the quartz crystal was well formed, singly terminated, and highly transparent, making the emerald inclusions clearly visible without magnification. A large cluster of emerald crystals reached the surface of the host quartz, which indicates they formed first and then the quartz grew over them. The largest of the inclusions was 23.50 mm long (figure 18), so an emerald spectrum was easily obtained when it was examined in transmitted white light with a handheld prism spectroscope. This is one of the most unusual "inclusion" specimens we have ever seen.

John I. Koivula and Shane F. McClure

Figure 17. This 74.05-mm-long specimen of emerald in quartz was recovered from the La Pita mine in Boyacá, Colombia.

Figure 18. The largest of the inclusions (23.50 mm long) in the quartz crystal revealed a characteristic emerald spectrum when examined with a handheld spectroscope.

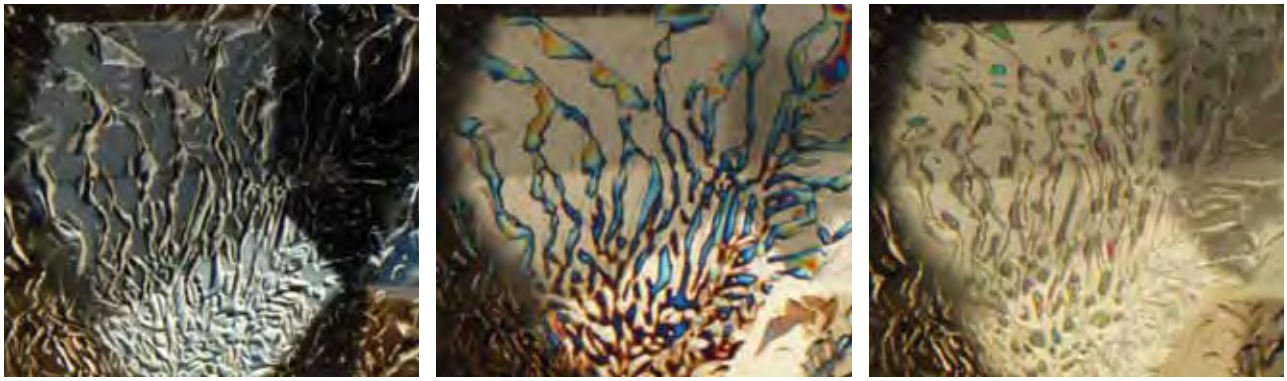

Figure 19. Raman analysis proved that this fluid-appearing layer of transparent inclusions in a grossular reportedly from Tanzania (left) was calcite. In one orientation in polarized light (center), some of the calcite inclusions display interference colors, while others do not. Upon 90° rotation of both polarizer and analyzer (right), the previously extinct portions now show interference colors, while the previously bright areas do not. Field of view 1.8 mm.

Calcite "Melt" in GROSSULAR

In the past, we have seen unusual-looking transparent features in pale-colored grossular from Lelatema, Tanzania, that appeared as if they might have been molten at the time they were included in their garnet hosts. Although those inclusions were examined microscopically, and under polarized light proved to be solid and birefringent, on these previous occasions we did not have the opportunity or capability to identify them.

Recently, we encountered a 0.39 ct transparent light green, round mixed-cut grossular—reportedly from Tanzania—with inclusions that were very similar to those we had previously observed. As shown in figure 19 (left), this feature was a transparent dendritic or fan-shaped layer of fluid-like inclusions that gave the strong appearance of once having been molten.

The pale green garnet host had the expected RI of 1.731. It exhibited a weak-to-moderate orange reaction to long-wave UV radiation, while the inclusion layer was inert. In polarized light, the transparent areas of the inclusion system behaved curiously. In one orientation of the polarizer and analyzer, a portion of the system showed bright interference colors while the remainder was extinct (figure 19, center). When the polarizer and analyzer were rotated in unison by 90°, the previously extinct area showed bright interference colors, while the previously bright portion went extinct (figure 19, right). This clearly revealed that *two* crystallographic orientations were present within this system. Examining all three photomicrographs side by side as a triptych made this curious relationship quite obvious.

We then employed laser Raman microspectroscopy to determine the nature of this feature. The results clearly showed that the melted-looking inclusions were calcite. Calcite is known to occur in garnets from this and other localities (such as hessonite from Sri Lanka), but it has not previously been reported with such a "liquid" form. An interesting bonus in this investigation was that a tiny, nondescript, rounded inclusion near the girdle and the pavilion surface, which was also analyzed, proved to be elemental sulfur, though it was too small to show its characteristic yellow color. Sulfur has not been encountered before as an inclusion in garnet. The investigation of this grossular showcases the power and increasing usefulness of Raman analysis in inclusion studies.

John I. Koivula and Alethea Inns

A Rare Yellow Trapiche SAPPHIRE

The 40.57 ct transparent-to-semitransparent yellow oval tablet in figure 20 was submitted to the New York laboratory as a "star sapphire." Standard gemological testing identified it as a natural sapphire. What caught our eye immediately, though, was that the star-like appearance was not asterism, but rather a "trapiche"

Figure 20. This 40.57 ct yellow sapphire (21.60 × 16.30 × 8.60 mm) exhibits the trapiche growth phenomenon.

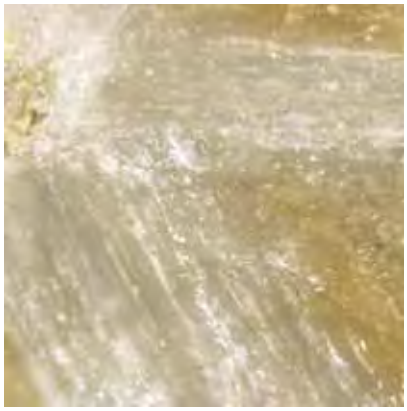

Figure 21. The core of the trapiche crystal is visible at upper left, with the arms formed by radiating spokes containing ribbons of thin films. Field of view ~3 mm.

pattern: a fixed reflective six-armed star with associated color zoning.

While trapiche patterns are common in emerald, they are less common in corundum, in which they are typically restricted to ruby (see, e.g., K. Schmetzer et al., "Trapiche rubies," Winter 1996 *Gems & Gemology*, pp. 242–250; I. Sunagawa et al., "Texture formation and element partitioning in trapiche ruby," *Journal of Crystal Growth*, Vol. 206, No. 4, 1999, pp. 322–330). Trapiche sapphire is considerably rarer (see, e.g., box A of T. Hainschwang et al., "Trapiche tourmaline from Zambia," Spring 2007 *Gems & Gemology*, pp. 36–46), and most is blue to gray: An extensive literature search with the help of staff members at GIA's Liddicoat gemological library revealed no published accounts of yellow trapiche sapphire.

Exposure to long-wave UV radiation caused this stone to fluoresce weak-to-moderate orange in the triangular growth sectors, while the "arms" fluoresced weak orange or were inert; the short-wave UV reaction was weaker. Fluorescent Cr lines at ~680 nm and an absorption line at 450 nm in the desk-model spectroscope indicated the presence of trace amounts of Cr and Fe, respectively.

A small core area parallel to the c-axis formed the center of the star formation. Reflected light best revealed the inclusions. The triangular growth sectors had a yellow bodycolor and were less included—with mostly fluid remnant "fingerprints," two-phase inclusions, and reflective films—than the radiating spokes. The arms were nearly colorless and to the unaided eye appeared to contain abundant needles. With magnification, these "needles" could be resolved into narrow ribbons of reflective thin-film inclusions in planes that were approximately perpendicular to the core or c-axis (figure 21). Metallic, small dark, or irregular transparent crystals were present in both the arms and triangular growth sectors.

These differences in inclusions, color, and growth structure suggest that the sapphire crystallized from its core outward, with the sectors and arms probably growing concurrently but at different rates. Note that the definition of *trapiche* varies, with some referring to it as skeletal growth resulting in inclusions trapped in the arms of the star, or being composed of a different material than the host (Hainschwang et al., 2007). Other definitions include preferential exsolution of inclusions in the dendritic and growth sectors, or structure- and growth-related chemical variations that result in color-causing mechanisms differentiating the arms (K. K. Win, "Trapiche of Myanmar," *Australian Gemmologist*, Vol. 22, No. 6, 2005, pp. 269–270). Although many of the reported trapiche corundums—and rubies in particular—have arms composed of distinct mineral phases, this stone was primarily composed of corundum throughout. Even so, the GIA Laboratory categorized this sapphire as "trapiche" due to its distinct core, inclusion pattern, and growth structure. It is the first yellow trapiche sapphire we have seen.

Donna Beaton

PHOTO CREDITS
Jian Xin (Jae) Liao—Figures 1, 6, 15, and 20; Wai L. Win—Figure 2; C. D. Mengason—Figures 3, 4, and 5; Paul Johnson—Figure 8; John I. Koivula—Figures 9, 12 (left), 14, and 19; Elizabeth Schrader—Figure 10; Karen M. Chadwick—Figures 12 (right) and 13; Wuyi Wang—Figure 16; Robert Weldon—Figures 17 and 18; Donna Beaton—Figure 21.

COLORED STONES AND ORGANIC MATERIALS

Using cucumbers to unearth dendritic agates in central India. Even though fashioned chalcedony from central India has been used in jewelry for over three centuries—at least since the reign of Maharaja Chhatrasal in the 1600s—relatively few examples of the superb dendritic agates produced there have been seen in the West. Tarun Adlakha, of Indus Valley Commerce, Ghaziabad, India, recently exhibited a large collection of them in the United States at the 2008 Tucson Gem and Mineral Show.

According to Mr. Adlakha, these agates (e.g., figures 1 and 2) are mined in Madhya Pradesh Province on the fringes of the Deccan Traps (thick basalt flows). These flows erupted at the end of the Cretaceous period, approximately 65 million years ago, forming one of the world's largest volcanic regions. Some agates are mined along tributaries of the Narmada River, but the vast majority are recovered some distance away, from gray-green volcanic ash deposits, at depths of 12–25 m. Mr. Adlakha noted that the Narmada River agates are found as waterworn pebbles and rocks that yield mostly transparent and finely imprinted dendritic gems, whereas the distal sources produce material that is largely translucent. The production includes colorless, orange, red, yellow and, rarely, purple material.

Editor's note: Interested contributors should send information and illustrations to Brendan Laurs at blaurs@gia.edu or GIA, The Robert Mouawad Campus, 5345 Armada Drive, Carlsbad, CA 92008. Original photos can be returned after consideration or publication.

GEMS & GEMOLOGY, Vol. 44, No. 3, pp. 262–282

Miners work the riverbed twice a year during the region's dry seasons. One unusual approach taken by local miners is to plant cucumbers and other deep-rooting vines in the riverbed, where the fast-growing roots reportedly loosen the soft alluvium, causing many nodules to rise to the surface. These are then easily collected for cutting.

Indus Valley Commerce fashions about 10,000 cabochons per year at their shops in Banda, Uttar Pradesh. Mr. Adlakha describes this production as "prime grades"; about 10% are considered "exceptional," but only a small amount, 5% or less, are dendritic. The most experienced and skillful cutters are used to fashion the rare dendritic pieces, because producing fine finished stones from this

Figure 1. This dendritic agate cabochon from central India measures 6.2 × 4.7 cm. The fern-like inclusions are composed of manganese and/or iron oxides trapped between layers of the agate. Photo by R. Weldon.

Figure 2. This shield-shape dendritic agate measures 6.1 × 5.2 cm. Photo by R. Weldon.

material is a specialized skill, particularly for large cabochons (e.g., 18–25 cm). Because the dendrites are only a few microns thick, the margin of error is extremely small; thus, the cabochons are cut by hand rather than with a saw. As a result, it can take a cutter several days to fashion a single stone. The finished cabs are typically 2–5 mm thick.

For more information on these agates, see M. C. Venuti and M. Pantò, "Il mistero delle dendriti indiane [The mystery of the Indian dendrites]," *Rivista Gemmologica Italiana*, Vol. 2, No. 3, 2007, pp. 181–191.

Robert Weldon (robert.weldon@gia.edu)
GIA Library, Carlsbad

Fluorite impersonating blue color-change garnet. Garnet comes in almost every color, but collectors continue the quest for stones showing a blue hue. This goal seemed within reach in the late 1990s, with the discovery of "blue" color-change pyrope-spessartine from Bekily, Madagascar. These stones commonly appear blue-green in daylight and purple in incandescent light (see K. Schmetzer and H.-J. Bernhardt, "Garnets from Madagascar with a color change of blue-green to purple," Winter 1999 *Gems & Gemology*, pp. 196–201). Yet only a few euhedral garnet crystals have been reported from Bekily (see Summer 2003 Gem News International [GNI], p. 156); most are irregularly formed fragments.

Therefore, one of us (JH) was quite excited about the prospect of documenting a relatively large (1.1 × 1.0 × 0.9 cm) well-formed crystal thought to be blue garnet from Madagascar. The gem-quality sample was seen at the 2008 Tucson gem shows, and kindly loaned by Jasun and Mandy McAvoy (Asbury Park, New Jersey). Its crystal form was similar to the previously published specimens of pyrope-spessartine from Madagascar, and it displayed a color change from violetish blue to purplish pink (figure 3).

Although the crystal's morphology, isotropic optic character, and color-change behavior were consistent with those of garnet, Raman analysis at the GIA Laboratory proved that it was actually fluorite. This was quite a surprise to all who were involved with this specimen, which apparently had never been tested. In hindsight, the crystal appeared remarkably similar—in its modified cubic crystal form as well as its color—to some of the color-change Ethiopian fluorites documented in the Summer 2007 GNI section (pp. 168–169).

Jim Houran (jim_houran@yahoo.com)
Mineralogical Association of Dallas, Texas

Brendan M. Laurs

Colorless forsterite from Mogok, Myanmar. During the BaselWorld show in April 2008, the SSEF Swiss Gemmological Institute received a colorless 2.48 ct stone (figure 4, left) for testing. According to Mark Smith (Thai Lanka Trading Ltd., Bangkok), it was cut from rough found

Figure 3. Resembling color-change garnet from Bekily, Madagascar, this ~1 cm fluorite is violetish blue in daylight (left) and purplish pink in incandescent light (right). Photos by Robert Weldon.

Figure 4. The 2.48 ct colorless forsterite on the left is reportedly from the Dattaw mining area near Mogok, Myanmar. A 4.77 ct synthetic forsterite is shown on the right. Photo by H. A. Hänni, © SSEF.

in the Dattaw mining area of Mogok, Myanmar. Originally the stone was sold as humite, a hydrous magnesium silicate, but its refractive indices (1.638–1.677), birefringence (0.039), and hydrostatic SG (3.27) did not quite match. With Raman spectroscopy, the specimen was readily identified as forsterite, a member of the olivine group. (The olivine group consists mainly of two end-members, forsterite [a Mg silicate] and fayalite [an Fe silicate]. The most common gem variety from this group, *peridot*, is a Mg-rich olivine that contains some Fe—typically 5–15 wt.% FeO—resulting in a yellowish green to dark green color.) After BaselWorld, we began seeing more of this material from Myanmar (figure 5), most of which was largely free of inclusions and colorless to slightly yellow. As these contributors had previously seen only synthetic colorless forsterite (e.g., figure 4, right), a detailed study was undertaken to confirm the natural origin of these stones.

Figure 6. Whereas the peridot/fayalite samples showed no photoluminescence, the natural and synthetic colorless forsterites had distinct PL bands at different positions.

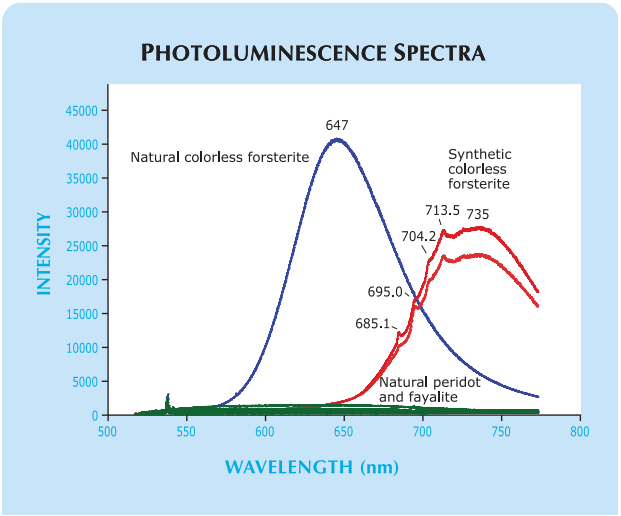

Figure 5. These nearly inclusion-free colorless forsterites from Myanmar range from 1 to 2 ct. Photo by Mark Smith, © Thai Lanka Trading Ltd.

Energy-dispersive X-ray fluorescence (EDXRF) analysis of the 2.48 ct stone revealed a minor amount of iron (0.1 wt.% FeO) and traces of Cr, whereas two colorless synthetic samples had only Mg and Si as main constituents and no Fe. The natural specimen showed a moderate red fluorescence to long-wave UV radiation, presumably related to its Cr content, whereas both synthetic samples fluoresced a weak chalky yellow. The reaction to short-wave UV was moderate yellow for the natural forsterite and weak yellow for both synthetic samples. Photoluminescence (PL) spectra excited with a 514 nm argon laser showed a broad luminescence band centered at 647 nm for the natural forsterite, while the two synthetic samples showed a band centered at 735 nm coupled with a series of small luminescence peaks at 685.1, 695.0, 704.2, and 713.5 nm; in contrast, five samples of natural peridot and fayalite (yellowish green to dark green and greenish brown) showed no photoluminescence (figure 6).

Using a microscope, we observed numerous hollow tubes and cavities (figure 7, left) in the synthetic samples. In contrast, the natural specimens showed partially healed fissures with fluid inclusions, as well as colorless idiomorphic (rhombic) crystal inclusions. These inclusions were identified by Raman spectroscopy as dolomite (figure 7, right), which fits well with the forsterite's reported origin in a marble deposit in the Dattaw area. The Mogok region is also known as a source for yellowish green to green peridot. The peridot is mined from the Pyanunggaung Mountains, in talc veins associated with ultramafic (Mg- and Fe-rich) rock (R. C. Kammerling et al., "Myanmar and its gems—an update," *Journal of Gemmology*, Vol. 24, No. 1, 1994, pp. 3–40).

Aside from their beauty, these new colorless forsterites may also prove enlightening to gemology students, as they clearly demonstrate the concept of isomorphous mixing within the olivine group. Between the forsterite and fayalite end-members are intermediate compostions with various amounts of iron replacing Mg on the same structural site (an isomorphous solid solution). The color is directly related to the iron concentration, ranging from colorless forsterite through yellowish green to dark green peridot, to dark brown fayalite (figure 8). As plotted in figure 9 (using the samples shown in figure 8, in addition to two samples of colorless synthetic forsterite), the greater substitution of Mg by Fe also leads to a marked increase in the RI and SG of the members of this solid solution. Similar observations

Figure 7. As shown on the left, abundant hollow tubes and cavities were seen in the synthetic forsterites (photomicrograph by H. A. Hänni, magnified 20×; © SSEF). On the right, this forsterite from Myanmar contains a somewhat regular pattern of fluid inclusions in a healed fissure, as well as rhombic dolomite inclusions (photomicrograph by M. S. Krzemnicki, magnified 35×; © SSEF).

are well known for other mineral groups with extensive chemical mixing, such as feldspars and garnets.

Michael S. Krzemnicki (gemlab@ssef.ch)
SSEF Swiss Gemmological Institute
Basel, Switzerland

Peter Groenenboom
AEL-Arnhem
The Netherlands

Colorless forsterite from Tajikistan. In addition to the gem-quality colorless forsterite from Myanmar now circulating in the trade (see the preceding GNI entry), colorless forsterite from Tajikistan recently became available. According to gem dealer Farooq Hashmi (Intimate Gems, Jamaica, New York), small quantities of this material have been produced from the Kukh-i-Lal skarn-type gem deposit in the southwestern Pamir Mountains, where it is found in association with clinohumite and spinel. Mr. Hashmi noticed a few of the colorless pieces of rough mixed with a 3+ kg parcel of clinohumite that he obtained in mid-2008. He cut a 3.54 ct gem from one of these pieces, and loaned it to GIA for examination.

Gemological characterization of this colorless pear-shaped brilliant (figure 10) yielded RIs of 1.637–1.669 (birefringence 0.032), a biaxial optic figure, and a hydrostatic SG of 3.26. It fluoresced weak orangy pink to short-wave UV radiation and weak red to long-wave UV. In addition to major amounts of Mg and Si, EDXRF spectroscopy revealed traces of Ca, Mn, and Fe. These properties are generally consistent with those reported for natural colorless forsterite (Spring 1999 Lab Notes, pp. 49–51; and K. Nassau, "Synthetic forsterite and synthetic peridot," Summer 1994 *Gems & Gemology*, pp. 102–108). The elements detected by EDXRF were confirmed with laser ablation–inductively coupled plasma–mass spectroscopy (LA-ICP-MS; calibrated with NIST glass standards), which

Figure 8. The 2.48 ct colorless forsterite is shown on the left, along with four peridot specimens and a fayalite. All members of the olivine group, these samples demonstrate the effect of increasing Fe concentration, from left to right. Data from these samples were used for figures 6 and 9. Photo by M. S. Krzemnicki, © SSEF.

*Figure 9. The SG and RI values of the olivine group (forsterite-fayalite) increase with Fe concentration, as shown here for the samples examined in this study. Similar relationships were illustrated by W. A. Deer et al. (*Rock-Forming Minerals—Orthosilicates*, Vol. 1A, 2nd ed., Longman, London, 1982, p. 184). The arrows show the points corresponding to the two synthetic forsterite samples; the other points correspond to the samples shown in figure 8.*

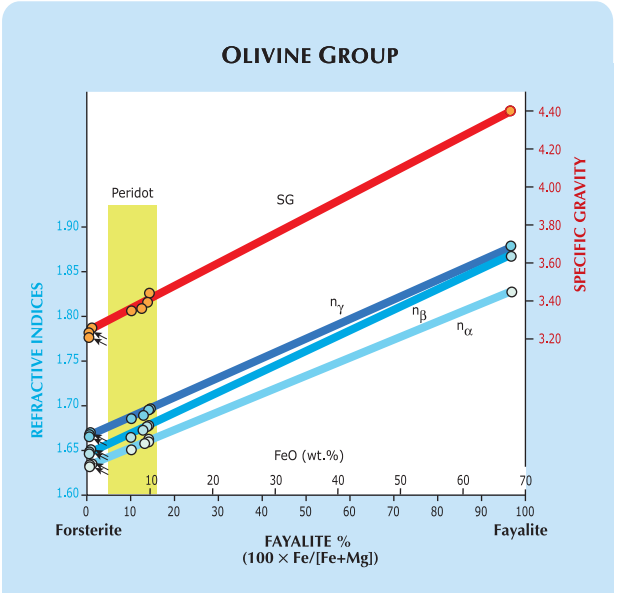

Figure 10. This colorless 3.54 ct forsterite reportedly came from Kukh-i-Lal, in the Pamir Mountains of Tajikistan. Photo by Robert Weldon.

showed average concentrations of 43.7 wt.% MgO and 0.34 wt.% FeO. As Mg is strongly dominant over Fe, the stone's composition lies near the forsterite end of the forsterite-fayalite series.

Microscopic examination showed a "fingerprint" composed of euhedral-to-subhedral inclusions (figure 11). With higher magnification and diffused lighting, these inclusions were observed to contain a white, fine-grained solid and—in some cases—a dark opaque crystal with a hexagonal outline (figure 12).

UV-Vis spectroscopy revealed weak absorption features at 451, 473, and 491 nm. Raman spectra taken with 488 and 514 nm laser excitation matched the forsterite and peridot spectra from our database. A 514 nm Raman scan was also taken up to 6000 cm^{-1} to investigate the fluorescence behavior. This showed a broad band with the maximum at approximately 4000 cm^{-1}, which is essentially equivalent to the fluorescent band reported for Burmese forsterite in the preceding GNI entry.

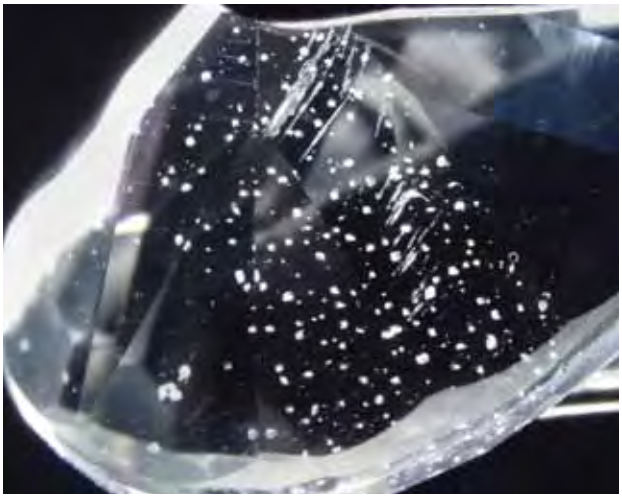

Figure 11. The forsterite contains a "fingerprint" composed of euhedral-to-subhedral inclusions. The linear features superimposed over the fingerprint are scratches. Photomicrograph by D. M. Kondo; field of view 7.2 mm.

David M. Kondo (david.kondo@gia.edu)
GIA Laboratory, New York

Natural impregnation of a rock by copper minerals. Rough stone buyer Werner Spaltenstein recently sent a blue-green rock (figure 13) to the SSEF Swiss Gemmological Institute for identification. The material was purchased in Tanzania, but its original locality is unknown. The blue portions resembled lapis lazuli, while the green patches looked like chrysocolla. This contributor had two cabochons polished to evaluate its suitability as an ornamental stone (again, see figure 13).

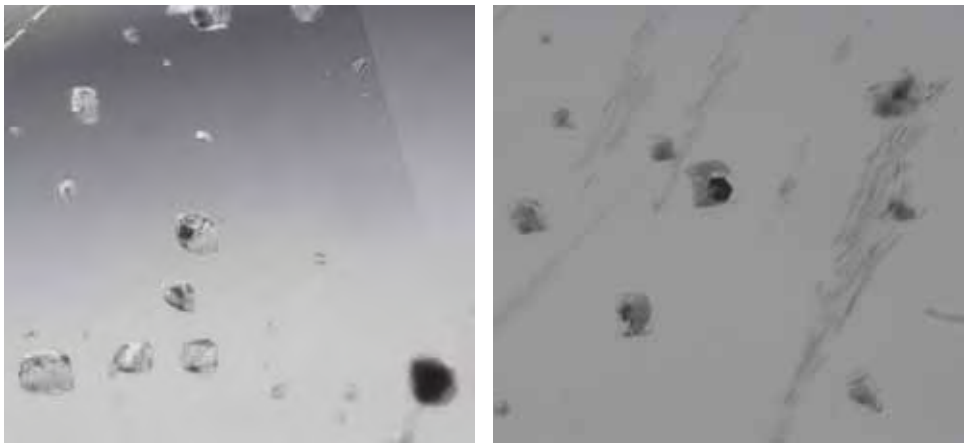

Figure 12. At higher magnification in diffused light, the inclusions forming the fingerprint in figure 11 were seen to consist of white solid phases (possibly within a liquid) and black particles. A hexagonal outline is evident for the black inclusion in the center of the right-hand photo. Photomicrographs by D. M. Kondo; fields of view 1.0 mm.

Viewed with low magnification, the material gave the initial impression of a color-treated coarse-grained igneous rock because of the numerous fractures and cleavage planes that were filled with a dark blue material (figure 14, left). With the client's permission, we prepared a petrographic thin section from the rock sample to analyze the component minerals and study their textural relationships (figure 14, right). Sodium-rich plagioclase, quartz, and muscovite mica were identified microscopically, and were confirmed via Raman spectroscopy. The blue material filling the fissures was not a dye but rather was identified as azurite; also present were malachite, chrysocolla, and chalcanthite. EDXRF chemical analysis showed Si, Al, Na, and some K and Ca. Copper was clearly present, as was Fe in low concentration.

The gemological properties of the material corresponded to the predominance of sodic plagioclase and quartz: The mean RI was 1.55, and the SG (by hydrostatic weighing of the large piece of rough in figure 13) was 2.69.

This ornamental material apparently formed when a plutonic rock was naturally fractured and impregnated with secondary copper minerals. "Jambolite" has been proposed as a trade name (*jambo* is a popular greeting in Swahili) for this colorful rock.

Henry A. Hänni

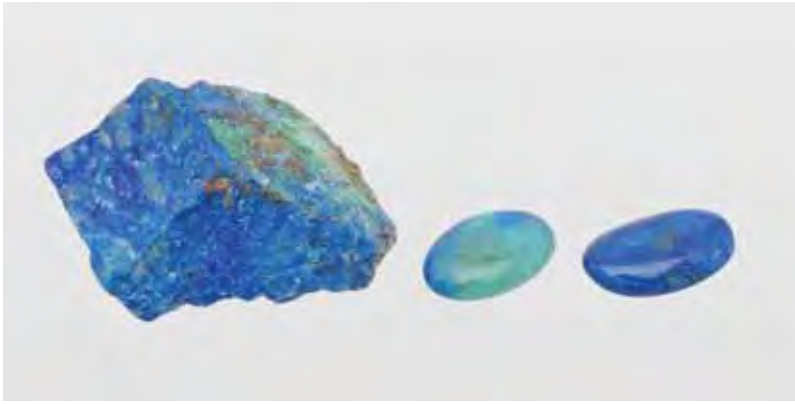

Figure 13. This feldspar-quartz-muscovite rock, sold in Tanzania, is naturally stained by secondary copper minerals. The blue color is due to azurite-filled veins, and the green is derived from malachite and chrysocolla. The cabochons are approximately 20 mm long. Photo by H. A. Hänni, © SSEF.

Update on the John Saul ruby mine, Kenya. In May 2008, this contributor and Dr. James E. Shigley of GIA Research visited the John Saul ruby mine, which is owned and operated by Rockland Kenya Ltd. in the Tsavo West National Park of southern Kenya. Our fieldwork was facilitated by Alice Muthama, director of Muthama Gemstones Ltd. in Nairobi. This report provides an update on underground mining activities and ore processing since the comprehensive Gem News entry on this deposit that was published by J. L. Emmett in the Winter 1999 issue of *Gems & Gemology* (pp. 213–215).

According to general manager Alfonse M'Mwanda and mine geologist/engineer Meshack Otieno, the underground mining began in late 2004, and is taking place in two locations on the property: the Kimbo shaft (in the former Kimbo pit), and the Gitonga shaft (in the former pit containing the Nganga and Miller open cuts; figure 15). The Kimbo shaft reaches a depth of 42 m and contains four levels of horizontal tunnels. It is currently the sole ruby producer, exploiting a mineralized zone that is 0.5–2 m thick. The Gitonga shaft is 21 m deep and contains one level. So far, no commercial ruby production has occurred from these exploratory workings but, according to old literature, good-quality stones were found in surface deposits in this area. Each shaft is joined to a separate ventilation shaft, and

Figure 14. At first glance (left), the rock appeared to contain a blue dye. Closer examination of a petrographic thin section with magnification (right) revealed the presence of azurite in veins crosscutting the feldspar-quartz-muscovite. Photomicrographs by H. A. Hänni, © SSEF; image width 5 mm (left) and image magnified 10× (right).

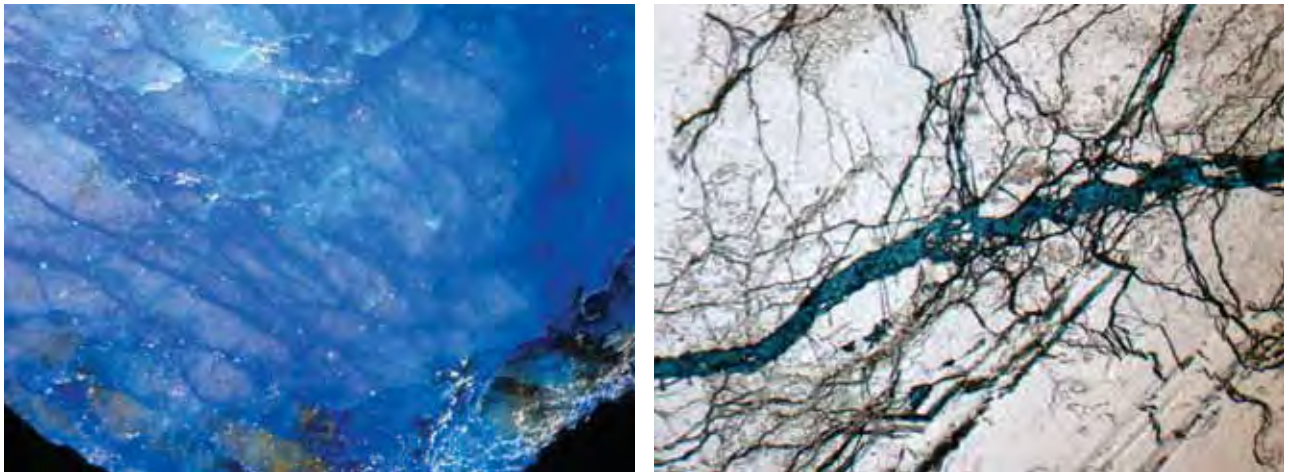

Figure 15. Underground mining at the John Saul ruby mine is taking place in two shafts, located at opposite ends of this large open pit. On the left is the Kimbo shaft, while the Gitonga shaft is visible in the distance to the right. The mine offices and sorting facilities are housed in the blue-green building on the left horizon. Photo by B. M. Laurs.

cranes are used to hoist the miners and the excavated material to the surface (figure 16). Mining is performed with pneumatic drills, and explosives are used only when necessary. The ruby-bearing material is transported underground in wheelbarrows (figure 17) before being loaded into a large container to be brought to the surface (again, see figure 16). The miners typically extend the tunnels 0.5 m day, and work 5½ days per week.

Of the 93 mine employees, 23 are involved with processing the ruby-bearing ore. The ore is stockpiled in a staging area, where it dries prior to being put through a rotating sieve. The fine-sized fraction is stockpiled, while the other material goes to a crusher and is then hand picked for ruby. Any matrix material is removed from the ruby by careful hammering and trimming as necessary with tile nippers (figure 18). The corundum is then sorted into three qualities, and each is sieved into several size fractions.

Since January 2008, the mine has produced approximately 200–500 kg per month of mixed-grade ruby and pink sapphire (excluding low-grade corundum). The rough is washed in hydrofluoric acid and heated in air to 1400°C for 12 hours (to brighten the darker colored material). Most of the rough is sent to Thailand for cutting, although a small amount is polished in Nairobi using Thai cutters.

Figure 16. Cranes are used to remove the excavated material from the shafts, as shown here at the Kimbo pit. A cage that is used for hoisting the miners is visible in the dump truck. Photo by B. M. Laurs.

Figure 17. Ruby-bearing material from the working face of the mine is moved to the haulage shafts in wheelbarrows. Photo by B. M. Laurs.

Figure 18. The corundum is carefully trimmed and sorted on site by Rockland Kenya Ltd. Photo by B. M. Laurs.

The cabochons are sorted into six quality grades, and only a small percentage possess top color and translucency (e.g., figure 19). At the time of our visit there was no facet-quality rough available, but the company anticipates better production as the deposit is explored at deeper levels.

Brendan M. Laurs

Ruby and other gems from Nanyaseik, Myanmar. The Nanyaseik (also called Namya or Nanyar Zeik) region of northern Myanmar has been known for nearly a decade as a source of fine-quality ruby, spinel, and other gems (see, e.g., H. Htun and G. E. Harlow, "Identifying sources of Burmese rubies," Fall 1999 *Gems & Gemology*, pp. 148–149, and Fall 2001 GNI, pp. 237–238). The mining area is situated about 50 km northwest of the town of Mogaung in Kachin State, at the southern edge of the Hukaung Valley, within an area extending from 25°35′15″ N, 96°31′00″ E to 25°39′30″ N, 96°34′20″ E. The following update on the localities and gem production from the area is derived mainly from field research by one of these contributors (KKW) for his PhD dissertation.

The region is generally flat, with a few hilly areas, and

Figure 19. The highest-quality ruby cabochons currently being produced at the John Saul mine show good translucency and a bright red color without any modifying tones. These heat-treated stones weigh approximately 1.2 ct each. Photo by B. M. Laurs.

densely forested. Within the area are two major rock units: granite and marble. Within the marble, associated minerals are variable in occurrence and consist of diopside, graphite, phlogopite, forsterite, spinel, and ruby.

Most of the gem production comes from secondary deposits that are worked by open-pit (*in-bye*) or square-shaft (*le-bin twin*) methods. There are five recognized mining areas within the Nanyaseik region:

- Ma Not Maw: First discovered in 2000, this area (25°37′12″ N, 96°32′45″ E) measures approximately 4 km^2 and experienced a major mining rush that subsequently led to the creation of Ma Not village. The gem-bearing layer (*byone*; 0.6–1.8 m thick) consists of reddish brown clayey soil that locally contains rock fragments. Within it have been found gem-quality ruby, sapphire, yellow-to-green zircon, pale yellowish green and dark green transparent epidote, and colorless topaz.
- Melin Chaung Maw: Situated near Nanyaseik village at 25°36′45″ N, 96°34′19″ E, this area is around 10 km^2 and produces large waterworn opaque rubies and sapphires that are locally called *carbolic*. Reddish brown transparent almandine, brown tourmaline, and zircon are also found. The gem-bearing layer is typically about 3 m thick and consists of clay and clasts of marble and granite.
- Khung Saing Zup Maw: The Khung Saing Zup village is located on the Mogaung-Phakant (Hpakan) road, and the mining area is situated ~100 m from the road. Here is found the largest open-pit mine (240 × 90 m) in the Nanyaseik region. The gem-bearing layer contains quartz, feldspar, mica, calcite, spinel, ruby, and epidote.
- Sabaw Maw: At 25°39′31″ N, 96°32′48″ E, this area lies in the northern part of the Nanyaseik region. Numerous shallow pits have produced quartz, spinel, sapphire, ruby, and pink painite.
- War Bu Maw: This area, located at 25°38′20″ N, 96°32′27″ E, is covered by swampy soil that overlays whitish clayey soil and organic material. Specific information on the gem materials from there is not available.

Nanyaseik rubies come in a variety of hues, including brownish red, orangy red, purplish red, and pinkish red. Colorless, yellow, pink, orange-yellow, "padparadscha," blue, and purplish blue sapphires are also found, though gem-quality blue sapphires are rare. Good-quality Nanyaseik rubies typically range from a few millimeters to one centimeter, while opaque stones up to 10 cm have been found. The crystals are usually somewhat rounded and equant, and may exhibit deep striations and rhombohedral parting. Conspicuous crystalline inclusions and oriented rutile needles have been noted. Trapiche specimens have also been found. Microprobe analyses of eight Nanyaseik rubies at HIAF (Heavy Ion Analytical Facility, CSIRO Exploration and Mining, North Ryde, New South Wales, Australia) revealed traces of V, Ti, Cr, Ga, Fe, Mn, Zr, Co, Cu, Ni, Sr, Y, and Pb. The low Fe content and presence of appreciable V and Cr apparently are responsible for the strong red fluorescence of Nanyaseik ruby.

Figure 20. This 0.56 g sapphire from Winza, Tanzania, is notable for its interesting color distribution. Note the purple-pink zone that is visible near the pinacoidal face, while the rest of the crystal appears colorless or blue of varying depth. Photo by G. Choudhary.

Figure 21. The sapphire crystal in figure 20 displayed numerous tiny hexagonal-to-subhexagonal growth hillocks on the pinacoidal face. Photomicrograph by G. Choudhary; magnified 80×.

Figure 22. The color distribution of the sapphire appeared to be restricted to zones with sharp edges that followed pyramidal directions within the crystal (left and center). The purple-pink areas also displayed alternating zones of lower and higher saturation along with some blue bands, oriented parallel to the pinacoidal face (right). Photomicrographs by G. Choudhary; magnified 35× (left), 45× (center), and 60× (right).

Nanyaseik spinel also shows strong fluorescence, and the crystals are commonly octahedral (sometimes combined with dodecahedral faces). The color is most commonly pink with an orange tint. Additional colors such as greenish blue, bluish green, pale pink, gray, orange, red, and brown have also been recovered. Internal features commonly consist of small translucent crystals, large prismatic crystals, octahedral spinel crystals, and fluid inclusions.

U Tin Hlaing (p.tinhlaing@gmail.com)
Dept. of Geology (Retired)
Panglong University, Myanmar

Kyaw Khaing Win
Yangon, Myanmar

An interesting zoned sapphire crystal from Winza, Tanzania. Recently discovered rubies from Winza in central Tanzania have gained popularity for their bright red color and transparency (Summer 2008 GNI, pp. 177–180). Sapphires have also been reported from this deposit (V. Pardieu and D. Schwarz, "Field report from Winza," *Rapaport*, Vol. 31, No. 26, 2008, pp. 173–175), but they have not received as much attention.

At the Gem Testing Laboratory in Jaipur, we had an opportunity to characterize a 0.56 g sapphire crystal (figure 20) that was brought to our attention by Shyamala Fernandes of Jaipur. She obtained the crystal from Jacob Hoyer of Italy, who purchased it directly from a Winza miner. The crystal's appearance immediately pointed to sapphire due to its characteristic pyramidal habit, which was terminated by a pinacoidal face; it also exhibited faint horizontal striations along the pyramidal faces, in addition to tiny hexagonal-to-subhexagonal growth hillocks on the pinacoid that were observed only at high magnification (figure 21).

The most interesting feature of the crystal was its color zoning. The area nearest the pinacoid was purple-pink, which gradually shifted to colorless and then blue (again, see figure 20). The latter color increased from light to deep blue to almost black toward the lower end of the crystal, making it appear opaque. When magnified, this color distribution seemed to be restricted to zones with sharp edges that mostly followed pyramidal directions within the crystal (figure 22, left and center). In addition, the purple-pink area displayed zones of alternating saturation along with some blue zones that were oriented parallel to the pinacoidal face (figure 22, right, also illustrated in M. S. Krzemnicki and H. A. Hänni, "New Tanzania mine uncovers source of exceptional rubies," *InColor*, Spring 2008, pp. 46–47).

When the crystal was viewed along the c-axis, we observed a transparent purple-pink core that was surrounded by a dark blue to black rim (figure 23). This effect reminded us of Mong Hsu rubies, where typically the central core is dark blue and the outer rim red; in this crystal, the zoning was reversed. However, we could not determine whether this core was colorless and the purple-pink color was visible because of the zone at the tip of the crystal, or if the core itself was purple-pink.

Figure 23. When the sapphire crystal was viewed along the c-axis, the central core appeared transparent purple-pink and was surrounded by a deep blue to black rim. The apparent pink color might be due to the presence of the pink zones near the pinacoid. Photomicrograph by G. Choudhary; magnified 35×.

Figure 24. This 2.5 g tourmaline, reported to be from Nigeria, proved to have an interesting internal feature. Photo by G. Choudhary.

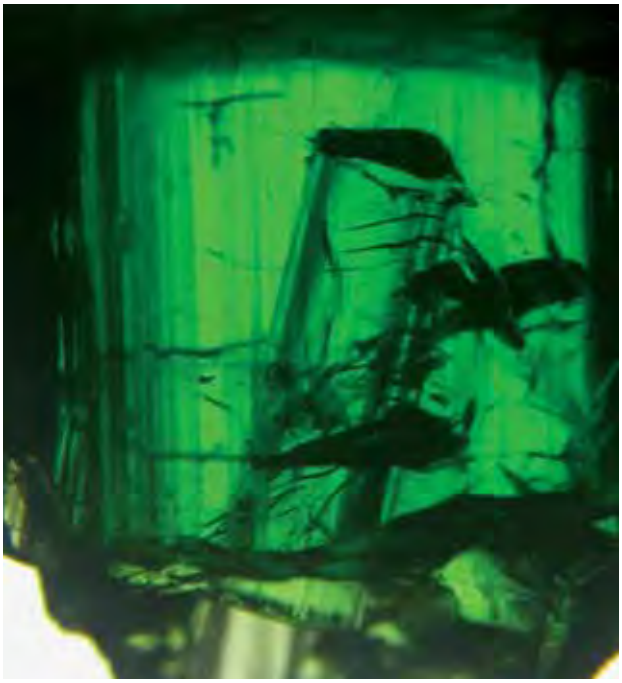

Figure 25. With transmitted light and magnification, the tourmaline in figure 24 was seen to contain an elongated crystal. It displayed weak striations on the prism faces, which were terminated by low-angle pyramidal faces (that appear dark in this image). Photomicrograph by G. Choudhary; magnified 10×.

No mineral or fluid inclusions were seen, possibly due to the dark color of most of the crystal; the color zones described above were observed only where the crystal was relatively transparent.

Since its discovery, the Winza deposit has produced some fine rubies, along with interesting specimens such as this sapphire. With further exploration, a wider range of material may be expected.

Gagan Choudhary (gtl@gjepcindia.com)
Gem Testing Laboratory, Jaipur, India

A tourmaline crystal within a crystal. Recently, we had the opportunity to study an unusual 2.5 g tourmaline crystal (figure 24) that contained an intergrowth of a second, smaller tourmaline. This specimen, reportedly from Nigeria, was loaned by Mr. S. K. Ajmera (Poorva's, Jaipur). It was transparent and displayed characteristic tourmaline morphology, including a prismatic habit, a roughly triangular cross section with broken terminations, and striations along the length of the prism. It was bright green when viewed from the sides, but much darker down the c-axis. From its appearance, the crystal was readily identified as tourmaline.

Figure 26. The included crystal displayed an etched surface along the length of its prism faces (left, magnified 80×). When examined at certain angles with fiber-optic light, the pyramidal faces of the included crystal appeared bronzy, revealing complex patterns of etching and/or growth hillocks (center, magnified 65×). Some angular growth features were present just below the pyramidal faces (right, magnified 80×). Photomicrographs by G. Choudhary.

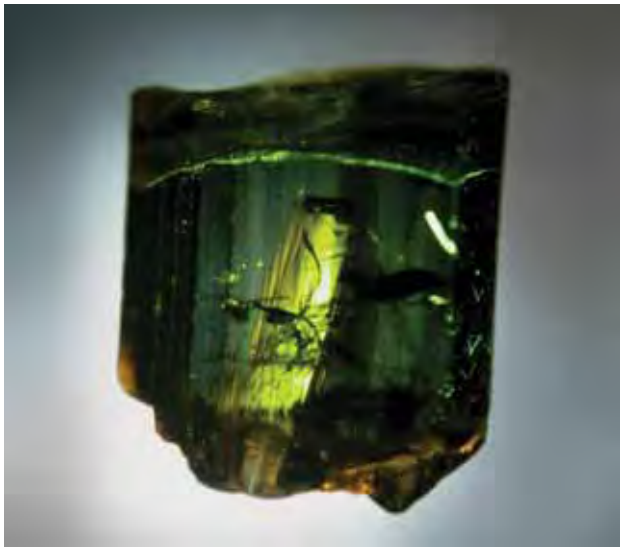

Figure 27. Between crossed polarizers, the included tourmaline remained bright when the host crystal came into an extinction position, indicating different planes of polarization for the two crystals. Photo by G. Choudhary.

Observed with transmitted light, the specimen's unusual feature became evident: It contained an elongated crystal that was inclined to the length of the main crystal (figure 25). With magnification, the prismatic habit of the included crystal was seen to be remarkably well developed. It displayed a pyramidal termination and a triangular cross section (again, see figure 25). Weak striations along the length of the prism also were visible. A small part of the included crystal extended beyond the host crystal, and it displayed a green color similar to that of the host.

At higher magnification, the prism faces of the internal crystal displayed fine etch marks (figure 26, left), which appeared angular (like two sides of a triangle). The pyramidal faces appeared to be coated with a bronzy material, and a complex pattern of triangular etching/growth hillocks was present (figure 26, center). In addition, this crystal displayed some angular growth zoning just below the pyramidal faces (figure 26, right). "Trichites" (hair-like fluid inclusions typically found in tourmalines) were present in both the host and the included crystal.

When observed between crossed polarizers, the specimen clearly showed an anisotropic nature. As expected based on the orientation of the crystal within its host, the internal crystal's polariscope reaction was distinctly different from that of the host crystal (figure 27).

The surface features of the included crystal recorded variations in its growth conditions. We believe it is protogenetic—that is, it formed before the main crystal. After the smaller crystal formed, its prism faces were apparently etched by residual fluids, and it was subsequently overgrown by the host tourmaline crystal.

Shyamala Fernandes (neethisjpr@gmail.com)
Indian Institute of Jewelry, Mumbai
Gagan Choudhary

Tourmaline from Muva, Mozambique. In late August 2007, two of these contributors (BML and JCZ) visited a new alluvial tourmaline deposit in northeastern Mozambique, in conjunction with field studies of the Cu-bearing tourmaline mines at Mavuco (see B. M. Laurs et al., "Copper-bearing [Paraíba-type] tourmaline from Mozambique," Spring 2008 *Gems & Gemology*, pp. 4–30). The deposit is located at 15°49′39.9″ S, 39°06′04.4″ E, which is only 13 km northeast of Mavuco.

At the time of our visit, there were approximately 100 miners working the deposit with picks and shovels in a series of shallow pits (figure 28). As at Mavuco, it was necessary to dig through some overburden (1–3 m) before reaching the tourmaline-bearing horizon. The thickness of this horizon could not be determined due to the presence of mud/water in the bottom of the pits. We were told by local miners and traders that about 50 kg of tourmaline were produced each week, as waterworn crystals ranging from near colorless to yellow to green and pink to brown

Figure 28. Miners work the Muva tourmaline deposit with picks and shovels in a series of shallow pits. Photo by J. C. Zwaan.

Figure 29. These pebbles (~0.8–2.9 g) show some of the colors of tourmaline that have been recovered from the Muva deposit. Photo by Kevin Schumacher.

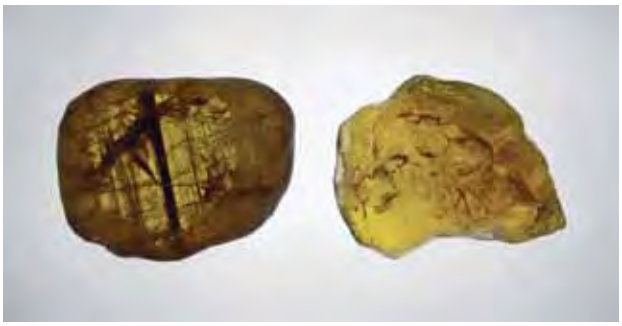

Figure 30. Some of the tourmaline from Muva is greenish yellow to yellow, as shown by these samples (8.66 and 8.59 g), which were gemologically characterized for this report. Photo by J. C. Zwaan.

(e.g., figure 29). Although the miners hoped to find Cu-bearing tourmaline at this deposit, the colors recovered there suggested that none contained Cu; however, the tourmaline had not yet been chemically analyzed.

From a parcel of rough material weighing approximately 1 kg, we selected 21 pieces for further study that encompassed the available range of colors. Flat faces were polished on all pieces, and two of them (both yellow, figure 30) were gemologically characterized using standard techniques at the Netherlands Gemmological Laboratory. The other 19 samples (pale yellow, yellow to yellowish green, and pink) were chemically analyzed by electron microprobe at the University of New Orleans.

The following properties were determined on the two rough samples (8.66 g greenish yellow and 8.59 g yellow, listed in respective order): pleochroism—very strong slightly greenish yellow and dark brown, and weak yellow and very light yellowish green; RI—1.627–1.648 and 1.622–1.643; birefringence—0.021; hydrostatic SG—3.09 and 3.07; fluo-

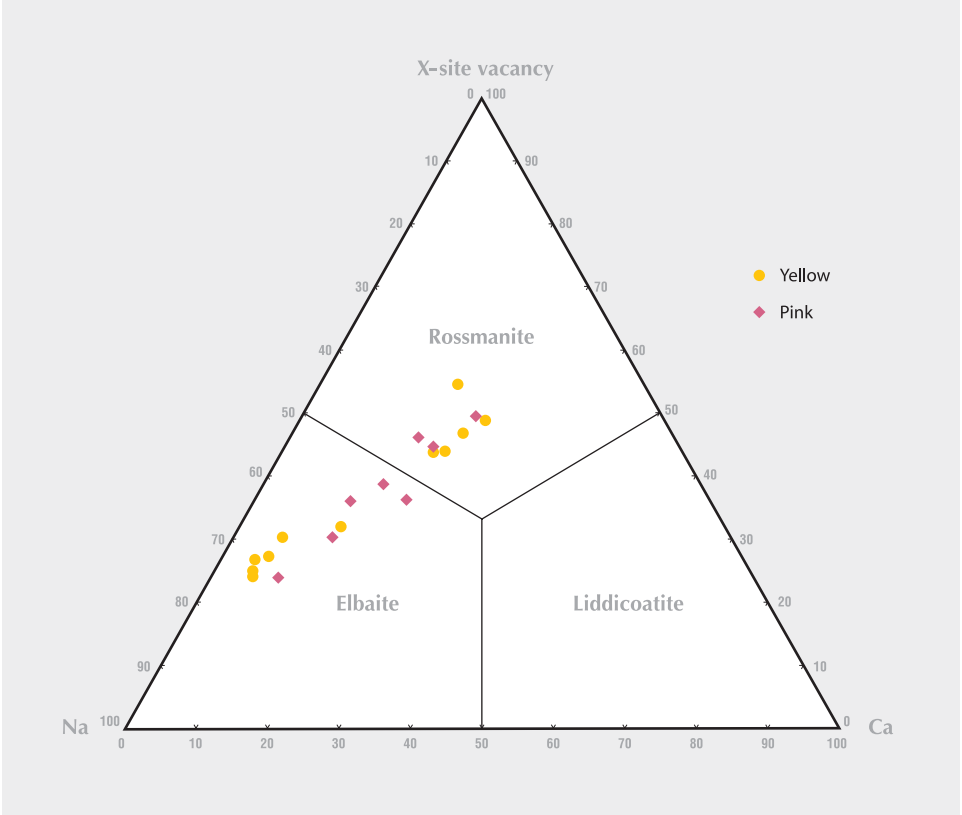

Figure 31. Electron-microprobe analyses of 19 samples of Muva tourmaline showed that they consisted of elbaite and rossmanite, and that there was no correlation between color and tourmaline species.

rescence—inert to long- and short-wave UV radiation; and no distinct features visible with a desk-model spectroscope. Microscopic examination revealed partially healed fissures, forming "trichites" composed of fine, thread-like, or wispy capillaries. Also present were hollow tubes that were mostly narrow and oriented parallel to the c-axis; some thicker tubes were stained reddish brown. The properties listed above are typical for gem tourmaline. EDXRF analyses of these samples showed that they contained high concentrations of Mn, and only trace amounts of Ca, Fe, and Ti.

Electron-microprobe analyses of the 19 samples showed that 11 were elbaite and eight were rossmanite. Some representative average analyses are available in the *G&G* Data Depository (see www.gia.edu/gemsandgemology). There was no correlation between color and tourmaline species (figure 31). No Cu was detected in any of the samples. The yellow to yellowish green samples contained significantly more Mn (3.99–7.44 wt.% MnO) than the pink samples (0.14–2.51 wt.% MnO), as well as slightly higher concentrations of Ti. The compositional data for the yellow to yellowish green samples was quite similar to those reported for tourmaline of similar colors from the Canary mining area in Zambia (see B. M. Laurs et al., "Yellow Mn-rich tourmaline from the Canary mining area, Zambia," Winter 2007 *Gems & Gemology*, pp. 314–331), except that some of the Mozambique stones contained much higher Ca, as well as slightly higher Fe and lower Na.

Brendan M. Laurs

J. C. (Hanco) Zwaan
Netherlands Gemmological Laboratory
National Museum of Natural History "Naturalis"
Leiden, The Netherlands

William B. ("Skip") Simmons and Alexander U. Falster
University of New Orleans, Louisiana

Figure 32. Pakistan is the source of this 31.9-mm-long aquamarine that contains a cloudy tornado-shaped concentration of fluid inclusions, as well as some interesting mineral inclusions. GIA Collection no. 37700; photo by Robert Weldon.

INCLUSIONS IN GEMS

Two unusual aquamarines. Two very unusual aquamarine specimens were recently brought to our attention by Dudley Blauwet (Dudley Blauwet Gems, Louisville, Colorado) and Jack Lowell (Colorado Gem and Mineral Co., Tempe, Arizona). The beryl crystal from Mr. Blauwet came from the Biensapi aquamarine pegmatite in the Braldu Valley in Baltistan, Pakistan, and he donated it to GIA because it contained some interesting inclusions. As shown in figure 32, this 31.9-mm-long crystal had a transparent termination and a cloudy lower portion with a tornado-like shape composed of numerous veils of minute fluid inclusions. The mineral inclusions in this aquamarine were also interesting. In addition to some obvious white feldspar crystals, a few small brownish green crystals were also visible (figure 33), although they were too deep in the host to allow analysis beyond what could be surmised through magnification. In this contributor's experience, the only brownish green crystals so far identified in Pakistani beryls have been monazite.

Figure 33. Although it was too deep in the Pakistan aquamarine to be analyzed, this 0.45 mm brownish green crystal inclusion surrounded by a tension halo appeared to be monazite. Photomicrograph by J. I. Koivula.

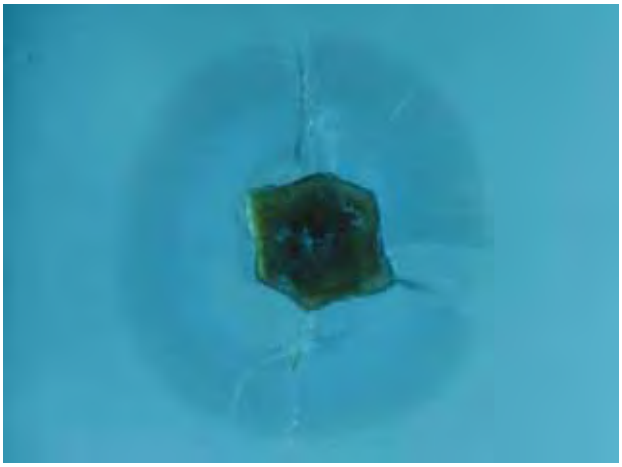

Figure 34. Some of the crystals in this 52.17-mm-wide aquamarine cluster from Namibia displayed an unusual trapiche structure on their terminations. Photo by Robert Weldon.

The specimen from Mr. Lowell reportedly came from the Erongo Mountains in Namibia. It measured 52.17 mm wide and was composed of a cluster of transparent-to-translucent greenish blue aquamarine crystals that were partially coated with a thin layer of pocket clay. The most interesting feature, which is clearly visible in both figure 34 and the photomicrograph in figure 35, was the distinctive trapiche structure apparent on several terminations. We have never before encountered such an obvious example of a trapiche pattern in aquamarine.

A 2006 issue of the *Mineralogical Record* (Vol. 37, No. 5) was dedicated to the minerals from the Erongo Mountains in Namibia, and though aquamarine was featured on the cover and thoroughly discussed and illustrated in the text, no mention was made of trapiche features and no photographs of this type of aquamarine were included. Although this appears to be a very unusual specimen, the fact that such material exists opens the possibility of trapiche aquamarine appearing in the gem market.

John I. Koivula (jkoivula@gia.edu)
GIA Laboratory, Carlsbad

An interesting rose quartz from Madagascar. In October 2007, Fabrice Danet (Style Gems, Antsirabe, Madagascar) informed us about a new find of rose quartz from Madagascar that contained some unusual inclusions. He first saw the material in April 2007, when a local dealer offered him a few kilograms of rather small pieces said to be morganite. About half the rough contained noticeable green inclusions, and Mr. Danet subsequently purchased 2 kg. In June 2008, he obtained 10 kg from a 100 kg parcel consisting mostly of small pieces. This time it was offered as rose quartz by a man who actually mined the material.

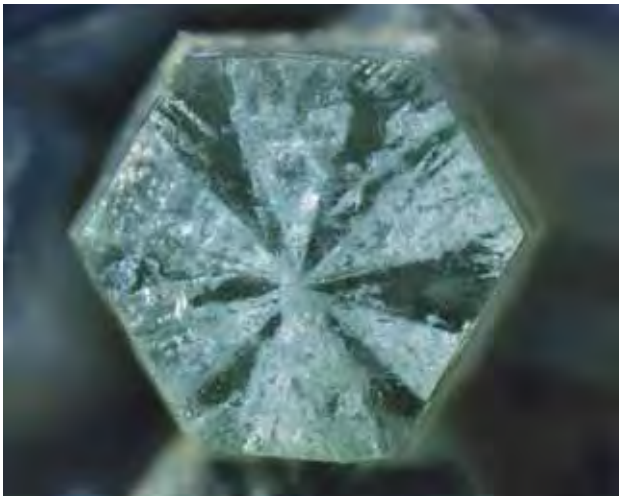

Figure 35. Looking down the c-axis, the hexagonal symmetry of the trapiche structure in this 5.87-mm-wide termination in the Namibian aquamarine cluster is clearly visible. Photomicrograph by J. I. Koivula.

He reported that it came from several small pits in a weathered pegmatite that contained beryl, black tourmaline, mica, clay, and areas of rose quartz. According to the miner and several local dealers, the deposit is located in the Ihosy area of southern Madagascar.

So far, Mr. Danet has cut about 200 stones, the largest of which weighs 27 ct. On examining the material with a loupe, he noticed that the green inclusions had a shape and color that were typical of diopside. Also present were orange hessonite-like inclusions and some very thin needles.

Figure 36. This 3.83 ct rose quartz from southern Madagascar contains an inclusion suite that has not previously been documented in such material from any locality. GIA Collection no. 37702; photo by Robert Weldon.

Figure 37. The green inclusions in this rose quartz from Madagascar proved to be diopside, and the orange crystalline masses were identified as grossular. Also present are some needles of epidote. Photomicrograph by J. I. Koivula; field of view 2.7 mm.

Mr. Danet donated to GIA a light pink 3.83 ct oval brilliant cut (figure 36) and three pieces of rough that contained obvious dark green and bright orange transparent-to-translucent inclusions. The faceted gem was confirmed as rose quartz by standard gemological testing. It contained a relatively large green inclusion adjacent to an orange inclusion (figure 37) that were both visible through the table facet and made excellent targets for Raman microanalysis. As suggested by Mr. Danet, the green inclusions were indeed diopside and the orange crystals were grossular. While we have encountered garnets before as inclusions in rose quartz (from Sri Lanka), this is the first time this combination of inclusions has been observed in rose quartz from any locality. As an added bonus, the very small blade-like to acicular inclusions in the stone were identified as epidote.

John I. Koivula and Karen M. Chadwick
GIA Laboratory, Carlsbad

Scapolite with diopside inclusions. In September 2007, Fabrice Danet obtained some yellow gem rough containing abundant stringers of dark inclusions that he was told came from the Amboasary region of Madagascar. The material was reportedly associated with mica, apatite, and large prisms (up to 50 cm) of yellow scapolite that were typically opaque. He obtained about 200 g of the inclusion-bearing material from a 5 kg parcel, and so far he has cut 16 stones ranging up to 7 ct. Mr. Danet donated to GIA a very light yellow 3.63 ct rectangular step cut (figure 38) and a few pieces of the rough material. Its overall appearance suggested that it might be heliodor, which is well known from Madagascar, but the inclusions were not typical of this beryl.

Standard gemological testing identified the faceted stone as scapolite. To the unaided eye, the inclusions appeared black and seemed randomly oriented. With magnification, their habits ranged from long rods to nearly spherical bul-

Figure 38. This 3.63 ct step cut, which was identified as scapolite, contains conspicuous randomly oriented inclusions that appear black to the unaided eye. GIA Collection no. 37701; photo by Robert Weldon.

bous masses that did not have visible crystal faces (figure 39). They were actually dark green in color, and even with magnification they had no apparent crystallographic orientation or relation to their host. Raman microspectroscopy identified them as diopside. In addition, a few extremely small light orange fuzzy-looking inclusions in association with the much more prominent diopside inclusions were identified as barite. The stone also contained some ultra-fine hair-like fibers that were too thin to identify by Raman analysis.

John I. Koivula and Karen M. Chadwick

Spodumene from Afghanistan with unusual inclusions. As a pegmatitic gem mineral, spodumene may occasionally display interesting inclusions that reflect its geologic character and the conditions of its growth and post-growth dissolution. This contributor recently examined two spodumene crystals that hosted some noteworthy features.

Figure 39. With magnification, it was evident that the inclusions in the scapolite were dark green; Raman analysis identified them as diopside. Photomicrograph by J. I. Koivula; field of view 3.3 mm.

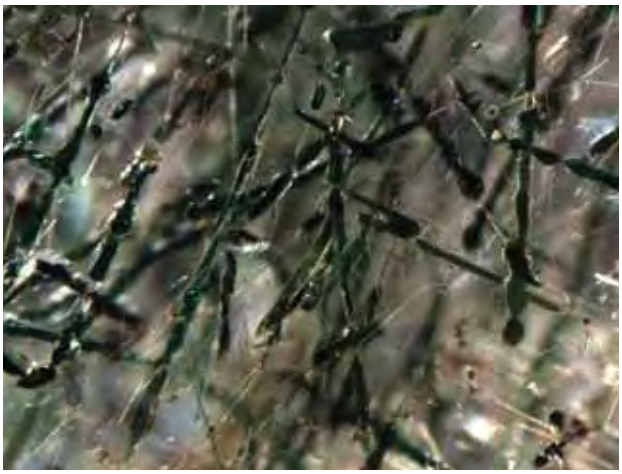

Figure 40. This 25.0-mm-long crystal of spodumene extends from a matrix of K-feldspar, creating an aesthetic mineral specimen that is reportedly from Afghanistan. GIA Collection no. 37699; photo by Robert Weldon.

Figure 41. Isotropic, transparent, and yellowish brown, these tetrahedral and modified octahedral inclusions in the spodumene in figure 40 resemble a mineral in the pyrochlore group, possibly pyrochlore itself. Photomicrograph by J. I. Koivula; field of view 2.6 mm.

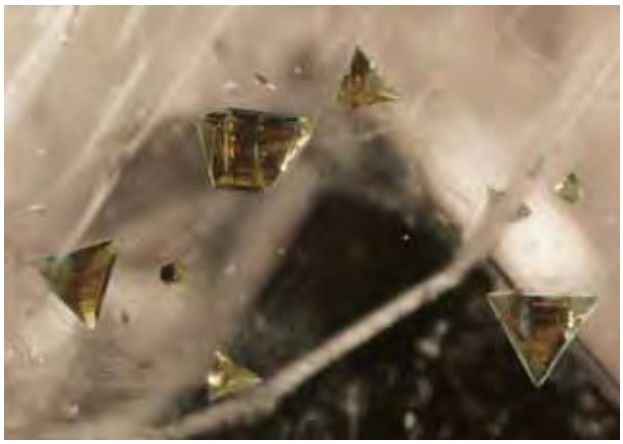

Figure 42. Also reportedly from Afghanistan, this 71.2-mm-long spodumene crystal has an etched spiral dislocation pattern extending through its entire length. Photo by Robert Weldon.

One of these specimens was donated by Dudley Blauwet. This pale yellow spodumene reportedly was mined from Kala, Darre Pech, Kunar Province, Afghanistan. As pictured in figure 40, the 25.0-mm-long transparent spodumene crystal extended from a matrix of K-feldspar and was very aesthetic. Scattered mineral inclusions were present near the base of the spodumene, but because of their positioning they could not be analyzed by Raman spectroscopy. Microscopic examination proved that the inclusions were isotropic and that they had a refractive index that was reasonably higher than their host. Their transparency and yellowish brown color, together with their tetrahedral to modified octahedral habit (figure 41), reminded us of inclusions we had encountered before in a beryl from Pakistan (E. J. Gübelin

Figure 43. The spiral dislocation pattern appeared to be epigenetically filled with off-white to reddish brown debris that was probably a mixture of clay minerals and iron oxides. Photomicrograph by J. I. Koivula; field of view 9.7 mm tall.

and J. I. Koivula, *Photoatlas of Inclusions in Gemstones*, Vol. 2, Opinio Publishers, Basel, 2005, p. 177). Those inclusions were conclusively identified by X-ray diffraction as pyrochlore, so the possibility exists that the inclusions in this specimen might also be pyrochlore or some other pegmatitic member of the pyrochlore mineral group.

The other spodumene, also reportedly from Afghanistan, was pale pink and measured 71.2 mm long (figure 42). It was sent to us for study by Jack Lowell because it had what appeared to be an etched spiral dislocation pattern extending through its entire length. The dislocation pattern was clearly visible even without magnification, and in some viewing directions it looked a bit like numerous tiny birds perched on a wire. Viewed with magnification through the natural surface, the etched dislocation had more of a fern-like or blade-like spiral pattern to it, with several relatively evenly spaced "petals" or curved "fan blades" extending from the edges along the length (figure 43). The whole of the dislocation also appeared to be filled with chalky-looking off-white to reddish brown epigenetic debris that was probably a mixture of clay minerals and iron oxides, which are commonly encountered as post-growth deposits in such features.

John I. Koivula

SYNTHETICS AND SIMULANTS

Two interesting synthetic rubies. Most synthetic rubies and sapphires are grown by flame-fusion (Verneuil), flux, or hydrothermal processes. Of these, Verneuil synthetics are the most common due to their low production cost. The Verneuil products are easily identifiable by internal features such as gas bubbles of various shapes and types, curved growth features (lines and color bands), and Plato lines.

However, some Verneuil synthetic rubies and sapphires display inclusion features that closely resemble those seen in their natural counterparts (e.g., Summer 2007 GNI, pp. 177–178). Recently, the Gem Testing Laboratory of Jaipur, India, encountered two synthetic rubies that were interesting because of their natural appearance. The rubies were purple-red mixed-cut ovals weighing 3.50 and 2.97 ct (figure 44). Upon initial observation, both specimens appeared to be ruby, which was supported by their RI and SG values.

When the 3.50 ct sample was observed carefully at low magnification, it appeared to be divided into two sections, one translucent and the other transparent (figure 45). These sections were separated by a distinct, slightly curved plane running throughout the specimen. The transparent portion displayed a cloud of fine "pinpoints" in a radiating pattern; this cloud was further surrounded by a circular zone (again, see figure 45). The circular zone was visible to the unaided

Figure 44. These 3.50 ct (left) and 2.97 ct (right) synthetic rubies, which were represented as natural, displayed interesting features. Note the distinct curved plane at the center of the 3.50 ct sample, dividing it into two parts, while the 2.97 ct gem displays surface breaks and a milky zone. Photos by G. Choudhary.

Figure 45. The transparent portion of the 3.50 ct sample displays a cloud of pinpoints in a radiating pattern, surrounded by a circular zone that confirms the ruby is synthetic. Photomicrograph by G. Choudhary; magnified 10×.

eye, and identified the sample as a flame-fusion synthetic. The translucent portion contained a dense concentration of globular and tubular inclusions (figures 46 and 47). When viewed in certain orientations, the inclusions were seen to be concentrated in parallel planes intersecting one another at angles that appeared to be 60°/120° (figure 46, right). The intersections of these planes formed rhomboid shapes that were very similar to those formed by the intersection of rhombohedral twin planes in natural corundum. It can be assumed that such features formed along the rhombohedral planes due to disturbances during the growth process. The translucent portion also contained a few blue pinpoints (again, see figure 47). Such blue-colored pinpoints have been noted previously in Verneuil synthetic corundum (ruby, as well as sapphire) by this contributor. The fact that the two portions of the sample displayed such distinct inclusion features seemed to indicate a composite stone, but this possibility was ruled out by the absence of a junction plane or flattened/trapped gas bubbles (again, see figures 45 and 46, left).

The 2.97 ct specimen had obvious surface breaks containing eye-visible orange stains, and also a milky zone toward one end. These features are common in natural rubies that have iron staining and host milky zones consisting of rutile silk or discs. When magnified, the surface breaks displayed distinct orange patches, with some flow-like patterns that indicated impregnation by a colored substance (figure 48, left). The milky zones had curved edges and were composed of fine gas bubbles (figure 48, right), which pointed to synthetic ruby. In addition, fine curved growth lines and scattered spherical and elongated gas bubbles were seen, as expected in Verneuil synthetics. In general, the substance used to fill fissures in gems is either colorless or is colored to match the stone's bodycolor. In this specimen, the use of a different-colored substance provided obvious evidence that it had been filled.

Gagan Choudhary

MISCELLANEOUS

Update on U.S.-Myanmar import restrictions. On July 29, 2008, U.S. President George W. Bush signed into law the Tom Lantos Block Burmese JADE (Junta's Anti-Democratic Efforts) Act of 2008. A supplement to the Burmese Freedom and Democracy Act of 2003, the new JADE Act significantly strengthens restrictions on the import of Burmese ruby and jadeite into the United States.

The 2003 Act imposed an import ban on all Burmese products, including Burmese gem materials, into the U.S. However, because of World Trade Organization Rules of Origin, Burmese gems that underwent a substantial transformation (e.g., cutting and polishing) outside Myanmar were not considered products of Myanmar and were not covered by the import ban (see, e.g., Spring 2005 GNI, p. 71). The 2008 JADE Act closes this loophole for ruby and jadeite. As of September 29, 2008, it is illegal to import into the United States:

- Jadeite mined or extracted from Myanmar
- Rubies mined or extracted from Myanmar
- Any articles of jewelry containing jadeite or rubies mined or extracted from Myanmar

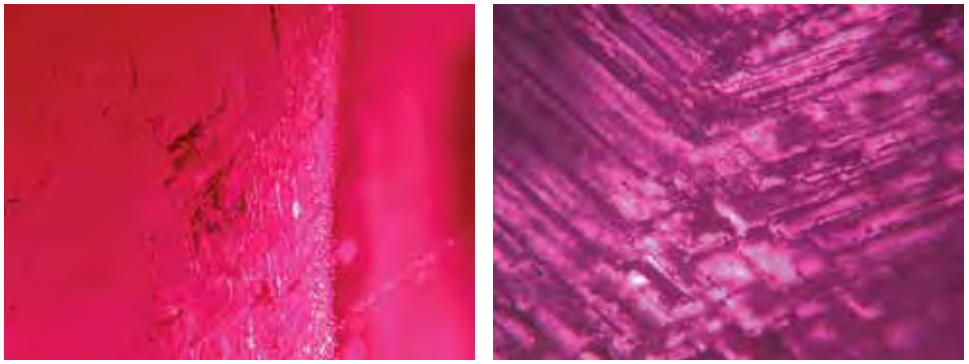

Figure 46. Part of the 3.50 ct synthetic ruby contains abundant inclusions that in places intersect at ~60°/120°. In the left image, no junction plane or trapped gas bubbles are present between the translucent and transparent areas, ruling out a composite gem. Photomicrographs by G. Choudhary; magnified 30× (left) and 65× (right).

Figure 47. Some of the globular and tubular inclusions in the 3.50 ct synthetic ruby were not arranged in intersecting planes, as shown here. Also note the scattered blue pinpoints. Photomicrograph by G. Choudhary; magnified 80×.

For both gem materials, the rules apply regardless of whether the gem is rough or fashioned. It is important to remember that the 2003 restrictions remain in effect, so it is still illegal to import other rough Burmese gem materials and all finished gemstones that are cut and polished in Myanmar.

An important element of this law is that importers of non-Burmese ruby and jadeite will be required to demonstrate the origin of their gemstones, and they must retain all information relating to the purchase, manufacture, and shipment of such goods for a period of not less than five years from the date of entry into the U.S. The only way these requirements can be waived is if the exporting country has itself implemented a similar set of restrictions to prevent the importation of Burmese gemstones into that country. The exact implementation of the law will be determined through the development of regulations, which are still being drafted.

The full text of the 2008 JADE Act is available at www.govtrack.us/congress/billtext.xpd?bill=h110-3890.

Thomas W. Overton (toverton@gia.edu)
GIA, Carlsbad

ANNOUNCEMENTS

***Gems & Gemology* wins two major awards.** On July 29, the American Gem Society presented Russell Shor with its annual Richard T. Liddicoat Journalism Award for Industry/Trade Reporting for his Fall 2007 *G&G* article "From Single Source to Global Free Market: The Transformation of the Cultured Pearl Industry." This marked the fifth prize for a *G&G* article since the Liddicoat Awards' inception in 2003.

G&G also received recognition for the quality of its printing, placing first in the 2008 Gold Ink Awards competition, in the category of Scientific and Technical Journals. Cosponsored by *Print Media* and *Printing Impressions* magazines, the Gold Ink Awards are recognized as the nation's most prestigious print competition. They are based on print quality, technical difficulty, and overall visual effect.

This brings to 29 the number of awards *Gems & Gemology* has won for editorial and printing excellence since moving to a larger format in 1981.

Conferences

Gem-A Centenary Conference and 2nd Annual European Gemmological Symposium. The Gemmological Association of Great Britain (Gem-A) will hold its annual conference October 25–26 in London. In conjunction with its centennial celebration, Gem-A will also be hosting this year's European Gemmological Symposium at the same time. Day one will highlight the history of gemology and the jewelry trade, and day two will discuss practical tips and new technologies for the modern gemologist. Visit www.gem-a.info/news--events/the-gem-a-conference.aspx.

Gems in objects of cultural heritage. An international conference titled *Geoarchaeology and Archaeomineralogy: Impact of Earth Sciences in the Study of Material Culture*

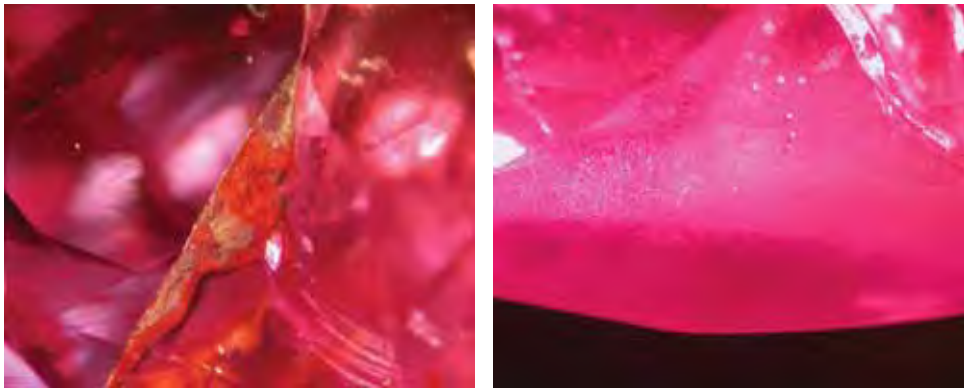

Figure 48. Surface breaks in the 2.97 ct synthetic ruby contain orange patches with flow-like patterns that indicate impregnation by a colored substance (left). Also note the fine curved growth lines, characteristic of a melt-grown synthetic, as is the curved milky zone on the right. Photomicrographs by G. Choudhary; magnified 80× (left) and 60× (right).

will take place in Sofia, Bulgaria, October 29–30, 2008. One of the conference topics will be "Archaeomineralogy and Gemmology." A field trip will focus on the "Role of Bulgaria in the History of World's Jewellery Art." Visit http://mgu.bg/docs/CircularEN.doc.

GIT 2008. The Gem and Jewelry Institute of Thailand will host the *2nd International Gem & Jewelry Conference* December 11–14 in Bangkok. The program will feature a two-day technical session, with oral and poster presentations, followed by a two-day excursion to the Kanchanaburi sapphire deposits. Visit www.git.or.th/conference/index.html.

IDCC-2. The *2nd International Diamond Cut Conference* will take place in Lausanne, Switzerland, March 22–25, 2009, just before the BaselWorld 2009 Watch and Jewellery Fair. A diamond cut exhibition will be offered at the fair. Visit http://idcc2.octonus.com.

MAEGS 16. Gemology will be one of the topics covered at the *Meeting of Association of European Geological Societies*, July 9–13, 2009, in Cluj-Napoca, Romania. Visit http://bioge.ubbcluj.ro/maegs16.

Gemological Research Conference. GIA will host its second Gemological Research Conference August 21–23, 2009, in San Diego, California. The program will feature oral and poster presentations and panel discussions in two parallel tracks (gemology and jewelry/business issues), as well as a photography competition and field trips to the gem pegmatites in San Diego County. Visit http://grc2009.gia.edu.

4th International Symposium on Granitic Pegmatites. Held in Recife, Brazil, August 30–September 6, 2009, this conference will explore the latest scientific advances in the study of granitic pegmatites. Field trips will include the Eastern Brazilian Pegmatite Province (Minas Gerais) and the Borborema Pegmatite Province (northeastern Brazil). Visit www.ufpe.br/geologia/peg2009brazil.

Exhibits

Exhibits at the GIA Museum. Through December 2008, "Facets of GIA" will explain the various gemological services that GIA provides, including diamond grading, gem identification, education, and public outreach. Also, on display in the Rosy Blue Student Commons are photo-essays by Robert Weldon, manager of photography and visual communications at the GIA Library, and *G&G* editor Brendan Laurs, depicting emerald mines in Colombia and the Paraíba-type tourmaline deposit in Mozambique, respectively (for more on the latter, see the article in the Spring 2008 issue of *G&G*). Advance reservations are required; to schedule a tour, call 760-603-4116 or e-mail museum@gia.edu.

The Aurora Collection at The Vault. "The Vault," a new permanent collection of rare gemstones and mineral specimens, is now open at the Natural History Museum in London. On temporary display is the Aurora Collection, currently comprising 296 naturally colored diamonds (267.45 carats total weight) assembled by collectors Alan Bronstein and Harry Rodman. Also on display is the 47.69 ct Star of Africa, which helped launch the 1869 diamond rush in South Africa, and the 1,385.95 ct Devonshire emerald crystal. Visit www.nhm.ac.uk/galleries/green-zone/vault.

Gold in the Americas. Now on display at the Musée de la Civilisation in Quebec City, Quebec, this exhibition will review the importance of gold to the cultures of North and South America, both ancient and modern. The 250 items on display will include gold objects and mineral specimens, as well as paintings, sculptures, and ethnographic objects. Visit www.mcq.org/or.

Portuguese and Brazilian jewelry. An exhibition of Portuguese and Brazilian jewelry is on display at the Royal Palace of Ajuda in Lisbon until November 30. The exhibit marks the 200th anniversary of the Portuguese royal court's arrival in Brazil, as they fled from Napoleon's troops. The curators chose 24 Portuguese and 24 Brazilian jewelry artists to work in pairs and create pieces based on the period. Brazilian diamonds and gold are featured, as well as colored stones from the Brazilian state of Minas Gerais.

Nature of Diamonds at the ROM. The Nature of Diamonds exhibit is on display at the Royal Ontario Museum from October 25, 2008, to March 22, 2009. The award-winning exhibition explores humankind's ongoing fascination with diamond, examining its geologic origins, mining, cultural significance in art, literature, and ornamentation, and numerous technological applications. Visit www.rom.on.ca.

BOOK REVIEWS

American Mineral Treasures

By Gloria A. Staebler and Wendell E. Wilson, Eds., 354 pp., illus., publ. by Lithographie LLC [www.lithographie.org], East Hampton, CT, 2008. US$85.00

In a very real sense, this book qualifies as an exhibition catalog. It was published to accompany and document a remarkable exhibition by the same name that was featured at the 2008 Tucson Gem & Mineral Society (TGMS) show. The project, which sprang from an impromptu discussion among a small group of people led by collector Gene Meieran at the 2005 TGMS show, grew to involve hundreds of participants and eventually culminated in what was likely the finest exhibition of minerals from the United States ever staged.

There is no need to rehash what went into producing the exhibition or the book here, as the reader can find brief synopses in the preface and afterword. For those who missed the exhibition or who were there and want to have their socks blown off all over again, this book is the next best thing.

The goal of the exhibition was to assemble the finest specimens produced by the most important U.S. mineral localities or regions of the past half-century, and to display those specimens by locality. The book follows the same approach, with a total of 44 locality chapters, each of which combines an article about the locality with a liberal selection of excellent photographs of many of the finest specimens that were displayed. Each chapter was written by one or more individuals knowledgeable about that locality, though perhaps *knowledgeable* is too tame a word. Coeditor Gloria Staebler describes the authors as passionate, and their passion certainly does permeate the text and will undoubtedly prove infectious to the reader.

As one might expect, a book with so many different authors (65 altogether) is bound to be somewhat uneven in style and approach. Every chapter has something to say about the history and specimen production of the locality; however, some chapters include discussions of the geology and mineralogy, while others consist essentially of personal reminiscences, stories, and anecdotes. Nevertheless, the editors are to be commended for their success in assembling this assortment of papers into a well-balanced and coherent whole that both informs and inspires.

A couple of other features deserve comment. The first is the lengthy introduction by *Mineralogical Record* editor-in-chief Wendell Wilson. Entitled "A Brief History of Mineral Collecting in America," this fascinating essay traces the American mineral collecting spirit from its beginnings in colonial times right up to the movers and shakers of the contemporary mineral hobby. There is also an equally fascinating foreword by Apollo 17 astronaut Harrison H. Schmitt. Schmitt's comments about lunar mineralogy might seem a bit out of place in a book devoted to American minerals, but one can only be inspired by hearing an astronaut relate how, as a youngster, he got hooked on geology when he went wulfenite collecting in an old Arizona mine with his father, only to end up years later collecting minerals on the moon.

ANTHONY R. KAMPF
Natural History Museum of Los Angeles County
Los Angeles, California

The Diamond Handbook: A Practical Guide to Diamond Evaluation, 2nd Ed.

By Renée Newman, 186 pp., illus., publ. by International Jewelry Publications [www.reneenewman.com], Los Angeles, 2007. US$19.95

Unlike the previous edition of Renée Newman's comprehensive guide to evaluating and identifying diamonds, which was directed to the consumer, this revision is aimed at the trade professional, gemology student, and serious diamond buyer. The first chapter lays the groundwork of the four Cs before moving on to more advanced concepts of evaluating diamonds.

Newman begins chapter 2 with an interesting discussion of the importance of transparency. Generally, not much thought is given in the trade to the concept of transparency vs. clarity, even though the two are distinct as well as intertwined. A cloud in a transparent diamond is a clarity issue, but if a diamond is cloudy throughout it is a transparency issue. Transparency, like the qualities of diamond cut and proportion, is one of the critical reasons why it is important to look at a diamond before purchasing it, rather than rely solely on a lab report. Transparency is usually noted on diamond grading reports only when it affects the clarity grade.

Light performance is another area where most consumers get confused, usually because sellers themselves often do not understand the concept. *Light performance* refers to the type and intensity of light distribution displayed by a diamond. It is a simple concept, but breaking down those components is where the battleground begins. Definitions vary according to who is using the terminology, and—to add potential confusion—not all labs evaluate light performance the same way, and some don't consider it at all. Newman discusses five laboratories and the nuances that differentiate each with regard to light performance—a valuable resource when presented with a lab report that includes analysis of this characteristic. Sample documents are provided to further the reader's understanding.

The "Synthetic Diamond" chapter is refreshingly calm and factual. The information in this section provides assurance that the various types of synthetic diamonds can be flagged by jewelers and gemologists, then sent to a lab for confirmation. With this book and my gemological background, I was able to confidently appraise a set of synthetic diamonds for a recent customer. High-quality color photos and four outstanding charts are included.

One of the more interesting discussions is the definition of *treatment* vis-à-vis *enhancement* in the "Diamond Treatment" chapter. Newman defines *treatment* as a process that is used to improve appearance but does not include cutting or cleaning. She maintains that *enhancement*, though often used as a synonym for *treatment*, can also refer to faceting and polishing. Some gem labs use the term *enhancement* for routine processes that are "accepted in the trade" (e.g., heat treatment of many gems). Conversely, they reserve the word *treatment* for "unacceptable" procedures (e.g., beryllium diffusion of ruby and sapphire). The feeling is that the term *enhancement* has a more positive connotation than *treatment*.

Each chapter makes an important contribution to the overall theme of diamond evaluation, and the readability of *The Diamond Handbook* makes this an invaluable resource for the jewelry professional.

GAIL BRETT LEVINE
National Association of Jewelry Appraisers
Rego Park, New York

Gems of the World

By Cally Oldershaw, 256 pp., illus., publ. by Firefly Books [www.fireflybooks.com], Buffalo, NY, 2008. $35.00

Gems & Minerals

By Andreas Landmann, 176 pp., illus., publ. by Schiffer Press, Atglen, PA, 2008. $29.99

Books intended as an introduction to scientific subjects outside of academia must perform a careful balancing act. They must take care not to overwhelm readers with too much technical material, while still providing enough information to avoid giving them a false sense of security in their newfound knowledge. Two books that arrived on my desk recently offer an introduction to the gemological world, though each has a slightly different emphasis.

Cally Oldershaw's *Gems of the World* is divided into two main sections. The first reviews gem formation, mining, and marketing, as well as physical and optical properties, among other related topics; the second describes known gem materials in detail. The first section is an excellent introduction to the world of gems, and it follows much of the beginning curriculum for a gemological diploma (though it will not serve to replace it). Attention is also given to considerations for buying diamonds and colored gems, both at home and abroad.

The second section is organized by chemical composition, an arrangement that takes some getting used to (for example, as the list starts with carbon, sulfides, and oxides, the first six gems discussed are diamond, sphalerite, pyrite, marcasite, cuprite, and spinel). The entries are rich in detail and useful information, including complete gemological properties. The illustrations, though not always of the highest quality, are more than adequate for their purpose. The book concludes with a useful series of maps of worldwide gem localities, a glossary of gem terms, and an index.

If there is a criticism to be leveled at *Gems of the World*, it is that this is a work that seems not quite sure what it should be. It is far too detailed for casual gem buffs, yet the organization makes it ill-suited as a reference for serious gemologists. However, it would be ideal for novice gem enthusiasts looking to begin their scientific study of the subject, and it should serve admirably as a counter aid for retail jewelers. The book's production values are solid, and the paper and binding are of sufficient quality to survive years of use.

Gems & Minerals is an English translation of Andreas Landmann's 2004 German original, *Edelsteine und Mineralien*. It is organized in straightforward encyclopedic format by mineral group, and covers all major gem materials in addition to mineral species popular with collectors but not normally used as gems, such as cinnabar and natrolite. Also covered are precious metals as mineral specimens and several synthetic materials. Each entry gives a general overview of the material, with basic physical properties (e.g., hardness, crystal system, cleavage, and chemical formula; other gemological properties are not given). The coverage is comprehensive, though not deep.

The book's main drawback is that the photos used are not always ideal for the material and the image choices at times are even a bit baffling. It may have been that the publisher did not have the means or resources to procure high-quality images for every section, but it is disappointing that so many of them fall well short of doing justice to the gems being discussed (the sapphire and alexandrite images in particular). The translation is occasionally un-

even, and I came across a few minor errors or obsolete information, such as ascribing the color of rose quartz to microscopic rutile inclusions (the most recent research attributes it to inclusions of a dumortierite-like mineral). Nevertheless, the wealth of information presented here makes this a useful work for novice collectors.

Those looking for an introduction to the world of gems and minerals will find value in these two works, though gem enthusiasts will be better served by the first, and budding mineral collectors by the second.

THOMAS W. OVERTON
Gemological Institute of America
Carlsbad, California

Southwestern Indian Jewelry: Crafting New Traditions

By Dexter Cirillo, photography by Addison Doty, 240 pp., illus., publ. by Rizzoli International Publishers [www.rizzoliusa.com], New York, 2008. US$55.00

Innovative contemporary Southwestern Indian jewelry is featured in this visually impressive and comprehensive book by Dexter Cirillo. The works of the 88 featured artists, primarily dating from the 1970s to the present, were inspired by such groundbreaking modern Indian artisans as Charles Loloma and Preston Monongye. Their jewelry merges modern design, new manufacturing techniques, and a variety of colored gemstones with traditional methods and materials. Many of the award-winning, museum-quality pieces are shown larger than life with the lavish photography of Addison Doty.

Cirillo's preface contains a brief history of the Native Americans of the southwestern U.S., followed by an introduction to modern design and its influence on the Native American artists who broke tradition by experimenting with new ideas and materials. There are three chapters on silver and metalwork, lapidary art, and objects and sculptural jewelry. Artist interviews touch on tribal lineage, education, and sources of inspiration. Many of the pieces featured have won nationally recognized awards at the Heard Museum (Phoenix, Arizona) and the Santa Fe Indian Market. Methods discussed include *mokume gane* (the process of laminating multiple layers of disparate metals) and tufa casting (i.e., casting in carved tufa stone). Cultural details include information on dances and ceremonies that are depicted in jewelry designs. Unusual, often stunning items such as a stamped sterling silver purse by Mike Bird-Romero are also included.

While some collectors might not find their favorite contemporary Indian artist, none will be disappointed with those featured. The author acknowledges the difficulty of narrowing the choices, given the caliber of contemporary Southwestern Indian artists. In addition, although values are not given for specific items, the book will serve as a useful resource for any purchase decision involving these products. And jewelry designers will be inspired by the uniqueness, precision, and ingenuity of the pieces. The book's extensive back matter includes notes, a glossary, suggested readings, artist and jewelry source lists, and an index.

Cirillo has created a well-written, interesting homage to the ever-evolving masters of Native American craft.

MARY MATHEWS
Gemological Institute of America
Carlsbad, California

OTHER BOOKS RECEIVED

Fleischer's Glossary of Mineral Species 2008. *By Malcolm E. Back and Joseph A. Mandarino, 345 pp., publ. by The Mineralogical Record [www.minrec.org], Tucson, AZ, 2008, US$26.00.* An update of the ninth edition, this larger-sized (6 × 9 in.) work includes both new mineral species and substantial nomenclature changes since 2004. Species name, chemical formula, crystal system, type locality, group, relationships to other species, and references are given for each entry. New to this edition is a comprehensive 80-page section on mineral groups.

TWO

Gemstones: Enchanting Gifts of Nature. *By R. V. Karanth, 48 pp., illus., publ. by the Geological Society of India [www.geosocindia.org], Bangalore, 2008, US$20.00.* This colorful booklet summarizes the basics of gemology as well as the characteristics of major gems such as diamond, corundum, and beryl. Emphasis is given to India's role in the gem world, and a map of the country's gem deposits is included.

TWO

Amazonite: Mineralogy, Crystal Chemistry, Typomorphic Features. *By M. N. Oustooumov, A. N. Platonov, and V. A. Popov, 253 pp., illus., publ. by Nedra, Moscow, 2008, Ru578 [in Russian].* This Russian-language book reviews the geology, characteristics, history, and recent research on amazonite.

TWO

Infrared Reflection Spectrometry in Advanced Mineralogy, Gemology and Archaeometry. *By Mikhail Oustooumov, 89 pp., illus., publ. by the National University of Mexico Institute of Geophysics [www.igeofcu.unam.mx], Mexico City, 2007 [in Spanish].* This Spanish-language monograph reviews the fundamentals of infrared reflection spectroscopy and its application in the nondestructive testing of gems, minerals, and cultural artifacts. Sixty pages of sample spectra for a variety of materials are included.

TWO

Traditional Jewelry of India. *By Oppi Untracht, 431 pp., illus., publ. by Thames & Hudson [thamesandhudsonusa.com], New York, 2008, US$49.95.* This is a paperback version of the 1997 hardcover. Like the original version, it presents a comprehensive review of India's rich jewelry history, numerous color photographs, and an extensive bibliography.

TWO

'08 GEMOLOGICAL ABSTRACTS

COLORED STONES AND ORGANIC MATERIALS

Production of designer mabe pearls in the black-lipped pearl oyster, *Pinctada margaritifera*, and the winged pearl oyster, *Pteria penguin*, from Andaman and Nicobar Islands, India. V. Kripa, K. J. Abraham, C. L. Libini, T. S. Velayudhan, P. Radhakrishnan, K. S. Mohamed, and M. J. Modayil, *Journal of the World Aquaculture Society*, Vol. 39, No. 1, 2008, pp. 131–137.

Although not as valuable as round cultured pearls, the assembled half-rounds known as mabes can be produced more easily and in significantly less time. The process entails attaching hemispherical beads or plastic shapes ("images") to the interior shell of the host oyster. Mabes can be produced from a number of mollusks, including *Pteria penguin* (the traditional mabe oyster), *Pteria sterna*, *Pinctada mazatlanica*, *Pinctada maxima*, and *Pinctada margaritifera*.

The authors studied the potential for developing a mabe pearl production industry in the Andaman and Nicobar Islands, an Indian territory located in the Bay of Bengal, using *P. margaritifera* and *P. penguin* oysters. Experiments were carried out to: (1) determine a standard dosage of menthol as a relaxant for the two types of oyster, (2) test the effectiveness of various adhesives for attaching the beads or images, and (3) test the efficiency of using images that are shell-cut (carved shell) or crafted (powdered shell fused with resin). The results indicated a range of menthol dosages and response times. Several locations were identified as ideal for attaching the mabe base, and glues containing polycarboxylate cement and the adhesive Fevikwik with cyanoacrylate gave the best results. Fevikwik was preferred, though, because of its avail-

ability and ease of application. Optimal clarity of the designer images was achieved when the mabes were harvested within 60 to 70 days. Good results were obtained with both shell-cut and crafted images; the shell-cut images were sharper, while the crafted images showed a better three-dimensional effect.

The authors conclude that the mabe industry could become an important source of employment for residents of the territory, which was devastated by the Indian Ocean tsunami in December 2004. *Stuart Overlin*

A spectrophotometric study of the thermal colour change of tanzanite. G. Pearson [grantpearson@optusnet.com.au], *Australian Gemmologist*, Vol. 23, No. 2, 2008, pp. 254–265.

The thermally induced color change of vanadium-bearing zoisite (tanzanite) was measured spectrophotometrically. The color enhancement of heat-treated tanzanite is caused by a substantial increase in spectral transmission in the blue-green and blue wavelengths (i.e., from ~400 to 510 nm) or, conversely, by the reduction of an absorption band between ~375 and 444 nm. The pleochroic color variations of an unheated tanzanite crystal viewed from different directions were also studied using this technique. *RAH*

What is vegetable ivory? M. C. Pedersen [info@maggiecp.com], *Organic Gems*, No. 8, March 2008, www.maggiecp.co.uk/subs/what_is_vegetable_ivory.htm.

Nuts from certain species of ivory palm, particularly the tagua nut from trees of the genus *Phytelephas*, have historically seen use as an ivory substitute, and accordingly have been called "vegetable ivory." These materials have been used since the 19th century for objects ranging from toys, umbrella handles, drawer knobs, and dice to carvings, jewelry, and (more recently) as buttons for the fashion industry. A few key features of vegetable ivory distinguish it from animal ivory, bone, antlers, and plastics—particularly its diagnostic cellular structure with magnification. Sample photographs show different forms of the vegetable ivory nut and examples of carvings. *Edward Blomgren*

DIAMONDS

Argyle type Ia pink diamonds: Gemmological properties, FTIR, UV-Vis and CL features. V. Rolandi, A. Brajkovic [anna.brajkovic@unimib.it], I. Adamo, and I. Fontana, *Australian Gemmologist*, Vol. 23, No. 1, 2008, pp. 194–203.

Examination of 36 pink diamond fragments from the Argyle mine in northwestern Australia revealed surface features consisting of hexagonal depressions, trigons, fractures, and dislocation planes. Anomalous birefringence with mosaic-like cross-hatch patterns was detected in all samples. IR absorption features indicated low nitrogen contents (<100 ppm). All diamonds were type Ia and showed A-defect absorption; hydrogen was always present. The most important UV-Vis absorption features were the 415 nm (N3) peak, the 390 nm band (often superimposed on the N3 center), and the 550 nm band, which possibly relates to dislocations and is responsible for the pink color. CL imaging revealed distribution patterns created by lattice defects; a green emission band is tentatively ascribed to traces of natural radiation damage. The CL spectra highlighted two broad components at 450 and 512–520 nm, which showed specific emission features such as N3, H3, and H4 centers.

Taking all these features into account, the authors conclude that the pink diamonds developed in a strongly N-impoverished eclogitic environment; experienced post-growth plastic deformation; and underwent annealing, dissolution, and resorption processes during mantle storage and eruptive emplacement. *RAH*

Diamond formation in the system $MgO–SiO_2–H_2O–C$ at 7.5 GPa and 1,600°C. A. G. Sokol [sokola@uiggm.nsc.ru] and Yu. N. Pal'yanov, *Contributions to Mineralogy & Petrology*, Vol. 155, No. 1, 2008, pp. 33–43.

Diamond crystallization was studied in the $SiO_2–H_2O–C$, $Mg_2SiO_4–H_2O–C$, and $H_2O–C$ subsystems at 7.5 GPa and 1600°C. It was found that dissolution of initial graphite is followed by spontaneous nucleation and growth of diamond on seed crystals. In 15-hour runs, the degree of graphite-to-diamond transformation was $\alpha = M_{Dm}/(M_{Dm}+M_{Gr})100$, where M_{Dm} is the mass of obtained diamond and M_{Gr} the mass of residual graphite. Transformation reached 100% in H_2O-rich fluids but was only 35–50% in water-saturated silicate melts. In 40-hour runs, an abrupt decrease of α was established at the weight ratio of $H_2O/(H_2O+SiO_2)\leq 0.16$ or $H_2O/(H_2O+Mg_2SiO_4)\leq 0.15$. The results indicate that α is a function of the concentration of water, which controls both the kinetics of diamond nucleation and the intensity of carbon mass transfer in the systems. The most favorable conditions for diamond crystallization in the mantle silicate environment at reliable *P–T* parameters occurs in the fluid phase with low concentrations of silicate solutes. In H_2O-poor silicate melts, diamond formation is questionable. *RAH*

Diamonds and associated heavy minerals in kimberlite: A review of key concepts and applications. T. E. Nowicki, R. O. Moore, J. J. Gurney, and M. C. Baumgartner, *Developments in Sedimentology*, Vol. 58, 2007, pp. 1235–1267.

Kimberlite pipes accounted for more than 70% of world diamond production by value in 2003. Kimberlite is an ultramafic, alkaline igneous rock that originates deep within the earth. Although most kimberlite intrusions do not contain significant concentrations of diamond, they may contain diamond-bearing xenoliths of upper-mantle rocks; the diamond content of these xenoliths varies widely.

Two key diamond sources are peridotites and eclogites. Peridotites can be subdivided into harzburgite and lherzolite. Harzburgitic diamonds formed in Archean time (~3300 million years ago [Ma]), while lherzolitic diamonds are much younger (2000–1900 Ma). Eclogitic diamonds formed from Archean through Proterozoic time (2900–990 Ma). After formation, the diamonds resided in the mantle for a significant period before they were incorporated into the kimberlite magma. Both peridotitic and eclogitic diamonds occur together in every known primary diamond deposit worldwide. There are also much younger diamonds (only slightly older than the host kimberlites) found as fibrous cubes and fibrous coatings on older diamonds.

Majorite, a very high-pressure mineral (stable only at ~200–450 km depths), is found very rarely as an inclusion in diamond. Its presence suggests that some diamonds may originate from the very deep mantle, such as the asthenosphere. During their ascent to the earth's surface, many diamonds are partially resorbed (mainly by oxidation), resulting in perhaps a 45% weight loss.

Thick continental cratons are the prime targets for diamond exploration. Volatile-rich ultramafic volcanism is required to transport diamonds rapidly to the surface. Mantle minerals such as garnet, chromite, ilmenite, Cr-diopside, and olivine are usually included in kimberlites, so they are important indicator minerals. Garnet, chromite, and ilmenite are resistant to chemical weathering and hence can easily be preserved in secondary deposits. Their high density, unique visual characteristics, and chemical compositions (such as relatively high contents of Mg and Cr) can be useful in identification. Other components, such as phlogopite and zircon, are valuable in dating kimberlites.

Diamond indicator minerals have unique chemical compositions compared to kimberlitic mantle minerals that are not associated with diamonds. In peridotite xenoliths, for example, diamonds are strongly associated with garnet harzburgite/dunites and least associated with garnet lherzolites (though they are the most common xenoliths in kimberlite). Chromites associated with diamonds have a high Cr concentration (typically >62.5 wt.% Cr_2O_3), whereas eclogitic garnets associated with diamonds have relatively high Na (>0.07 wt.% Na_2O) and Ti. Using detailed flow charts, the authors explain the step-by-step use of diamond indicator minerals in exploring for and evaluating primary diamond deposits. *KSM*

Distribution of diamond contents as reflecting the self-organization processes in kimberlites of Catoca pipe (Angola). V. N. Dech [agat@bp2956.spb.edu], V. N. Zinchenko, and V. A. Glebovitsky, *Proceedings of the Russian Mineralogical Society*, Vol. 137, No. 1, 2008, pp. 11–21 [in Russian with English abstract].

In the polygenic kimberlites of the Catoca pipe in northeastern Angola, diamonds were found to follow a classic Boltzmann distribution when studied statistically. The distribution of diamonds according to their number in the grade of their mass corresponds to Bose-Einstein statistics, confirming the quantum nature of their growth. The nature of the distribution is substantiated genetically by statistical thermodynamics, which is important for a well-grounded evaluation of the diamond contents needed for the calculation of the reserves of the diamond-bearing pipe. *RAH*

Evaluation of brilliance, fire, and scintillation in round brilliant gemstones. J. Sasian [jose.sasian@optics.arizona.edu], J. Quick, J. Sheffield, J. Caudill, and P. Yantzer, *Optical Engineering*, Vol. 46, No. 9, 2007, pp. 093604-1–093604-25.

The authors used four types of gem evaluation maps (color-coded face-up representations) to quantify the light-handling abilities of a faceted diamond:

1. Angular spectrum maps indicating the set of ray-angle directions that can make facets appear illuminated
2. Dispersion maps showing a stone's potential to produce fire and illustrating the amount of dispersion that a ray of white light will undergo when reaching an observer's eye
3. Scintillation maps disclosing aspects of the size and form of virtual facets while depicting the gem's "intrinsic light scrambling properties"
4. Glare maps indicating the directions that can produce glare

Matrices of face-up maps and tilt-view maps permit the user to find the proportions with the best light performance.

The authors describe a concept they refer to as the "cutter's line." This is a line across a matrix of maps that follows what the authors determined to be the best proportions for "gemstone performance." Maps in the article illustrate why the Tolkowsky cut—and other adjacent cuts along the cutter's line—are the best round-brilliant cuts. In contrast, the "anti-cutter's line" demonstrates where optical properties change significantly across minor proportion-space differences; they change little along the cutter's line. The authors recommend going parallel to the cutter's line when adjusting proportions; if modifications deviate perpendicular to the cutter's line (i.e., along the anti-cutter's line), changes in appearance will be more extreme with only a minor departure in proportions. *Al Gilbertson*

Gem diamonds: Causes of color. H. Kitawaki [h-kitawaki@gaaj-zenhokyo.co.jp], *New Diamond and Frontier Carbon Technology*, Vol. 17, No. 3, 2007, pp. 119–126.

This article briefly reviews the causes of color in natural gem diamonds. These include: the presence of foreign atoms such as hydrogen, boron, and nitrogen (along with the state of aggregation of the nitrogen atoms, and optical centers involving nitrogen); structural defects and vacan-

cies due to radiation damage and other phenomena; and defects thought to be related to natural plastic deformation of the diamond lattice. In each case, the diamond absorbs a portion of the spectrum of the incident light while transmitting the remaining portions to exhibit coloration.

Fancy-color diamonds are highly valued in the gem marketplace. In the 1950s, artificial coloring processes began to see commercial use. Radiation exposure, low- to moderate-temperature annealing, and, more recently, high-pressure, high-temperature (HPHT) annealing have all been used to enhance color in diamonds. Correctly identifying treated-color diamonds is an ongoing challenge for gem-testing laboratories that issue origin-of-color reports. In general, this detection is based on a combination of gemological properties and visible, infrared, and luminescence spectral features. *JES*

Hydrogen-related optical centers in natural diamond: An update. E. Fritsch [emmanuel.fritsch@cnrs-imn.fr], T. Hainschwang, L. Massi, and B. Rondeau, *New Diamond and Frontier Carbon Technology*, Vol. 17, No. 2, 2007, pp. 63–89.

Many absorption features in both the infrared and visible regions of natural diamond spectra are related to the presence of hydrogen as an impurity. The most important one in the IR range is the 3107 cm^{-1} system, which is thought to be due to hydrogen strongly bonded to carbon and weakly linked to nitrogen. When the intensity of this absorption feature is greater than that due to the intrinsic band at 2450 cm^{-1}, the diamond is called "hydrogen-rich" and may exhibit specific optical properties. Three color groups of H-rich diamonds have been recognized—"brown to grayish green to green," "gray to blue to violet," and "chameleon"—each of which is associated with particular patterns in the UV-visible absorption spectrum.

This article presents a detailed classification of six groups of IR spectra for H-rich diamonds, which can be quite complex since about 90 distinct absorption bands or systems have been found so far (some quite common, others rare). There does not appear to be a direct relationship between the H-related optical centers that produce infrared and visible absorptions, and many of the hydrogen defects responsible for these centers are not yet fully understood. The concentration of hydrogen in diamonds is thought to be on the order of 500–1000 atomic parts per million (ppma), but the amount responsible for the various optical centers is not known. All natural H-rich diamonds appear to have formed by cuboid growth, which seems to preferentially incorporate this impurity as compared to octahedral growth. *JES*

The ordered creation of paramagnetic defects at plastic deformation of natural diamonds. R. M. Mineeva [mineeva@igem.ru], A. V. Speransky, S. V. Titkov, and N. G. Zudin, *Physics and Chemistry of Minerals*, Vol. 34, No. 2, 2007, pp. 53–58.

Plastically deformed diamonds are common in many deposits throughout the world. While residing in the earth's mantle, and during their transport in kimberlite or lamproite magmas to the surface, diamonds are subjected to stresses that produce this kind of deformation. Such deformation creates different types of structural defects in the diamond lattice that are responsible for the widespread brown and less common pink (red) and purple colorations of diamonds.

An electron paramagnetic resonance spectroscopic study of 15 natural purple diamonds of varying saturations from the Internationalaya and Sputnik kimberlite pipes in eastern Siberia revealed differing amounts of several well-known paramagnetic defect centers, including P1, P2, W7, N2, and M2. The distribution of the M2 defects and the purple color were restricted to parallel lamellae that the authors interpret as the result of twinning on a microscale. The W7 defects were found in both the lamellae and within the main body of the samples, while the remaining three centers were found only in the main body. Both the M2 and W7 centers involve a pair of substitutional nitrogen atoms in different carbon atom sites. Mechanical twinning appears to be one result of plastic deformation, but the transport conditions that produced deformation in this manner seem to be uncommon, given the rarity of natural purple diamonds. *JES*

GEM LOCALITIES

Minerals of the Lipovka granite pegmatites, central Urals, Russia. I. V. Pekov and L. R. Memetova, *Mineralogical Almanac*, Vol. 13, 2008, pp. 7–44.

The Lipovka granitic pegmatite field is the largest source of gem tourmaline in Russia. Located in the Rezh district of the Sverdlovsk region in the central Urals, it is considered a classic mineralogical locality. This article provides a thorough discussion of the pegmatites' structure and their mineral composition. The authors include a brief discussion of each of the more than 60 minerals that have been identified in the Lipovka pegmatites. Other types of geologic formations in the same area also provide a variety of minerals. Information on the occurrence and geochemical features of these minerals is discussed as well.

Dennis Zwigart

Role of basin-wide landslides in the formation of extensive alluvial gemstone deposits in Sri Lanka. A. Gunatilaka [gunat@asianet.lk], *Earth Surface Processes and Landforms*, Vol. 32, No. 12, 2007, pp. 1863–1873.

The tectonically stable central highlands of Sri Lanka and their associated alluvial valleys represent one of the most prolific Quaternary gem provinces in the world. The focus of this study was the geomorphic factors controlling the distribution of these gem deposits. The known denudation

rates of these highlands and the resulting sediment fluxes in river systems are inadequate to deliver the volume of sediments that would be required to concentrate the known placer gem deposits. Based on an extensive field study, the author suggests that large-scale, unstable, and slow-moving landslides and debris flows throughout the region have been the dominant mechanisms both today and in the past for the mass-wasting of hill slopes and the bulk delivery of sediments to the alluvial valleys. Monsoonal rains that occur several times a year in the highlands play a major role in the generation of these landslides. A review of geologic information databases revealed a significant spatial overlap and direct causal link between numerous landslide occurrences and the location of alluvial gem mining areas. Landslide phenomena play an important role in the development of landscapes in all mountainous terrains where there is high annual rainfall. *JES*

Some observations on the composition and origin of opals from Java. H. C. Einfalt [hcv.einfalt@gmx.de], *Journal of Gemmology*, Vol. 30, No. 7/8, 2007, pp. 383–398.

The gemological properties, composition, and geologic environment of play-of-color and common opals from Banten Province (Rangkasbitung, West Java, Indonesia) are described. The opals have a restricted occurrence as isolated nodules in a decomposed tuff layer containing montmorillonite and clinoptilite (a zeolite). Internal features in the opals consist of flow texture, microcrystalline granular quartz/chalcedony, and zeolite inclusions. Several samples showed indications of stress: (1) hidden latent microfractures in brown and black opals, (2) play-of-color fields exhibiting bent color lamellae, (3) crosscutting microfractures penetrating several color fields with a displacement of fragments relative to one another, and (4) a subparallel arrangement of elongated color fields interpreted as the result of shearing or squeezing. These may contribute to the poor stability of some Indonesian opals, which often develop fractures during polishing and wear.

All but one of the opals studied showed pseudo-birefringence. One unusual "inverse" hydrophane opal lost its play-of-color when immersed in water. Along with the red, orange, and green play-of-color commonly observed in Indonesian opals, subordinate patches of deep blue were also seen. The comparatively large size of the silica spheres in the Indonesian samples explains the dominance of red to green colors in these opals. XRD patterns and SEM micrographs of hydrofluoric acid–etched samples divided the opals into three types: opal-A, opal-CT, and opal-C. *Elise Skalwold*

INSTRUMENTS AND TECHNIQUES

Applications of diamond crystal ATR FTIR spectroscopy to the characterization of ambers. M. Guiliano [michel.guiliano@univ-cezanne.fr], L. Asia, G. Onoratini, and G. Mille, *Spectrochimica Acta A*, Vol. 67, No. 5, 2007, pp. 1407–1411.

Fourier-transform infrared (FTIR) spectroscopy is an important analytical tool used to characterize a variety of materials. In this study, geologic and archeological samples of amber and copal from several sources (including Poland, France, Madagascar, and Colombia) were examined by FTIR using the attenuated total reflection (ATR) method, which involves minimal sample preparation. Although the infrared spectra of amber and copal were complex, they exhibited a number of distinguishing features. In addition, their imitations can be recognized. The article summarizes the specific infrared spectral features that are characteristic of these two natural resins. *JES*

PIXE and ionoluminescence for Mesoamerican jadeite characterization. J. L. Ruvalcaba-Sil, L. Manzanilla, E. Melgar, and R. L. Santa-Cruz, *X-Ray Spectrometry*, Vol. 37, No. 2, 2008, pp. 96–99.

"Greenstones" consisting of jade (jadeite and nephrite), serpentine, and possibly other minerals were highly prized as gem materials in pre-Hispanic Mesoamerica, with jadeite being the most valued. This study concerns a greenstone necklace that was a temple offering recovered from an excavation of the ~155 AD palatial structure of Xalla at Teotihuacan, Mexico. Eleven light-to-dark green rounded beads (2.1–4.8 cm in diameter) were investigated by two nondestructive analytical techniques. Particle (or proton)-induced X-ray emission (PIXE) gives information on the chemical elements in a sample to the parts-per-million level. Ionoluminescence (IL or IOL) is an efficient way of exciting luminescence in a material by exposure to the same proton beam.

The range of chemical composition data indicated several different sources for the 11 beads, and from an archeological viewpoint, these sources may have been widely distributed, considering that trade extended throughout the region at the time. Only one bead (labeled sample C) had chemical features consistent with jadeite from Manzanal in the Motagua River area of Guatemala—the only known source of jadeite in Mesoamerica. Two other beads (A and B) may have come from this source or from elsewhere, while the provenance of the remaining eight beads remains uncertain. Bead samples A, B, and C all displayed green and violet IL (blue-violet for bead A). The green emission is due to Mn^{2+}, while the violet IL is due to Ce^{3+} or Al^{3+} emissions. The similar IL reactions among the three beads provides evidence for a possible common source. *JES*

JEWELRY RETAILING

Place your Bidz. *Retail Merchandiser*, Vol. 48, No. 1, 2008, pp. 38–40.

Sales are down for many retail jewelry firms, yet Bidz.com, an online jewelry auctioneer founded in 1998, is growing fast and expects to become a billion-dollar-plus company in the next few years. The brainchild of CEO David Zinberg, Bidz.com offers its products through live auctions with only a $1 minimum bid. After running pawn shops for more than 20 years, Zinberg discovered that "the easiest way to get rid of jewelry was online." Bidz.com operates primarily on a closeout model, buying overstock. However, 30% of the jewelry it sells is manufactured specifically for the site.

Bidz.com has some features not found on competitor eBay. For example, a last-minute bid on Bidz.com extends the auction period by 15 minutes. The site received between four and six million unique visits each month in January and February 2008. Fourth-quarter 2007 projected revenues exceeded the predicted $56–$58 million, and 2008 revenues are expected to be around $225–$230 million, with a pre-tax income of approximately $23.5–25.5 million and a gross margin of approximately 27–28%. The site recently completed a major upgrade of its auction platform at a cost of about $1 million. Its new LiveBid system supports a broad range of browser software.

Edward Johnson

PRECIOUS METALS

Colorizing metals with femtosecond laser pulses. A. Y. Vorobyev and C. Guo [guo@optics.rochester.edu], *Applied Physics Letters*, Vol. 92, 2008, pp. 041914-1–041914-3.

A femtosecond 800 nm Ti:sapphire laser system was used to alter the color of polished samples of aluminum, gold, and platinum. The laser caused a modification of the optical properties via surface restructuring on nano-, micro-, and sub-millimeter scales. Gold, black, and gray colors were achieved. UV-Vis-IR reflectance spectroscopy showed that treated aluminum samples exhibited decreasing reflectance toward the UV end of the spectrum; the decrease was more linear in the gray and black samples than in the gold-colored samples, which showed greater absorption in the blue and green regions. By changing the laser fluence and pulse rate, the authors produced some samples that exhibited different colors at different viewing angles. SEM analysis determined that the viewing-angle effect was caused by nanostructure-covered laser-induced periodic surface structures (NC-LIPSS). The authors noted that since the spacing of such structures can be controlled, this femtosecond laser technique offers a versatile way to modify the optical properties of the metal. They concluded that this technique has many potential applications because it can process a variety of metal sizes as well as complex shapes.

Michele Kelley

SYNTHETICS AND SIMULANTS

Nonuniform distributions of color and luminescence of diamond single crystals. H. Kanda [kanda.hisao@nims.go.jp], *New Diamond and Frontier Carbon Technology*, Vol. 17, No. 2, 2007, pp. 105–116.

Synthetic diamonds grown from a metal solution at high pressures and temperatures, or from a vapor by chemical vapor deposition at high temperatures but near-vacuum conditions, can incorporate impurity atoms such as N, B, H, Si, P, Ni, and Co as optically active lattice defects. Of these elements, all except Si, P, and Co can produce coloration and luminescence.

In both forms of synthesis, growth begins from a diamond seed crystal, with carbon and impurity atoms migrating from the growth medium and depositing on the surface(s) of the seed. This impurity incorporation depends on the arrangement of carbon atoms at the surface as well as on growth kinetics and other factors. The structure of the growing surface depends on crystal orientation; the structure of an octahedral {111} face, for example, is different from that of a cube {100} face. As a result, impurity atoms are incorporated to varying degrees—in some cases, almost not at all—on different surfaces (growth sectors). This variation creates a nonuniform distribution of impurity atoms within the synthetic diamond, which in turn causes a zonal distribution of color and luminescence. Such visual features are characteristic of many synthetic diamond crystals. Because of this, it is very difficult to grow synthetic diamonds with uniform impurity distributions, a prerequisite for some technological applications. *JES*

TREATMENTS

Color centers in topaz: Comparison between neutron and gamma irradiation. K. Krambrock [klaus@fisica.ufmg.br], L. G. M. Ribeiro, M. V. B. Pinheiro, A. S. Leal, M. Â. de B. C. Menezes, and J. M. Spaeth, *Physics and Chemistry of Minerals*, Vol. 34, 2007, pp. 437–444.

Even though topaz has been irradiated commercially for more than 30 years, the nature of its radiation-induced defects and color centers is still not well understood. Recently, O^- hole centers were found to be associated with blue color in topaz. It also has been suggested that small polarons (quasiparticles composed of an electron plus its accompanying polarization field) are candidates for color centers in oxide materials, including topaz. To understand more about the color centers, neutron- and gamma-irradiated topazes from four different regions in Brazil were examined by electron paramagnetic resonance and optical absorption spectroscopy.

Neutron irradiation can produce O_2^- and O^- hole centers, which are independent of the sample origin. By con-

trast, gamma irradiation generates O^- hole centers that are origin-dependent. It was confirmed that O^- hole centers are responsible for the blue color. These centers could be correlated to a 620 nm absorption band, and they could be annealed out at ~500°C (along with the blue color). Neutron irradiation was found to be the preferred method for blue color enhancement, and the best blue can be produced commercially by a high integrated flux of fast neutrons, regardless of the topaz's origin and composition. Using a Cd shield during the neutron irradiation process will eliminate thermal neutrons, thus reducing induced radioactivity to a minimum level.

A brown color may be caused by the X center, which shows absorption at ~0.15 eV and is stable between 150 and 200°C. This defect is believed to be associated with a bound polaron along with an O^- hole center. More detailed studies are essential to a thorough understanding of a model for the X defect. *KSM*

Diagnostics of natural and synthetic diamonds with the aid of low-temperature optical spectroscopy. R. S. Serov and M. A. Viktorov, *Moscow University Geology Bulletin*, Vol. 62, No. 1, 2007, pp. 46–48.

The authors investigated the low-temperature UV-Vis and IR absorption spectra of a total of 100 natural and synthetic diamonds (0.1–6 ct), both rough and faceted. They summarized the properties according to diamond type, color, and natural or synthetic origin. The N3 defect was observed in all the colorless and yellow natural type Ia diamonds; the N2, N4, and N5 defects were usually observed as well. The presence of these nitrogen-related defects did not correlate to depth of color as it changed from colorless to fancy yellow. The three natural type IIa diamonds studied showed a distinct band at 270 nm that is associated with single nitrogen atoms (C defect).

The authors studied five type Ib synthetics that showed features at 1290 and 1135 cm^{-1}—related to C defects—in their IR spectra. The UV-Vis spectra showed several Ni-related peaks, confirming their synthetic origin. One type IIa and one type IIb synthetic were studied as well. No diagnostic features were seen in the absorption spectra. All the synthetic diamonds were grown by HPHT methods using a nickel catalyst. However, the Ni-related defects were not observed in the type II (i.e., nitrogen-free) samples. Therefore, the authors conjectured that the optically active Ni-related centers in the type Ib synthetics have a form that involves nitrogen, such as Ni-N. Additionally, they observed a correlation between the intensity and quantity of the Ni-related peaks in the type Ib diamonds and the increasing concentration of C defects. *SE-M*

Features of low-temperature optical absorption spectra of natural and treated diamonds. R. S. Serov and M. A. Viktorov, *Moscow University Geology Bulletin*, Vol. 62, No. 2, 2007, pp. 127–130.

The authors investigated the low-temperature UV-Vis and IR absorption spectra of untreated and treated diamonds. They summarized the properties according to diamond type and treatment. In three irradiated type Ia diamonds, they observed lines at 393 and 741 nm related to the negatively charged vacancy and the neutral vacancy, respectively. These defects also can be seen in naturally irradiated diamonds, but their intensities are much lower. Subsequent annealing was confirmed by the presence of features at 594 and 724 nm.

In an irradiated type Ib synthetic diamond, features appeared at 526, 617, 626, 637, 644, 649, and 655 nm. It also showed a considerable decrease in the concentration of single substitutional nitrogen after treatment. The authors connected this decrease with the transformation of the nitrogen to N^+ defects. The authors tested 150 HPHT-treated type Ia diamonds and found that these were characterized by defect lines at 637 and 986 (H2 defect) nm. The authors indicated they have not yet found any diagnostic signs of treatment in type IIa and type IIb diamonds, partly because they do not have detectable amounts of nitrogen defects. *SE-M*

HPHT annealing of natural diamond. F. de Weerdt [fdw@euphontnet.be] and A. T. Collins, *New Diamond and Frontier Carbon Technology*, Vol. 17, No. 2, 2007, pp. 91–103.

This article reports the results of high-pressure, high-temperature (HPHT) annealing experiments involving brown diamonds at pressures of 6–9 GPa and temperatures above 2500°C. The samples were type Ia diamonds with a range of A and B nitrogen-aggregate concentrations. During the treatment process, vacancies in the starting material were released to move through the diamond lattice and become incorporated into various nitrogen-vacancy defects. As a result, brown diamonds became yellow-green after relatively short annealing times (several minutes) and yellow after longer annealing times at identical pressure and temperature conditions. Type IaB brown diamonds became near colorless or yellow, depending on the annealing conditions. Results of experiments such as these provide a better understanding of the color changes produced by HPHT annealing, and additional means of detecting HPHT-treated diamonds. *JES*

Optical centres produced in diamond by radiation damage. A. T. Collins [alan.collins@kcl.ac.uk], *New Diamond and Frontier Carbon Technology*, Vol. 17, No. 2, 2007, pp. 47–61.

Radiation exposure produces optically active (and color-causing) defects in diamond that can be detected by absorption or luminescence spectroscopy. Any particle radiation with sufficient energy can produce damage to the diamond lattice in the form of vacancies (vacant carbon atom sites). Two important radiation defects are the GR1 (zero-phonon line [ZPL] = 741 nm), due to a vacancy in a

neutral charge state, and the ND1 (ZPL = 393 nm), due to a vacancy in the negative charge state. A broad region of absorption between ~550 and 750 nm, associated with the GR1 defect, produces green-to-blue coloration in diamond. Heating an irradiated type I diamond at several hundred degrees at ambient pressure for one hour reduces the intensity of these radiation-damage absorptions, but creates new absorption bands related to vacancies that have migrated in the lattice to become trapped with various forms of nitrogen. These new absorptions can result in yellow-green, yellow, orange, or red (pink) colors.

Which defects are destroyed and which are created by this subsequent heating depends on the nitrogen concentration, the perfection of the lattice, and the particular heating conditions. Heating above 900°C results in the disappearance of the vacancy-related absorptions mentioned above and, in nitrogen-containing diamonds, the formation of an optical center consisting of a vacancy trapped with a single nitrogen atom. The absorptions associated with this N-V center are located at 575 and 637 nm; another nitrogen center produces an absorption band at 594 nm. Trapping of a vacancy by nitrogen A or B aggregates produces absorptions due to H3 and H4 defects (ZPL = 503 and 496 nm, respectively). Heating to higher temperatures (>1500°C) destroys or further alters many of these nitrogen-vacancy centers with accompanying changes in absorption spectra.

The effects of radiation and annealing on optical centers have been a major focus of diamond research for more than 50 years. While the details of many of these optical centers are now well known, the nature of others remains the subject of ongoing research. *JES*

MISCELLANEOUS

Africa wants to cut its own diamonds. F. Misser, *The Courier*, No. 4, January-February 2008, pp. 27–28.

Africa accounts for 60% of global rough diamond supply, and "resource nationalism" is a growing phenomenon in which diamond-producing countries in Africa are developing their own cutting and polishing operations. This campaign, also described as "beneficiation," stems from the argument that while Africa supplies most of the raw materials for the world's jewelry industry, it only receives the equivalent of 10% of the overall revenue generated (US$150 billion). Producing countries in southern Africa want to use the value added from cutting and polishing to improve their balance of trade and stimulate employment.

Countries such as Botswana, South Africa, Angola, the Democratic Republic of the Congo, and Namibia want access to large diamonds, for which labor costs are proportionately lower. This would allow them to compete against lower-cost processing centers in Asia. In South Africa, the State Diamond Trader has the authority to buy 10% of all stones cut in the country, preferably for companies that promote black economic empowerment. In Namibia, 11 diamond-cutting plants will be supplied with rough between 2007 and 2011. Botswana is increasing the turnover of its 16 cutting plants; its capital city, Gaborone, is now home to the largest sorting and distribution facility of the De Beers Diamond Trading Company, which relocated some of its operations from London in March 2008. This new African supply oligopoly will strengthen in 2008 when global demand begins to outstrip supply, as is predicted by both Rio Tinto Diamonds and Alrosa. *Edward Johnson*

Conflict diamonds: Still threatening. F. Misser and O. Vallée, *The Courier*, No. 1, July-August 2007, pp. 31–32.

The Kimberley Process, ratified in 2003, has been effective in slowing the entry of conflict diamonds into the mainstream market. By limiting all forms of illicitly traded rough diamonds, the Kimberley Process also has increased export earnings for diamond-producing nations. However, reducing surveillance could lead to resumption of illicit trade. This report cites examples of diamonds from war-torn Ivory Coast being represented as Ghanaian. Karel Kovanda, the newly appointed Kimberley Process chairman, hopes to see the measures extended to other gemstones and resource exports, and expanded to include associations of small-scale alluvial miners. *RS*

The diamond industry as a virtual organization: Past success and challenging future. E. I. Mostovicz, N. K. Kakabadse [nada.kakabadse@northhampton.ac.uk], and A. P. Kakabadse, *Strategic Change*, No. 16, 2007, pp. 371–384.

This paper argues that the global diamond trade functions like an organization, where members have close-knit, defined relationships, rather than an industry with diverse players that often have little or no contact with one another.

The authors examine how changes since 1980—namely the loosening of De Beers's control and the rise of new players (primarily Indian manufacturers) and new requirements in the form of grading reports—have created paradoxes in which the solution to one problem often means worsening a second problem inside the "organization." The authors cite a number of examples, including a tendency for older diamond people to blame De Beers for the industry's problems while seeking its assistance in a difficult market.

To succeed, the diamond industry must recognize these paradoxes and take appropriate action, particularly longer-term thinking and closer collaboration between various groups, instead of passing blame and responsibility. *RS*